Synthesis, characterisation and activity of Ruthenium/N-doped multi-walled Carbon nanotubes catalysts

Letlhogonolo Fortunate Mabena

A thesis submitted to the Faculty of Science, University of the Witwatersrand, in fulfillment of the requirements for the degree, Doctor of philosophy Degree (PhD) in chemistry

Supervisor   : Prof Neil Coville
Co-supervisor   : Prof Suprakas Sinha Ray

Johannesburg, 2013

DECLARATION

I declare that this thesis is my own, unaided work. It is being submitted for the degree of Doctor of Philosophy in the University of the Witwatersrand, Johannesburg. It has not been submitted before for any degree or examination in any other university.

Signature: ……………………………………………………

Date: ……………………………………………………

DEDICATION

This thesis is dedicated to

My two daughters DIMPHO & DINTLE

My son MBHUDUMA "DITIRO"

My lovely husband ERNEST SOZABILE MABENA
&
My mother

OMPHILE DOROTHY MATLHOKO

ACKNOWLEDGEMENTS

ABSTRACT

Nitrogen doped carbon nanotubes (N-CNTs) were synthesised using thermal-Chemical Vapour Deposition (CVD). The obtained material was purified, characterised and used as a support for ruthenium nanoparticles. The catalytic performance of the Ru/N-CNTs was investigated in different chemical reactions. Thus, this thesis is divided into two sections. The synthesis of the nanomaterials, the catalyst performance of nanomaterials in the oxygen reaction reduction (ORR) and activity in the oxidation of styrene and benzyl alcohol.

In the first section N-CNTs were synthesised using a thermal-CVD method in a horizontal split-tube furnace. The reactions were carried out in a tubular quartz reactor. Cyclohexanol was used as carbon source, aniline as a nitrogen source and ferrocene as catalyst. A mixture of cyclohexanol-aniline-ferrocene was placed in a quartz boat that was directly introduced in the centre of the first furnace and vaporised at 280 °C. The resultant vapours were transferred to the second furnace where the N-CNTs were grown at a temperature of 900°C under the carrier gas flow (nitrogen or 5% H_2 balanced in argon gas). The N-CNTs formed had a fairly crystalline structure, constituted by a periodical bamboo like structure with tubes diameters of 35 - 100 nm and nitrogen content up to 1.3 at. %.The N-CNTs with 0.8 at.% were selected to be used becaused of the quality and the amount of CNTs produced.

N-CNTs were then used to support ruthenium (Ru) nanoparticles using a microwave assisted reduction technique. The synthesised nanostructured materials were characterised by TEM, SEM, TGA, and XRD.

The TEM images of the Ru catalysts supported on N-CNTs revealed homogenous dispersion of Ru nanoparticles with a narrow sizes

distribution and small particle size with an average diameter of 2.5 nm when 500 W power was used.

In the second section, part A; four catalysts with different Ru wt. % supported on N-CNTs were prepared: the amount of Ru deposited on the N-CNTs was varied between 0 −10 wt. %. The activity of the prepared nanocatalysts towards the oxygen reduction reaction (ORR) was characterised using the rotating disk electrode and voltammetry techniques. The ORR activity was higher at lower concentrations of Ru on N-CNTs. The 4e- pathway of ORR was more favourable on 2 and 5 % Ru loaded N-CNTs than as 10 % Ru loaded N-CNTs.

In Part B; prepared Ru/CNT and Ru/N-CNT catalysts were calcined and used for the liquid-phase oxidation reaction of styrene and benzyl alcohol. The influence of various reaction parameters such as reaction time, catalyst mass, solvent nature and reaction temperature were evaluated. It is interesting to note that the RuO_2 on carbon material catalyst was more active for styrene oxidation than for benzyl alcohol oxidation reaction. The conversion of styrene was 41 % and the selectivity to benzaldehyde was 85 % when 5 % RuO_2/CNTs catalyst was used with 1,4-dioxane as a solvent at 80 °C in 4 h. The highest conversion of benzyl alcohol was 11 % also with 85 % benzaldehyde selectivity. The benzyl alcohol oxidation was performed at 110 °C for 5 h.

Ru/N-CNTs were shown to exhibit better activity for a styrene oxidation reaction. Therefore further investigations on the activity of nitrogen doped carbon nanotubes (N-CNTs*) prepared by reaction of acetylene (C_2H_2) and acetonitrile (CH_3CN) at 700 °C over a 10 % Fe-Co supported on calcium carbonate ($CaCO_3$) catalyst was investigated for styrene oxidation. In this case the nitrogen doped carbon nanotubes (N-CNTs*) with 2.2 at. % nitrogen content was used. A 5 % Ru/N-CNT* catalyst was highly selective as compared to the previous N-CNT supports used in the styrene oxidation reaction. Comparing the support it was deduced that the

nitrogen present in the support is playing a major role. With the increase in the nitrogen content in the matrix of the CNTs the conversion of styrene decreased but with an increase in the selectivity. The selectivity towards benzaldehyde was 96 % after 4 h when N-CNTs* were used as support for the styrene conversion reaction. In comparison for the RuO_2 on CNTs and N-CNTs the styrene conversions were 85 and 87 % respectively.

PUBLICATIONS AND PRESENTATIONS ARISING FROM THIS THESIS

Publications

1. Letlhogonolo F. Mabena Suprakas Sinha Ray, Neil J. Coville, Microwave Irradiation of Ruthenium on Nitrogen-Doped Carbon Nanotubes. Ceramic Engineering and Science Proceedings 32: 33-42 (2011)

2. Letlhogonolo F. Mabena, Suprakas Sinha Ray, Sabelo D. Mhlanga, Neil J. Coville, Nitrogen-Doped Carbon Nanotubes as a Metal Catalyst Support: Review: Applied nanoscience 1: 67-77 (2011)

3. Letlhogonolo F. Mabena, Remegia M. Modibedi, Suprakas Sinha Ray, Neil J. Coville. Ru supported on nitrogen-doped carbon nanotubes for the oxygen reduction reaction in alkaline media", **Journal of Fuel cells 12: 862-868 (2012)**.

4. Synthesis of Nitrogen-Doped Carbon Nanotubes Using Two Stage Furnace (To be sumitted).

5. Studies on styrene oxidation over nitrogen doped carbon nanotube supported ruthenium (To be submitted).

Oral Presentations

1. Microwave Irradiation of Ruthenium on Carbon Nanotubes, 35th International Conference and exposition on advanced Ceramic and composite (Florida, US), January 2009.

2. Ru supported on nitrogen-doped carbon nanotubes for the oxygen reduction reaction in alkaline media, Nanoscience young Researcher Symposium (Vaal university of Technology), October 2011.

Poster Presentations

1. Microwave Polyol Synthesis of Ru/CNT catalysts. Catalysis Association of South Africa Conference (Cape Town) December 2009.

2. Synthesis Of Nitrogen-Doped Carbon Nanotube Cups Using Two Stage Furnace, 35th International Conference and exposition on advanced Ceramic and composite (Florida, US), January 2011.

3. Ru supported on nitrogen-doped carbon nanotubes for the oxygen reduction reaction in alkaline media. SA-Korea Fuel Cell Workshop (Warmbath), July 2012.

TABLE OF CONTENTS

Section   **_Page_**

LIST OF FIGURES

LIST OF SCHEMES

LIST OF TABLES

LIST OF ABBREVIATIONS

Ar	argon
at.%	atomic concentration by percentage
AFC	Alkaline fuel cells
Au	Gold
CNTs	carbon nanotubes
CV	cyclovoltammetry
CVD	chemical vapour depositio
DMFC	direct methanol fuel cell
EDS	energy dispersive X-ray spectroscopy
EG	ethylene glycol
F	Faraday constant
Fe	iron
GC	Gas Chromatography
HNO_3	nitric acid
K-L	Koutecky–Levich
LSV	linear sweep voltammetry
MWCNTs	multi walled CNTs
MCFC	Molten carbonate fuel cell
N_2	nitrogen
N-CNTs	nitrogen-doped CNTs
nm	nanometer
O_2	Oxygen
ORR	oxygen reduction reaction
PEMFC	Proton exchange membrane fuell cells
RDE	rotating disk electrode
Ru	Ruthenium
SAED	selected area electron diffraction
SEM	scanning electron microscopy
SOFC	Solid oxide fuel cell
SWCNTs	single walled CNTs

TEM	transmission electron microscopy
TGA	Thermogravimetric analysis
T	temperature
t	time
wt. %	weight percentage
XPS	X-ray photoelectron spectroscopy
XRD	X-ray diffraction

CHAPTER 1

BACKGROUND

1.1   Introduction

The term "catalysis" was first used in 1836 by Berzelius to describe the phenomenon that was capable of promoting the occurrence of a chemical reaction by a catalytic contact. Today catalysis plays an important role in the production of over 90 % compounds found in numerous fields such as fine chemical and petrochemical industries, the production of fuel, foodstuffs, pharmaceuticals and other numerous manufactured goods. The catalysts and the products derived from catalytic reactions, directly or indirectly, impact on a large portion of the gross domestic product of any nation. Catalytic reactions played a key role in the development of the industrial revolution [1]. In 1991, it was estimated that the total value of chemical and fuels derived from the chemical industry was above 900 billion dollars/year. In 2003 global sales of catalysts exceeded 12 billion dollars which was up from 9.3 billion in 1998 [2,3,4,5].

1.2   Types of catalytic reactions

Catalysts can be divided into two main types - heterogeneous and homogeneous catalysts. In both types chemical bonds are broken and new chemical bonds are formed during the catalytic process. These events occur repeatedly, usually without a significant change of the catalyst. In the absence of the catalysts, this chemical transformation would either not occur or would take place with lower efficiencies or at slower rates. Heterogeneous catalysts are usually immobilised on a cheaper material to stop them agglomerating, and catalysts of this form are called supported metal catalysts. In homogenous catalysis, the

catalyst is in the same phase as the reactants. The catalyst and reactants will both be present either as a gas or as liquids. The catalyst usually takes part in a reaction but it is not used up in the reaction.Table 1.1 summarise the advantages and disadvantages of both homogenous and heterogeneous catalysis.

Table 1.1. Homogeneous versus heterogeneous catalysis [6]

Properties	Homogeneous	Heterogeneous
Activity	Excellent	Good/poor
Selectivity	Excellent	Good/poor
Catalyst Recycling	Difficult, Expensive	Easy, cheap
Thermal Stability	Poor	Good

Homogeneous catalysts have the attractive property of potentially perfect selectivity and activity. However, many homogeneous catalytic systems cannot be commercialized because of difficulties associated with separating the products from the catalyst [7,8].

1.3   History of catalysis

According to Lindstorn and Petterson the evolution of catalysis can be divided into five periods [9]. The first period of catalysis, from alchemy to chemistry (300 B.C. - 1834) dates back to the dawn of civilisation, at a date lost when mankind was producing wine and beer (fermentation). This alchemy period was dominated by the search for a "magical catalyst" that could convert base metals into noble metals [10].

Emperics to science (1835 - 1887) is the second era of catalysis where there was an increase in understanding of chemical reactions and how

they influenced catalysis development. The development of reaction engineering was the main driving force in this era.

The birth of industrial catalysis between 1898 and 1918 was the third advancement in catalysis. It was marked by the discovery and implementation of new catalytic processes. It was in this period that the ammonia process was developed. Bulk ammonia produced was used in the production of nitrogen based explosives and fertilizers. The period ended in disgrace since many catalytic developments related to producing weapons of destruction [10].

1918 - 1945 was the fourth period which corresponded to the increase in global mobility and the use of catalysts in developing catalytic fuel processes. There were large number of constantly catalytic process developed leading to evolution in this era. The first development came in 1920 when the Standard Oil Company developed the large scale industrial production of isopropanol from petroleum. The process is still employed by several companies, including SASOL and Shell. In 1926, DuPont began producing synthetic methanol. A year later Hinshelwood presented his kinetic theory based on the findings of Langmuir. The Hinshelwood-Langmuir theories are now applied in the design and chemical engineering principles of catalysts. The ammonia process catalyst from the third period was also improved in this era when Temkin published a detailed description of the kinetics of the process. The fourth period ended in 1945 with World War Two [9,11].

The transition from war to peace (1946 - 1970) resulted in a natural shift in the demand of chemicals. The petroleum industry continued to play a vital role in advancing catalysis even in the fifth period. The only difference with the previous era was a shift in the use of the catalysts for the production of commodities/chemicals. The highlight of this period was in 1954 when Eischen and co-workers developed the first method for characterising catalysts. They developed a method for studying carbon

monoxide (CO) adsorption on copper catalysts, with IR-spectroscopy. This work soon included approaches to characterize active sites for adsorption on metal, metal oxide and acidic sites as well as distinguishing Brønsted and Lewis acid sites. In 1960 three industrially important processes were also introduced into the commercial market [9]:

- Ethylene to acetaldehyde - Wacker Chemistry

- Benzene to cyclohexene (Hydrar process) - UOP

- World's first acrylonitrile Plant - SOHIO.

The fifth period ended without any clear transitions into the sixth period [2].

The current (sixth) period which started in 1970 is called the environmental catalysis period. The period is influenced by environmental driving forces and the integration of science with new technologies. The older technologies and the new research may lead to new ideas which have impact on the methods that are used for new catalytic systems. It is in this era that reforming catalysts were revolutionised, for e.g. Sinfelt developed a bimetallic platinum–iridium catalyst for the production of lead-free gasoline. Highly dispersed clusters or crystallites of metals on supports were investigated. Haag also helped to bridge the gap between homogenous and heterogeneous catalysts through his studies of transition-metal complexes anchored on organic resins [5].

1.4   Nanotechnology for catalysis

Nanotechnology is one of the technologies that was developed in the current 6th catalytic period. It refers to a process that offers the ability to manipulate the design, synthesise and control of materials and devices at small scale length scales ranging from 1-100 nm. There are exciting prospects to use nanotechnology in health, electronics and manufacturing

industry etc. [12,13]. While nano-scale technology in multifaceted in its application, the study of nano-crystals as catalysts has become possible by use of new characterisation techniques. Nano-materials are more effective than large sized catalysts due not only to their small size but also because nanomaterials produce a large surface atom/ bulk atom ratio not found in their macroscopic counterparts [14,15].

The ultimate aim in catalysis is to design catalysts that can achieve perfect selectivity and activity. A reaction showing perfect selectivity would generate no waste products, and thus reduce energy and process requirements for the separation of products from each other [16]. For instance, in an automobile, hydrocarbons ignite to create, water and carbon dioxide and energy to drive the piston of an engine. Furthermore, impurities and inefficient reactions in a car engine yield by-products such as nitrogen monoxide and carbon monoxide which are harmful to our environment. These by-products are responsible for the acid rain and depletion of the ozone layer. Catalysts have the potential to make automobile combustion up to 100 % selective and produce fewer by-products. This control may be achievable by using controlled small size catalyst particles.

There is no doubt that the catalysis community is following developments in nanotechnology closely to capitalise on these developments to further the purpose of designing catalysts to achieve ideal selectivity in a catalytic reaction. There is much progress in applying nanotechnology in catalysis developments but there are many challenges that still remain [14,17].

1.5   Desired catalysts

Many attempts to obtain high surface area catalysts in order to enhance catalytic activity, selectivity and stability have been developed [4,18,19]. This is achieved by depositing the catalyst particles on a support. Oxides of the transition metals such as silicon dioxide, titanium dioxide, etc., are

amongst the most commonly used heterogeneous catalyst supports [19,20]. In catalysis control of the particle size, as well as the distance between particles is required. Catalysts deposited on a support are affected by the surface reactivity and the microstructure of the support [4,21]. An efficient way of increasing the surface area of the catalyst is by dispersion of the catalyst on a high surface area material [21]. The morphology and the nature of catalyst supports are considered to be one of the main factors in obtaining a high dispersion of nanoparticles [18]. The surface area of the metal or metal oxide catalysts can be increased by enhancing the surface area of a support by corrosive treatment to develop cracks and pores in the catalyst surface. This treatment alters the uniformity in the shape of the catalyst particle. The support is also found to influence the performance of the catalyst through electronic interactions and migration effects [22].

In the field of heterogeneous catalysis, numerous carbon materials have also been used to disperse and stabilise nano-sized metallic particles [23]. In this project, the use of carbon nanotubes (CNTs) as a support media for stabilising small metal particles to develop novel heterogeneous catalysts will be presented. CNTs are envisaged as possible supports for many catalytic applications [3,24]. They are attractive supports in a heterogeneous catalytic process owing to their properties that can be tailored to meet specific needs. They are employed as supports due to:

- Their high surface area

- Resistance to acidic/basic media

- High mechanical strength

- Stability at high temperature

- Possibilities of controlling both their porous structure and

- Chemical nature of their surface [18,25,26,]

CNTs have been extensively studied as supports for metal catalysts [27,28,29,30]. However, less work has been done on using nitrogen-doped carbon nanotubes (N-CNTs) as catalyst supports. N-CNTs are expected to have an influence on the dispersion of the metals and the activity of the catalyst. This thesis is focused on producing nitrogen doped supported catalysts for use in various chemical reactions. The metal that will be supported on the CNTs will be Ru. N-CNTs will be used to disperse the ruthenium metal nanoparticles for the study of two reactions:

- Oxygen reduction reactions (ORR) in alkaline media for use in fuel cells

- Oxidation reactions.

1.6 Aims and objectives

The main objectives of this research were as follows:

- To synthesise nitrogen-doped CNTs using the chemical vapour deposition method. This was achieved by controlling various parameters such as temperature, precursors, and gas flow rates.

- To study the physico-chemical properties of the CNTs using a range of techniques such as scanning electron microscopy (SEM), Energy-dispersive X-ray spectroscopy (EDS), thermal gravimetric analysis (TGA), Raman spectroscopy, X-ray photoelectron spectroscopy (XPS) and high resolution transmission electron microscopy (TEM).

- To determine the optimum conditions for the deposition of ruthenium nanoparticles on both undoped and nitrogen-doped

CNTs using both thermal and microwave irradiation techniques in order to make homogenously dispersed particles with a narrow distribution of diameter sizes.

- To characterise the metal supported undoped and N-doped MWCNTs by X-ray diffraction (XRD), TEM and XPS techniques.

- To test the selectivity and the catalytic activity of supported Ru in various chemical reactions. i.e. the catalysts were tested in ORR in alkaline media for use in fuel cells and in the oxidation of styrene and benzyl alcohol.

1.7 The layout of the dissertation

The chapters in the thesis have been written in the style of Journal articles. As the chapters were written independently of each other, reappearance of the basics and some experimental results will lead to some duplication of material. Nevertheless, this does allow each chapter to be read independently, with each having its own introduction, experimental, results and conclusion sections. The outline of this thesis is given below:

Chapter 1: This gives a motivation for the work presented in the subsequent chapters. Although each chapter briefly introduces itself, the information contained in this chapter is of a general nature. The main objectives of the study are also presented in this chapter.

Chapter 2: This gives a literature review of N-CNTs as a catalyst support. Pristine CNTs have been studied as supports for metal catalysts. However, less work has been done on using N-CNTs as catalyst supports. Synthesis of N-CNTs is briefly discussed. Furthermore, the role of N-CNT supported metal catalysts with reference to previous studies and literature reports is given.

Chapter 3: This chapter describes the **Synthesis of Nitrogen-Doped Carbon Nanotubes Using Two Stage Furnace**. It gives a description of the procedures that were used to prepare and characterise the nitrogen-doped carbon nanotube.

Chapter 4: The use of microwave irradiation to load Ru onto CNTs is given in this chapter. This has been published in a paper titled "**Microwave Irradiation of Ruthenium on Nitrogen-Doped Carbon Nanotubes**" was published in Ceramic Engineering and Science Proceedings, 32 (2011) 33-42.

Chapter 5: This chapter is entitled "**Ru supported on nitrogen-doped carbon nanotubes for the oxygen reduction reaction in alkaline media**". This work was published in Journal of Fuel cells 12: 862-868 (2012).

Chapter 6: The results and discussion of work done on "**Supported ruthenium catalyst for the oxidation of styrene**" is presented in this chapter. The results show the effect of variables such as reaction temperature, reaction time, the loading of Ru on support material and the type of support material used.

Chapter 7: This chapter is an extension of chapter 6. **Studies on styrene oxidation over nitrogen doped carbon nanotube supported ruthenium**. Nitrogen CNTs prepared differently to those in previous chapter are used as Ru support and studies on styrene oxidation reaction were fully investigated.

Chapter 8: The results and discussion of work done on "**selective oxidation of benzyl alcohol to benzaldehyde over carbon nanotubes supported ruthenium**" is presented. The results show the effect of variables such as reaction temperature, reaction time, the loading of Ru on support material and the type of support material used.

Chapter 9: Presents a general summary and conclusion of the work presented in this thesis. The successes and the limitations of work performed in the study and the usefulness of the results found in the study are highlighted in this chapter.

References

1.   S. M. George, Chemical Reviews 95 (1995) 475-476.

2.   J. N. Armor, Catalysis Today 163 (2011) 3-9

3.   B. M. Reddy, K. N. Rao, G. K. Reddy, P. Bharali, Journal of Molecular Catalysis A: Chemical 253 (2006) 44-51.

4.   M.J. Ledoux, C. Pham-Huu, Catalysis Today 102-103 (2005) 2-14.

5.   J. K. Smith, History of Catalysis, in: Encyclopedia of Catalysis, John Wiley & Sons, Inc., 2002

S. M. George, Chemical Reviews 95 (1995) 475-476.

6.   E. Farnetti, R. D. Monte, J. Kaspar, Homogenous and heterogenous catalysis, in: I. Bertin (Ed.) Inorganic and Bio-Inorganic chemistry, *Encyclopedia of Life Support Systems,* vol II, EOLSS, Italy, 2009, pp. 50 - 86.

7.   I. W. C. E. Arends, R. A. Sheldon, Applied Catalysis A: General 212 (2001) 175-187.

8.   D. J. Cole-Hamilton, Science 299 (2003) 1702-1706.

9.   B. Lindström, L. J. Pettersson, CATTECH 7 (2003) 130-138.

10.   A. Robertson, Platinum Metals Review 2 (1975) 64-69.

11.   J. Happel, Catalysis Reviews 6 (1972) 221-260.

12.   J. C. Osuwa, P. C. Anusionwu, Asian Journal of Information Technology 10 (2011) 96-100.

13.   G. M. Whitesides, Small 1 (2005) 172-179.

14.   H. H. Kung, M. C. Kung, Catalysis Today 97 (2004) 219-224.

15.   J. Liu, B. Zhou, S. Hermans, G. A. Somorjai, Advanced Electron Microscopy in Developing Nanostructured Heterogeneous Catalysts Nanotechnology in Catalysis, in: Springer US, 2004,. 361-402.

16.   M. Zach, C. Hagglund, D. Chakarov, B. Kasemo, Current Opinion in Solid State and Materials Science 10 (2006) 132-143.

17.   M. C. Roco, M. C. Hersam, C. A. Mirkin, E. L. Hu, S. M. Davis, R. Davis, E. Scher, Applications: Catalysis by Nanostructured Materials

Nanotechnology Research Directions for Societal Needs in 2020, in: vol 1, Springer Netherlands, 445-466.

18.   G.Y. Gao, D.J. Guo, H.L. Li, Journal of Power Sources 162 (2006) 1094-1098.

19.   P. Francesco, Catalysis Today 41 (1998) 129-137.

20.   S. Martínez-Méndez, Y. Henríquez, O. Domínguez, L. D'Ornelas, H. Krentzien, Journal of Molecular Catalysis A: Chemical 252 (2006) 226-234.

21.   D. K. Chakrabarty, (1990).

22.   S. Mhlanga, Carbon nanotubes with CaCO3 as support for catalysts, in: Chemistry Department, vol PhD, University of the Witwatersrand, Gauteng, 2009.

23.   B. Coq, J. Marc Planeix, V. r. Brotons, Applied Catalysis A: General 173 (1998) 175-183.

24.   L. Guczi, G. Stefler, O. Geszti, Z. Koppány, Z. Kónya, É. Molnár, M. Urbán, I. Kiricsi, Journal of Catalysis 244 (2006) 24-32.

25.   T. W. Ebbesen, H. J. Lezec, H. Hiura, J. W. Bennett, H. F. Ghaemi, T. Thio, Nature 382 (1996) 54-56.

26.   H. Dai, J. H. Hafner, A. G. Rinzler, D. T. Colbert, R. E. Smalley, Nature 384 (1996) 147-150.

27.   Y. Liang, H. Zhang, B. Yi, Z. Zhang, Z. Tan, Carbon 43 (2005) 3144-3152.

28.   A. Esmaeilifar, S. Rowshanzamir, M. H. Eikani, E. Ghazanfari, Energy 35 (2010) 3941-3957.

29.   M. Cano, A. Benito, W. K. Maser, E. P. Urriolabeitia, Carbon 49 (2011) 652-658.

30.   H. Tong, H.L. Li, X.-G. Zhang, Carbon 45 (2007) 2424-2432.

CHAPTER 2

LITERATURE REVIEW:

NITROGEN-DOPED CARBON NANOTUBES AS A CATALYST SUPPORT

2.1 Introduction

In recent years, different forms of carbon have been used to support different kinds of metals. In particular the use of carbon nanotubes (CNTs) has been reported. To achieve good interaction between the CNT and the metal, functionalisation or doping of CNTs has been attempted. The most common dopant used to modify the behaviour of CNTs is nitrogen to give the so called nitrogen-doped carbon nanotubes (N-CNTs). The work reported to date, using N-CNTs as support materials for catalysts, is reviewed below.

A catalyst support is a material on which an active metal nanoparticle is deposited. It can be a granular, fibrous or a monolithic material with high thermal stability. Examples include either naturally occurring materials such as clays and zeolites or synthetic materials like silica, titania, alumina and zirconia [1]. A challenge related to the use of the above supports is that they are not easily removed from the products at the end of the reaction due to their high degree of insolubility. To overcome the above challenge CNTs have been used as supports for various catalytic applications [2,3,4,5,6,7,8,9]. These can in principle be removed by oxidation.

2.2   CNTs

CNTs can be described as a one dimensional form of a fullerene with a well-defined direction along the nanotube axis that is analogous to the in-plane directions of graphite. CNTs can be single-walled CNTs (SWCNTs), double-walled CNTs (DWCNTs) or multi-walled CNTs (MWCNTs). Ideally, SWCNTs are made of a perfect graphene sheet, rolled up into a cylinder and closed by two caps [10,11]. The diameters of SWCNTs are typically in a range of 0.4 - 3 nanometres (nm), while the length can be up to several microns. Typically MWCNTs can be considered as a series of concentric SWCNTs with inner diameter of 1 - 30 nm and with outer diameter of up to 100 nm (Figure 2.1) [11]. Since the report of CNTs by Iijima in 1991, their physical and electronic properties have generated considerable interest. The most noticeable properties are their superior mechanical toughness, good electrical conductivity and high tensile strength which are required for numerous applications [12,13].
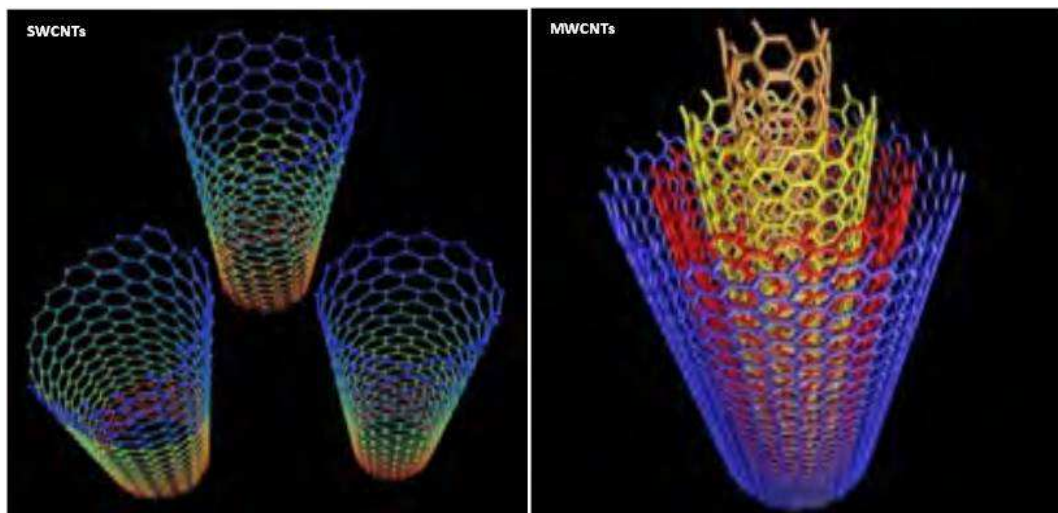
Figure 2.1. Computer generated models of single-walled (SWCNTs) and multi-walled carbon nanotubes (MWCNTs) [14].

One of the first observed major commercial applications of MWCNTs was their use as an electrically conducting material with dramatically increased

14

modulus and strength [15]. Porous CNT arrays have a high electrochemical accessible surface area and combined with their high electronic conductivity and useful mechanical properties, these materials are attractive as electrodes for devices that use electrochemical double layer charge injection [11]. Therefore, they are used for energy storage, *i.e.* for fuel cells that power electric vehicles or laptop computers [16]. They can be applied as field emission electron sources, for flat panel displays, lamps, gas discharge tubes providing surge protection and as X-ray and microwave generators [11].

CNTs are attractive supports in heterogeneous catalytic processes owing to their ability to be easily tailored to meet specific needs. They are employed as supports due to their high surface area, resistance to acidic/basic media, stability at high temperatures and the possibilities of controlling both their porous structure and the chemical nature of their surface [8,17,18]. CNTs have been studied as supports for metal catalysts and they are known to enhance the catalytic performance in such a way that the activity of a catalyst becomes higher than that encountered with traditional catalyst supports in both the gas phase and liquid phase reactions [19,20,21,22]. Nanotubes are special because they have small dimensions, a smooth surface topology and perfect surface specificity.

Nieto-Márquez, et al. [23] revealed that CNTs possess fascinating physical and chemical properties with electronic behaviour varying from metallic to semiconducting depending on their structural composition, chirality and diameter. It is still a challenge to precisely control these parameters in the growth process of the CNTs; it is also not easy to control the properties or the reactivity of the outer wall of the CNTs [24]. The CNT surfaces are usually chemically modified by acid treatment which considerably reduces the chemical and electronic performance of the tubes due to the introduction of a large number of defects. Other surface modification is done by doping CNTs with heteroatoms.

2.3   Nitrogen doped carbon nanotubes (N-CNTs)

The doping of CNTs with heteroatoms offers a practical path to tailor both the physical and chemical properties of the CNTs by creating new states that modify their electronic structure [25,26]. Boron and nitrogen are among the most effective dopants used because of their small atomic size that is similar to that of the carbon atom. They thus have a reasonable probability of entering the nanotube lattice [27,28,29,30,31]. In particular, the substitutional doping of CNTs by nitrogen has received attention because significant changes in hardness, electrical conductivity and chemical reactivity of CNTs have been theoretically predicted and experimentally observed after doping [32]. Additional lone pairs of electrons on N atoms with respect to the delocalised π-system of a graphite-like hexagonal framework enhance the electron properties [33,34,35].
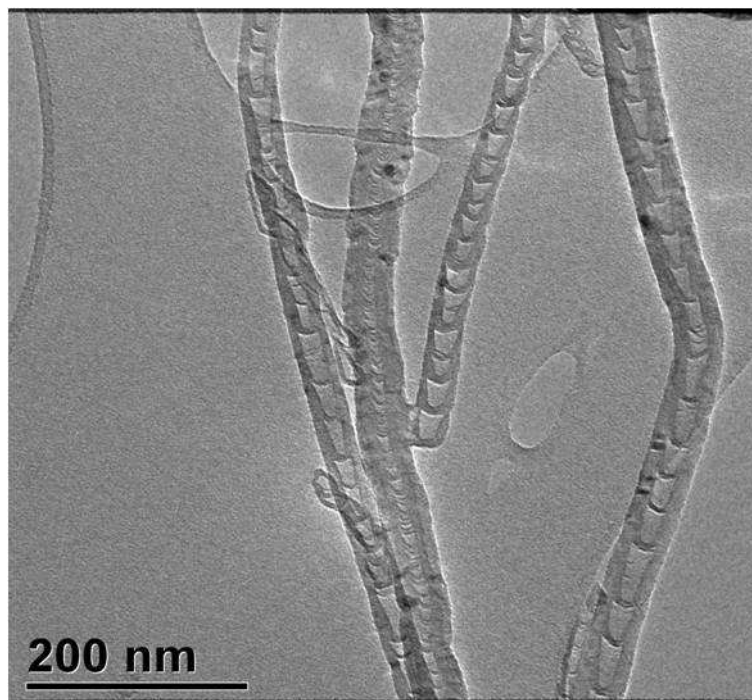
Figure 2.2. Representative TEM micrographs of N-CNTs with a bamboo-like structure along the tube axis

It is observed that doping with nitrogen also has a significant effect on the structure of the carbon material. In most cases, MWCNTs doped with nitrogen usually exhibit a bamboo-like structure with regularly arranged compartments (refer to Figure 2.2). N-CNTs are found to be exclusively metallic conductors or with a narrow energy gap, thus increasing their storage capacity. This offers the possibility of greater electrical conductivity when compared to undoped CNTs [33,36,37,38].

Nitrogen atoms entering the graphene sheets as a substituent for carbon could also modify the adsorption strength of the nanotube towards foreign elements quite significantly. This will in turn, greatly modify the overall catalytic activity as well as selectivity of a catalyst [39]. Generally, nitrogen is incorporated into the CNT lattice during growth. The possible bonding configurations for N in graphitic networks are shown in Figure 2.3. The three most common bonding configurations are: (A) pyridine-like sp2 - hybridized 6-fold ring arrangement, (B) pyrrole-like sp2 - hybridized 5-fold ring arrangement, (C) substitutional sp3 - hybridized 6-fold ring arrangement and (D) oxidised pyridine [40,41].
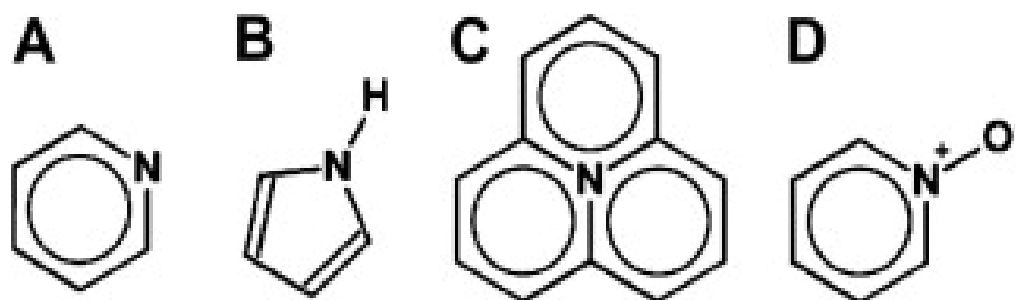
Figure 2.3. Types of nitrogen species found in N-CNTs: (A) pyridinic, (B) pyrrolic, (C) quaternary and (D) oxidized pyridinic [42].

N-CNTs contain promising activated carbons that demonstrate enhanced chemical reactivity for electron transfer processes. Although many studies

have evaluated the structure-composition-property relationships of these N-doped carbons, the influence of nitrogen doping has not been fully established [36].

2.4   N-CNTs synthesis

Several techniques have been developed to produce nanotubes in sizeable quantities. Currently there are three major techniques to produce high quality CNTs viz. arc-discharge, laser ablation and chemical vapour deposition [42,43]. This same method can be used to make N-CNTs. In the first two processes, energy from either the arc or the laser is used to preferentially evaporate the carbon (graphite) material in the presence of an inert gas and metal catalysts like iron or cobalt. The temperatures involved in these methods are close to the melting temperature of graphite, 3000 - 4000 °C [45]. The disadvantages of arc discharge and laser ablation processes are:

I.   These processes are not very well controlled, nor are they continuous processes;

II.   The removal of impurities using simple, cheap purification methods is difficult;

III. It is not easy to grow well aligned nanotubes as they require the use of sophisticated instrumentation [44].

The chemical vapour deposition (CVD) method, however, has certain advantages such as a high yield and controllable growth conditions. Scalability is not a problem in the CVD process. A drawback of the CVD process in the production of poor quality CNTs that contain defects, particularly because the structures are created at much lower temperatures of between 600 - 1000 °C as compared to arc and laser techniques, where the environment of the plasmas are larger than 2000

°C. It is most likely that in laser and arc technique defects can be annealed by high temperature during a growth proces [45,46].

2.4.1 Arc Discharge

In this method nanotubes are synthesised through arc vaporisation of two carbon rods placed end to end; which are separated by approximately 1 mm in an enclosure that is usually filled with inert gas such as helium or argon at low pressure of between 50 - 700 mbar. A direct current of 50 - 100 A, driven by approximately 20 volt direct current (VDC), creates a high temperature discharge between the two electrodes. The discharge vaporises the anode carbon rod and forms a cigar-like deposit on the cathode. The outer part of the deposit is grey and hard and is usually discarded. The inner core is black and soft and contains nanomaterial [47]. During vaporisation there soot is formed on the sides of the arc chamber, which also contains a lesser amount of nanomaterial. Stéphan et al. [48] initiated the synthesis of doped MWCNTs; they produced boron-nitrogen doped MWCNTs using the arc-discharge method.

2.4.2 Laser ablation

Laser ablation uses intense laser pulses to vaporise carbon graphite containing a small atomic percent of metal catalyst. The target is placed in an oven heated to 1200 °C. A laser beam is focussed onto the target and a flow of inert gas typically helium or argon, is passed through the growth chamber to carry the nanotubes downstream to be collected on a cold finger. The synthesis of B-C-N nanotubes by a laser ablation in which a pressed pellet of carbon, BN and metal mixture are ablated by a high-power pulsed laser in flowing nitrogen gas was reported by Zhang et. al,. [49].

Laser ablation operates similar to arc-discharge, the optimum background gas and catalytic mix is the same as in the arc-discharge process. They

both use the condensation of carbon atoms produced from the vaporization of graphite targets [47].

2.4.3   Chemical vapour deposition (CVD)

CVD synthesis is achieved by decomposing a carbon source and using an energy source, such as a plasma or a resistively heated coil, to impart energy to the gaseous carbon molecules. This process occurs in a typed temperature range of 650 - 900 °C. Commonly used carbon sources include methane, carbon monoxide, acetylene, etc. The energy source is used to dissociate the molecule into reactive (radical) species. These reactive species then diffuse to the substrate, which is heated and coated with a catalyst (usually a first row transition metal such as Ni, Fe or Co), where CNTs grow on the catalyst. The CVD method enables the selective production of MWCNTs or SWCNTs, depending on the reaction chemistry and process parameters, such as temperature.

2.5   Review of the literature of N-CNTs synthesis

In this section we review the synthesis of N-CNTs as described in the literature. The doping of a carbon nanostructure with nitrogen can be divided into two types:

I.   Doping directly during the synthesis of carbon nanostructure materials, which can be called an "in situ" doping process and

II.   Post-treatment of pre-synthesised CNTs with nitrogen-containing precursors such as N_2, and NH_3, i.e. a post doping process.

The 'in situ' doping method is the most commonly used method used to make N-CNTs [50]. Incorporation of foreign atoms into CNTs was first performed by Stephen and co-workers [51] who doped CNTs with boron and nitrogen using the arc discharge technique. The arc discharge,

chemical vapour deposition (CVD) and laser ablation methods have all been employed in the synthesis of CNT structured material and these methods are also suitable for the synthesis of N-CNTs. These techniques produce the N-CNTs with regular internal bamboo cavities (refer to Fig. 2.2.) whose growth mechanism is not fully understood. A recently proposed growth model is depicted in Figure 2.4. During synthesis, carbon and nitrogen species are generated and deposited on the metal catalyst particle and react exothermically with the metal. Diffusion of N-C species through the metal catalyst particle is accountable for N-CNT growth in the same way that carbon diffusion leads to CNTs. The encapsulation of N in the N-CNTs is caused by the decomposition of unstable reactive intermediates. The compartments are caused by the different precipitation rates of different N and C species. When precipitation is slow, and there is a lack of material to maintain inner CNT growth, layers will suddenly close [41].
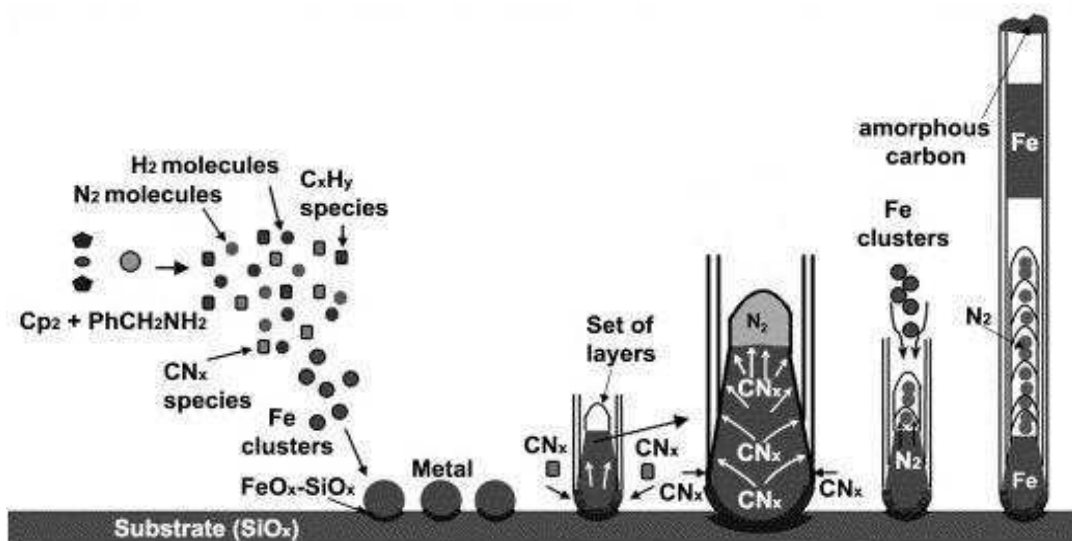
Figure 2.4. Proposed growth mechanism for N-CNTs [47].

When NH_3 is used as a N-source, it requires the co-addition of a carbon precursor. This process has been found difficult to control [52]. To

overcome this difficulty of using ammonia, precursors containing both carbon and nitrogen have been adopted. Ghosh et al., [27] obtained highly aligned bamboo-shaped CNTs by the catalytic pyrolysis of ethanolamine/ferrocene mixtures over the temperature range 700 – 900 °C by a CVD method. During the deposition ethanolamine decomposed to form ammonia, which is very effective for the growth of N-CNTs. MWCNTs containing nitrogen have also been grown by aerosol CVD of a ferrocene/benzylamine solution [27]. Scanning tunneling microscopy (STM) measurements showed that the local density of states of nanotubes in these materials is asymmetrical, with a higher density of states above the Fermi level. Approximately 9.7 wt. % nitrogen was determined by Energy dispersive spectroscopy [53]. Nxumalo et al. [54] studied the effect of varying the N-source concentration on the production of N-CNTs by a floating catalyst CVD method using a ferrocene/aniline/toluene solution. A ferrocene/aniline catalyst of 15 wt. % produced pure N-CNTs with a small amount of by-products. It was also revealed that the diameters of the tubes can be controlled by varying the N-source concentration. Well-aligned as-grown N-CNTs bundles having lengths of about 430 μm were reported. In another study spray pyrolysis of ferrocene/acetonitrile solutions was used [55]. X-ray-photo electron spectroscopy studies revealed that the wt. % of N content was indirectly proportional to the growth temperature and TEM showed that the bamboo compartment distance increase with an increased in growth temperature [55].

Albeit several articles have been published regarding the synthesis of N-CNTs it is very difficult to compare the results obtained from different reports since different experimental condition have been reported by the various authors.

2.6   Metal/CNT catalyst preparation

The primary aim in the preparation of a supported catalyst is to have a high surface area of a reduced metal deposited on a high surface area material (Figure 2.5). In order to use the N-CNTs effectively as a support for catalyst, metal nanoparticles must be well dispersed on the support surface. Supported metal catalysts are typically prepared by reducing a metal salt and binding it onto a support material [1,56]. The dispersion of a metal on a support is still largely based on conventional catalyst preparation techniques, such as precipitation and impregnation methods followed by chemical reduction, CVD deposition and ion exchange. Egg shell catalyst, plasma and sol gel methods are other methods that are less commonly used to prepare supported catalysts [6,57]. These techniques can play a role in metal finishing operations. However, many have high unit-deposition costs. Other disadvantages of most reported methods are the required pre-treatment of the support. Carbonaceous are often treated support, with strong acids, ionic liquids surfactants, specific solvents, or reagents prior to metal salt addition [58]. In addition, certain requirements are not always fulfilled when these methods are used. Below are some of the challenges experienced during catalyst preparation:

- Particle mean size is not well controlled.

- Wide particle size distribution of metals on CNTs.

- Particles are agglomerated and not uniformly dispersed [59].

- Cost issues associated with up-scaling.
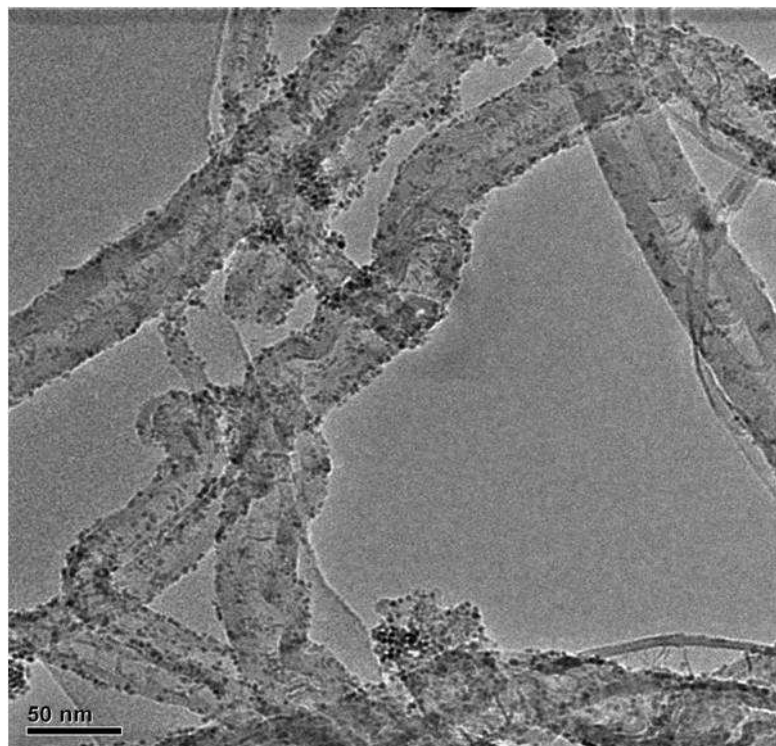
Figure 2.5. HRTEM image of metal/MWCNT composites

The nitrogen atom has an extra electron compared to carbon, and from an electronic point of view, therefore the surface of CNTs is expected to be more electronegative [60]. This results in N-CNTs possessing high surface nucleation sites, which allow the anchorage and high dispersion of the metal active phase on the support surface.

In order to gain more insight into the exact localization of the metal particles with respect to the N-CNT, Chizari et al. [38] used TEM tomography to study a Pd/N-CNT catalyst (Figure 2.6). According to the results, the palladium particles were exclusively restricted on the outer surface of the N-CNT, which provided a highly effective metal surface contact for the reactants.
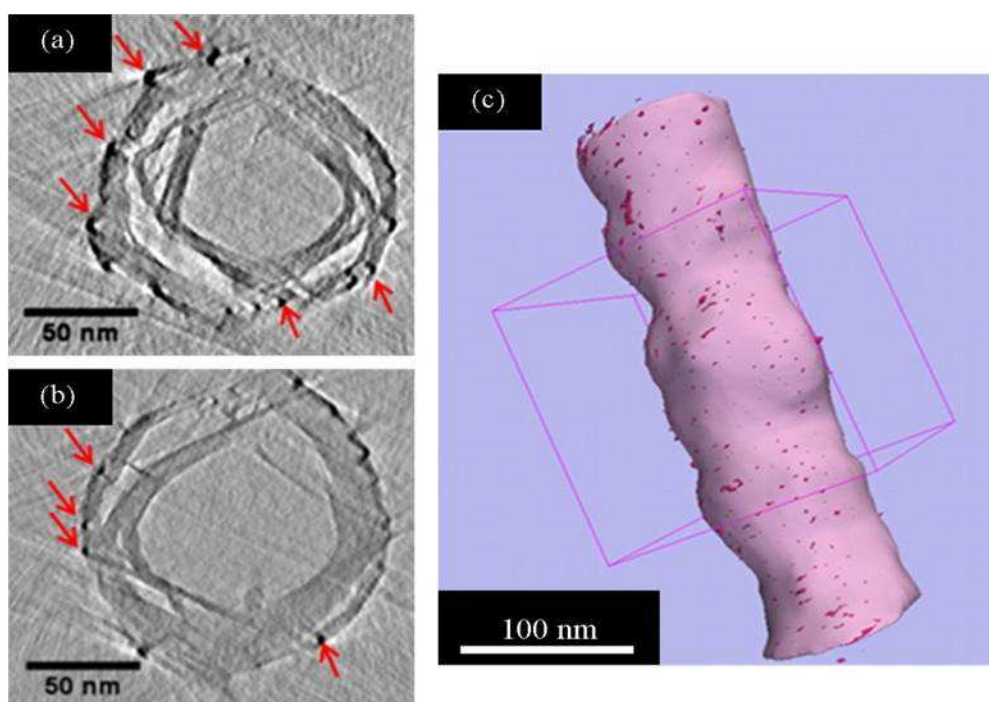
Figure 2.6. TEM tomography (a) and (b) arrow showing the metal particles (c) 3D image showing the localization of the Pd particles on the outer surface of the N-CNT support [38].

Molecular dynamics simulations were used to investigate the effect of ruthenium on the stability of N doped MWCNTs. Figure 2.7a depicts a model of nitrogen that has been doped (substitutionally) onto a CNT network. The system has been hydrogen-terminated to account for dangling bonds. Ruthenium was placed 2.048 Å (stable configuration) above the CNT surface and after simulations ruthenium was seen to be repelled from the surface to a distance of 4,044 and 3.147 Å for pristine CNTs (Figure 2.7b) and N-CNTs (Figure 2.7c) respectively. The configuration shown in Figure 2.7c was comparably found to be the most stable structure. The results show that the nitrogen atoms act as donor-like atoms and not directly as binding sites for the deposited metal active phase.
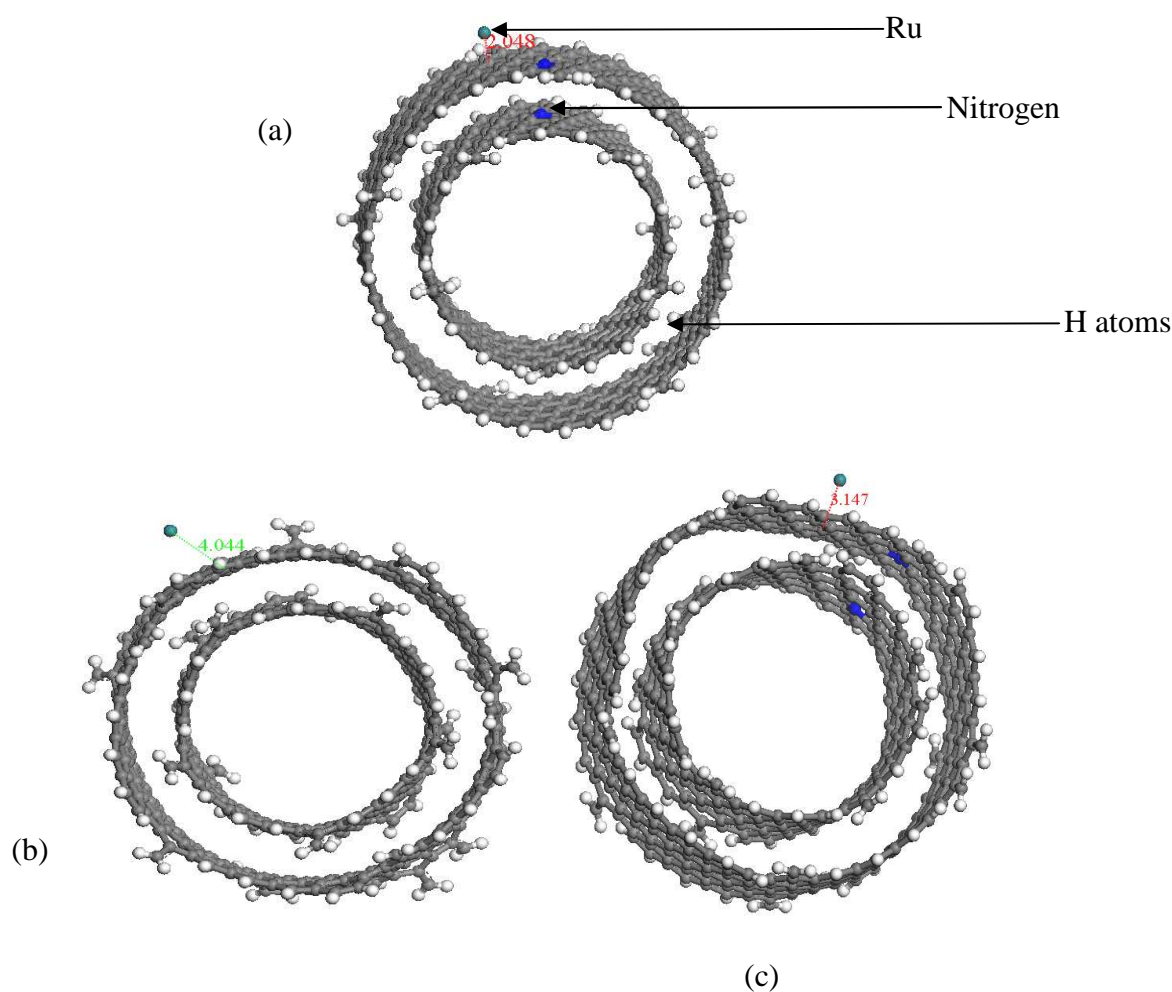
Figure 2.7. Molecular Dynamics simulation studies of the physisorption of ruthenium (a) stable configuration before simulation (b) pristine CNT (c) N-CNT support.

2.7 Catalyst preparation methodologies

2.7.1 Impregnation method

Impregnation is the most simple, least expensive and most prevalent method to prepare a supported metal catalyst. In this method a high surface area support is contacted with a liquid solution containing dissolved metal ions. After slurries of the support and metal precursors are dried they are heated in various oxidising and reducing environments in

order to remove the ligands and to reduce the metal to its active elemental state [61,62,63]. The advantage of this method in the preparation of the supported noble metal catalysts is the deposition of small amounts of metals on the surface of support in a finely dispersed form.

The impregnation process may involve an incipient wetness or a dry method. The incipient wetness method is an impregnation method in which a support is contacted with a volume of precursor solution slightly in excess of the total pore volume of the support; after addition, the slightly wet powder is allowed to dry [63,64,65]. In the dry impregnation method a thick paste formed from contacting the support with just the right amount of liquid needed to fill the pore volume is used. The solution contains a precise metal loading and the product does not need to be filtered. Drawbacks of impregnation methods arise when metal precursors do not interact strongly with a support surface. Metal complexes that remain in the solution can migrate significantly during drying [57].

2.7.2 Precipitation methods

The precipitation method is the preferred method for preparing a supported catalyst with a metal loading higher than 10 - 15 %. It can be either achieved by co-precipitation or deposition-precipitation. Co-precipitation is a process whereby solutions containing the metal salt and a salt of a compound that will be converted into the support are contacted while stirring with a base in order to precipitate the metal ions as hydroxide or carbonate. In principle deposition-precipitation is similar to co-precipitation but with an aim of allowing the precipitation material to form inside the support pores [66].

2.7.3 Microwave assisted method

Unlike the impregnation method whereby chemical reduction is used, the microwave assisted method uses microwave irradiation for metal

reduction. It is a more novel technique which gives a good control of particle size and morphology, which are the factors that influence the catalytic activity [6]. The microwave assisted method can allow synthesis to be achieved using shorter reaction times, reduced energy consumption and better yields that can be achieved by impregnation methods [67].

Classical synthesis processes can be time consuming since they include multiple steps such as long ageing, drying and calcination of the samples.

2.8   Application of metal/N-CNTs in catalysis

A number of applications for the use of N-CNTs as a support in fuel cells have been reported (Table 2.1). Currently, the degradation of an electro-catalyst and their supports is recognized as one of the main contributors to the long-term degradation of fuel cells [68]. Another major limitation to the commercialization of fuel cells is the high cost of their components. A study of catalysts for the oxygen reduction reaction (ORR) using nitrogen-containing carbon has propelled the use of N-CNT supported catalysts in fuel cells research.

N-CNTs have been shown to be a highly active catalyst for the ORR in a proton exchange membrane (PEM) fuel cell environment. The conductivity of N-CNTs material were slightly less than, but still comparable to, materials used in fuel-cells [69].In addition, Chen et al., [80] evaluated the electrochemical activity of N-CNTs prepared with different catalysts using a rotating ring disc electrode (RRDE) voltammeter. The results showed that the nitrogen content of N-CNTs is crucial for ORR. A high degree of N-CNT surface defects was observed, and these enhanced ORR activity by exposing more edge plane nitrogen groups such as pyridinic and pyrollic nitrogen, which could take part in the ORR though the lone pair electrons on the nitrogen.

Table 2.1. Applications of N-CNTs

Metal	N %	Loading %	Reaction application	Ref
Pd	1 - 5.5		Cinnamaldehyde hydrogenation	[38]
Pd	4	10	Cinnamaldehyde hydrogenation	[39]
Pt	1.5 - 8.4	30	PEM fuel cells	[68]
Ru	0.1 - 1.9	0.8	Ammonia Decomposition	[70]
Ru	4	2	Ammonia Decomposition	[71]
Pt-Ru	unknown	40	Methanol oxidation	[72]
Pt-Ru	4	9	Methanol oxidation	[73]
Pt	0 - 16.7		Methanol oxidation	[74]
Pt	unknown		Methanol oxidation	[75]
Pt	unknown	23	Ethanol oxidation	[76]
Pt	unknown	11	PEM fuel cells	[77]
Pt	3.5		Electrochemical performance	[78]
a	8.4	-	ORR	[79]
a	2.5 - 3.8	-	ORR	[7]
a	2.7 - 2.9	-	ORR	[80]
a	2.9 - 6.0	-	ORR	[81]
a	4 - 6	-	ORR	[82]
a	1.4 - 7.7	-	ORR	[83]

a- no metal used

In another study, the N-CNTs were used as a cathode material for the ORR in alkaline medium [81]. Furthermore, the material proved to be more active as compared to a commercially available Pt/C catalyst. The improved electrocatalytic activity showed two important features; a significant shift of the oxygen reduction and an increase in the oxygen reduction current, which likely related to a higher average number of electrons transferred per oxygen molecule [81].

Lin [78] also investigated the effects of nitrogen incorporation in CNT structures on their electrochemical (EC) properties. Studies were carried out by correlating the nitrogen content of CNTs with EC performance. The results showed that nitrogen incorporation provided a simple pathway to modifying the electronic bonding structure. N-CNTs with an optimal 3.5 % N promoted a substitutional graphite-like defect structure, which is favourable for fast ET in electrochemistry. Albeit there is a lack of a proposed mechanism for the ORR that includes a non-metallic active site, several studies have suggested how nitrogen improves the ability of carbon to reduce oxygen due to the ability of nitrogen to donate electrons to O_2 [34].
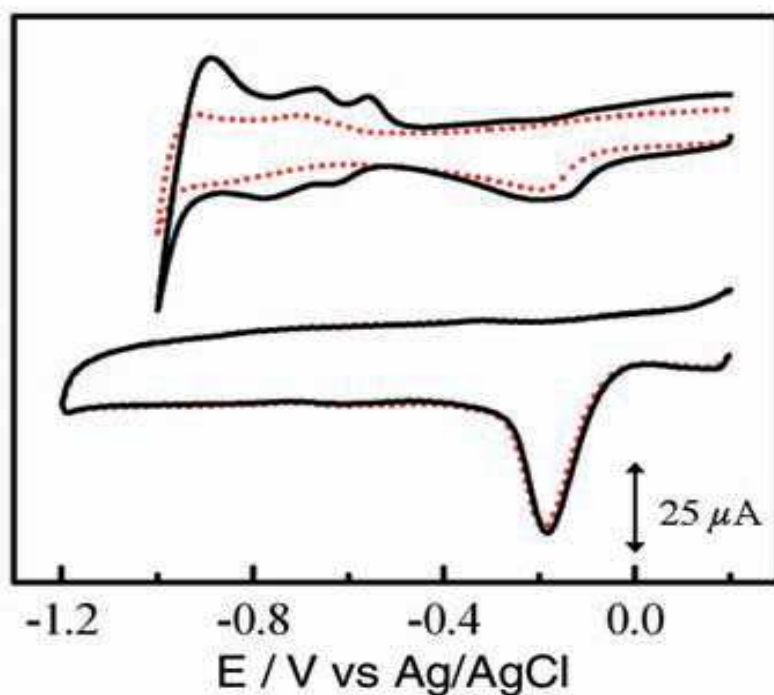
Figure 2.8. CVs for the ORR at the Pt-C/GC (top) and N-CNT/GC (bottom) electrodes before (solid black curves) and after (dotted curves) a continuous potentiodynamic swept for ~100,000 cycles in an air saturated 0.1 M KOH solution at room temperature [82].

N-CNTs also appear to give a better electrode than Pt-C/glassy carbon (GC) since there was a substantial enhanced steady state diffusion current

(~ 0.8 mA) for N-CNTs/GC with respect to Pt-C/GC electrodes (Figure 2.8). Furthermore, N-CNT electrodes show stronger diffusion-limited currents and lower over potentials when compared to their nitrogen-free counterparts [82]. Studies have indicated the importance of the nitrogen heteroatom in N-CNTs on their electrocatalytic activities for the ORR/fuel cells [80]. Given that nitrogen has an effect on the surface chemical activity and creates surface properties such as polarity, basicity and heterogeneity, N-CNTs as a catalyst support should increase the durability of the resultant catalyst [73].

Chen et al. [68] have shown that N-CNTs as support have advantages over pristine CNTs when Pt catalysts are used. In the study, the electrochemical surface area (ESA) was used to characterise the proton exchange membrane fuel cell (PEMFC) catalyst. The degradation of the ESA is plotted in Figure 2.9.
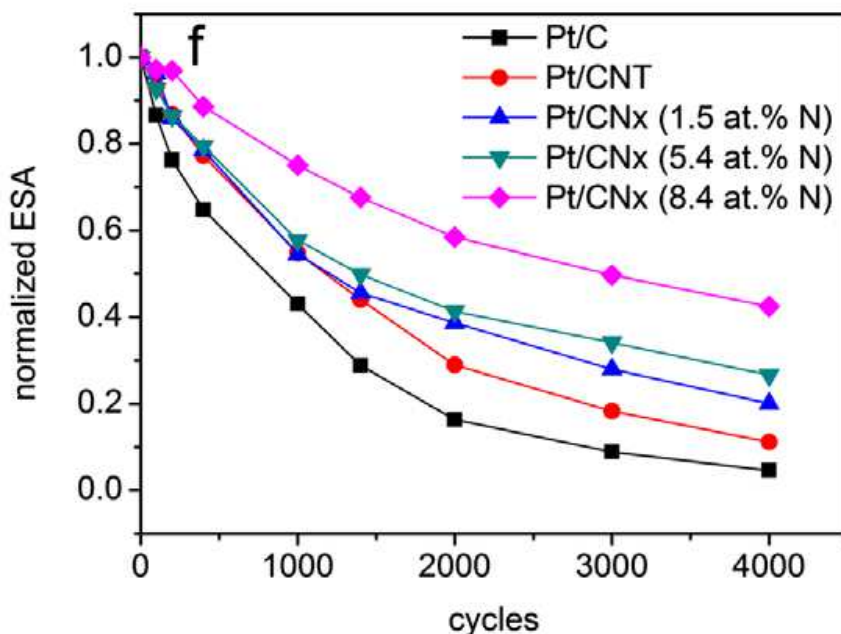
Figure 2.9. Cyclic voltammograms comparing the degradation of the five catalysts. Scan rate: 50 mV/s [68]. CN_x refers to N-CNTs

The durability of Pt/C was found to be much lower than that of Pt/CNTs. After 4000 cycles, only 4.6 % of the initial ESA of Pt/C remained while 11.2 % of the initial ESA for Pt/CNTs was removed. It is also clear that Pt/N-CNTs have a higher stability than Pt/CNTs. Not only did the ESA increase, but accelerated durability tests and TEM results indicated that the stability of the Pt catalyst was increased by doping with N. Similar studies were done by Saha and co-workers [77]. They revealed that the Pt/N-CNTs electrodes exhibited a greater electrochemical surface than the Pt/CNT electrodes as well as a higher single-cell performance in a H_2O_2 fuel cell.

In another study, Pt catalysts were loaded on three different supports, viz. graphite, CNTs and N-CNTs. In order to see the effect that incorporated nitrogen would have, the catalytic activity was evaluated by increasing the amount of nitrogen in the CNTs from 0 - 16.7 %. The catalytic activity of methanol oxidation increased with the increase of the nitrogen content up to 10.5 %. As shown in Table 2.2 the activity of an electrode with 10.5 % nitrogen was higher than that obtained from other N-CNTs, CNT and commercial Pt/C electrodes.

Table 2.2. Electro-catalytic activity of methanol oxidation on various electrodes [74].

Electro-catalyst	N content (%)	Activity Ip(mA/cm^2)
Pt	–	0.076
GC/E-TEK 20% Pt/C-Nafion	–	1.3
GC/CNT–Pt–Nafion	0.0	12.4
GC/N-CNT[1]–Pt–Nafion	6.63	16.2
GC/N-CNT[2]–Pt–Nafion	10.5	21.4
GC/N-CNT[3]–Pt–Nafion	16.7	18.6

The increasing order of stability of various electrodes is: Pt < Pt/Vulcan (E-TEK) < Pt/CNT< Pt/N-CNT[1] < Pt/N-CNT[2] < Pt/N-CNT[3]. It was also found that the metal particle distribution on the N-CNT support and the metal-support interactions was an important parameter contributing to the activity of the catalyst. Thus, the higher activity of the Pt/N-CNT[3] electrode with 10.5 % nitrogen content may be attributed to the small particle size, the higher dispersion of platinum and the nature of the CNT supports [74].

Another advantage of N-CNTs as a support for fuel cell application was illustrated by study of PtRu nanoparticles dispersed on N-CNTs [73]. The obtained catalyst was used to investigate the catalytic activity and the data compared to data for oxidised CNT supports and a commercial catalyst. The cyclic voltammograms (Figure 2.10) were recorded for the oxidation of methanol (1 $mol.dm^{-3}$) at a scan rate of 50 $mV.s^{-1}$ for PtRu/N-CNT, PtRu/O-CNT, PtRu/C E-TEK and PtRu/Vulcan catalysts. An improvement in the activity was observed for the PtRu catalyst supported on N-CNTs confirmed by the lower onset potential and significantly higher oxidation current (curve (i)) in the forward sweep. The oxidation peak observed in the reverse scan at around 0.4 V is associated with the oxidation of adsorbed intermediate species in the forward scan. The onset potential for PtRu/N-CNT was 0.21 V, while that for PtRu/O-CNT was 0.33 V. In principle, with respect to the methanol electrooxidation mechanism, the onset potential is related to the breaking of C-H bonds and the subsequent removal of the CO_{ads} like intermediates by oxidation with OH_{ads} species supplied by Ru-OH sites. In the CO stripping study, PtRu supported on N-CNTs showed the lowest onset potential confirming the easier oxidation and removal of the CO_{ads} intermediates, which is reflected here by the significantly higher methanol oxidation current.
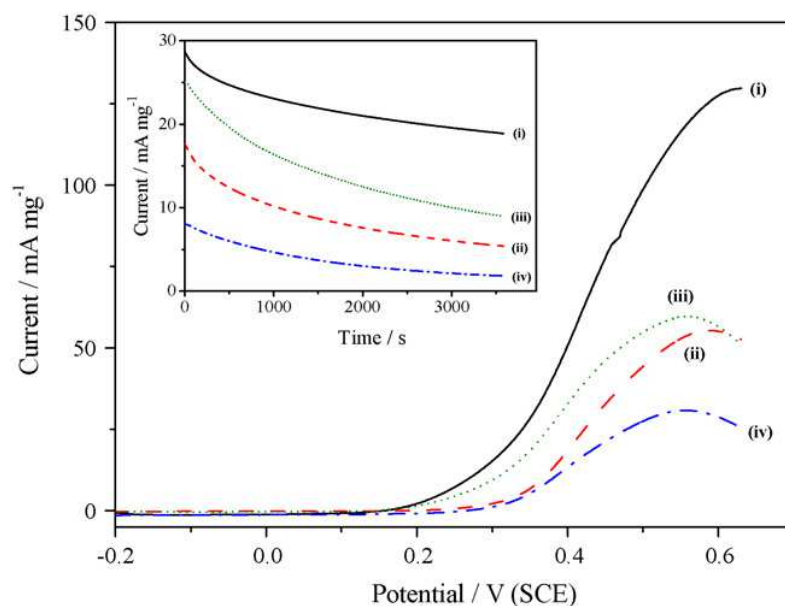
Figure 2.10. LSV at 1 mV s−1 scan rate for the oxidation of 1 mol dm^{-3} methanol in 0.5 mol dm^{-3} H$_2$SO$_4$ at room temp. Inset showing the chronoamperometric response recorded at 400 mV. (i) PtRu/N-CNT, (ii) PtRu/O-CNT, (iii) E-TEK PtRu/C and (iv) PtRu/Vulcan catalysts [73].

2.9   Other catalytic applications of N-CNTs

This high surface reactivity of N-CNTs is not only exploited in electrocatalytic reactions but can be used in other reactions e.g. Ru catalysts have been tested in catalytic ammonia decomposition reaction. The N-CNTs and conventional CNTs prepared under the same conditions were used as a support for Ru. The activity of Ru improved significantly when supported on N-CNTs; the differences in the activity could not be accredited to the Ru particle size effect since the sizes were similar in both cases [71].

Chen et al. [70] and Garcia-Garcia [71] also demonstrated that the decomposition reaction of ammonia was enhanced by the presence of a Ru catalyst on the N-CNTs. It was concluded that the catalytic activity of the Ru-based catalyst depends on the electron transfer ability and the dispersion of Ru nanoparticles. Recently, N-CNTs were used as a catalyst

support for palladium in the liquid-phase hydrogenation of cinnamaldehyde [38]. The palladium active phase supported on the N-CNTs showed C=C bond hydrogenation activity and selectivity higher than that found for the undoped CNTs. The specific areas of the two supports were similar (183 and 176 m^2/g, respectively). This is in agreement with the findings of Chen et al. [70] that the activity depends on the dispersion of the metal catalyst. The high dispersion of metal on the N-CNTs is attributed to the electronic interactions with the sp^2 hybridized nitrogen, with an unbonded electron pair being able to complex the empty orbital of the metal ion as a ligand [38].

2.10   Conclusion

This chapter summarised the current literature on the use of N-CNTs as a catalysts support. Currently most applications related to the use of N-CNTs as a catalyst support relate to fuel cell applications. N-CNTs are still in their early stages of development but they have been showed to be exceptional nanomaterials due to their properties. In order for the N-CNTs to demonstrate their ability to act as nanoparticles for supports, appropriate metal addition methods for nanoparticles to CNTs must be exploited.

References

1. D. K. Chakrabarty, Adsorption and Catalysis by Solids, Wiley Eastern Limited, 1990

2. L. Guczi, G. Stefler, O. Geszti, Z. Koppány, Z. Kónya, É. Molnár, M. Urbán, I. Kiricsi, Journal of Catalysis 244 (2006) 24-32.

3. B. M. Reddy, K. N. Rao, G. K. Reddy, P. Bharali, Journal of Molecular Catalysis A: Chemical 253 (2006) 44-51.

4. E. Antolini, Applied Catalysis B: Environmental 88 (2009) 1-24.

5. C.C. Chen, C.F. Chen, C.M. Chen, F.T. Chuang, Electrochemistry Communications 9 (2007) 159-163.

6. W.X. Chen, J. Y. Lee, Z. Liu, Materials Letters 58 (2004) 3166-3169.

7. Z. Chen, D. Higgins, Z. Chen, Carbon 48 (2010) 3057-3065.

8. G.Y. Gao, D.J. Guo, H.L. Li, Journal of Power Sources 162 (2006) 1094-1098.

9. J. Garcia, H. T. Gomes, P. Serp, P. Kalck, J. L. Figueiredo, J. L. Faria, Carbon 44 (2006) 2384-2391.

10. J. Li, Y. Zhang, Physica E: Low-dimensional Systems and Nanostructures 28 (2005) 309-312.

11. Y.-Y. Fan, A. Kaufmann, A. Mukasyan, A. Varma, Carbon 44 (2006) 2160-2170.

12. L. A. Montoro, J. M. Rosolen, Carbon 44 (2006) 3293-3301.

13. E. T. Thostenson, Z. Ren, T.-W. Chou, Composites Science and Technology 61 (2001) 1899-1912.

14. P. F. Harris, Carbon Nanotubes and Related Structures: New Materials for the Twenty-first Century, Cambridge University Press, Cambridge, 1999.

15. M.S. Dresselhaus, G. Dresselhaus, P. C. Eklund, Science of Fullerenes and Carbon Nanotubes, New York, NY,, 1996.

16. M.-F. Yu, O. Lourie, M. J. Dyer, K. Moloni, T. F. Kelly, R. S. Ruoff, Science 287 (2000) 637-640.

17.   H. Dai, J. H. Hafner, A. G. Rinzler, D. T. Colbert, R. E. Smalley, Nature 384 (1996) 147-150.

18.   T. W. Ebbesen, H. J. Lezec, H. Hiura, J. W. Bennett, H. F. Ghaemi, T. Thio, Nature 382 (1996) 54-56.

19.   M. C. Bahome, L. L. Jewell, K. Padayachy, D. Hildebrandt, D. Glasser, A. K. Datye, N. J. Coville, Applied Catalysis A: General 328 (2007) 243-251.

20.   G. Wu, B.-Q. Xu, Journal of Power Sources 174 (2007) 148-158.

21.   Y. Liang, H. Zhang, B. Yi, Z. Zhang, Z. Tan, Carbon 43 (2005) 3144-3152.

22.   P. Collins, P. Avouris, Scientific American 283 (2000) 62-69.

23.   A. Nieto-Márquez, J. C. Lazo, A. Romero, J. L. Valverde, Chemical Engineering Journal 144 (2008) 518-530.

24.   X. Y. Tao, X. B. Zhang, F. Y. Sun, J. P. Cheng, F. Liu, Z. Q. Luo, Diamond and Related Materials 16 (2007) 425-430.

25.   E. Cruz-Silva, D. A. Cullen, L. Gu, J. M. Romo-Herrera, E. MuÃoz-Sandoval, F. LÃpez-UrÃas, B. G. Sumpter, V. Meunier, J.-C. Charlier, D. J. Smith, H. Terrones, M. Terrones, ACS Nano 2 (2008) 441-448.

26.   M. S. Saha, A. Kundu, Journal of Power Sources 195 (2010) 6255-6261.

27.   P. Ghosh, T. Soga, K. Ghosh, R. A. Afre, T. Jimbo, Y. Ando, Journal of Non-Crystalline Solids 354 (2008) 4101-4106.

28.   A. A. Koós, M. Dowling, K. Jurkschat, A. Crossley, N. Grobert, Carbon 47 (2009) 30-37.

29.   S. Iijima, Nature 354 (1991) 56-58.

30.   B. G. Sumpter, V. Meunier, J. M. Romo-Herrera, E. Cruz-Silva, D. A. Cullen, H. Terrones, D. J. Smith, M. Terrones, ACS Nano 1 (2007) 369-375.

31.   F. Villalpando-Paez, A. Zamudio, A. L. Elias, H. Son, E. B. Barros, S. G. Chou, Y. A. Kim, H. Muramatsu, T. Hayashi, J. Kong, H. Terrones,

G. Dresselhaus, M. Endo, M. Terrones, M. S. Dresselhaus, Chemical Physics Letters 424 (2006) 345-352.

32.   S. Maldonado, S. Morin, K. J. Stevenson, Carbon 44 (2006) 1429-1437.

33.   K. Ghosh, M. Kumar, T. Maruyama, Y. Ando, Carbon 48 (2010) 191-200.

34.   P. H. Matter, E. Wang, U. S. Ozkan, Journal of Catalysis 243 (2006) 395-403.

35.   P. M. Ajayan, Chemical Reviews 99 (1999) 1787-1800.

36.   R. H. Baughman, A. A. Zakhidov, W. A. de Heer, Science 297 (2002) 787-792.

37.   M. M. J. Treacy, T. W. Ebbesen, J. M. Gibson, Nature 381 (1996) 678-680.

38.   K. Chizari, I. Janowska, M. Houllé, I. Florea, O. Ersen, T. Romero, P. Bernhardt, M. J. Ledoux, C. Pham-Huu, Applied Catalysis A: General 380 (2010) 72-80.

39.   J. Amadou, K. Chizari, M. Houllé, I. Janowska, O. Ersen, D. Bégin, C. Pham-Huu, Catalysis Today 138 (2008) 62-68.

40.   S. Van Dommele, A. Romero-Izquirdo, R. Brydson, K. P. de Jong, J. H. Bitter, Carbon 46 (2008) 138-148.

41.   H. J. Burch, Bioapplications of Nitrogen-doped Carbon Nanotubes, in: Department of Physics, vol PhD, University of Oxford, 2006.

42.   B. Zheng, Y. Li, Liu, J., Applied Physics A 74 (2002) 345-348.

43.   T. Suzuki, K. Suhama, X. Zhao, S. Inoue, N. Nishikawa, Y. Ando, Diamond and Related Materials 16 (2007) 1116-1120.

44   A. Merkoaci, M. Pumera, X. Llopis, B. Perez, M. del Valle, S. Alegret, TrAC Trends in Analytical Chemistry 24 (2005) 826-838.

45.   Dresselhaus M. S., Dresselhaus G, P. Avouris, Carbon nanotubes: synthesis, structure, properties, and applications Springer, 2001.

46.   H. Li, N. Zhao, C. He, C. Shi, X. Du, J. Li, Q. Cui, Materials Science and Engineering: A 476 (2008) 230-233.

47.   G. Nicole, Materials Today 10 (2007) 28-35.

48   O. Stephan, P. M. Ajayan, C. Colliex, P. Redlich, J. M. Lambert, P. Bernier, P. Lefin, Science 266 (1994) 1683-1685.

49   Y. Zhang, H. Gu, K. Suenaga, S. Iijima, Chemical Physics Letters 279 (1997) 264-269.

50.   Y. Shao, J. Sui, G. Yin, Y. Gao, Applied Catalysis B: Environmental 79 (2008) 89-99.

51.   O. Stephan, P. M. Ajayan, C. Colliex, P. Redlich, J. M. Lambert, P. Bernier, P. Lefin, Science 266 (1994) 1683-1685.

52.   P. Ghosh, M. Tanemura, T. Soga, M. Zamri, T. Jimbo, Solid State Communications 147 (2008) 15-19.

53.   Z. K. Osváth, A.A.; Grobert, N.; Vértesy, Z.; Horváth, Z.E.; Biró, L.P., Journal of Nanoscience and Nanotechnology 9 (2009) 6139-6143.

54.   E. N. Nxumalo, P. J. Letsoalo, L. M. Cele, N. J. Coville, Journal of Organometallic Chemistry 695 (2010) 2596-2602.

55.   R. Yadav, P. Dobal, T. Shripathi, R. Katiyar, O. Srivastava, Nanoscale Research Letters 4 (2009) 197-203.

56.   K. J. Puttlitz, K. A. Stalter, Handbook of lead-free solder technology for microelectronic assemblies, Marcel Dekker, 2004.

57.   P. Serp, M. Corrias, P. Kalck, Applied Catalysis A: General 253 (2003) 337-358.

58.   M. Cano, A. Benito, W. K. Maser, E. P. Urriolabeitia, Carbon 49 (2011) 652-658

59.   Y. L. a. J. L. B. Zheng Applied Physics A 74 (2002) 345-348.

60.   P. Ayala, R. Arenal, M. Rümmeli, A. Rubio, T. Pichler, Carbon 48 (2009) 575-586.

61.   R. Richards, Surface and nanomolecular catalysis, CRC/Taylor & Francis, 2006.

62.   J. R. Regalbuto, Catalyst preparation: science and engineering, CRC Press/Taylor & Francis, 2007.

63.   B. C. Gates, Chemical Reviews 95 (1995) 511-522.

64. J. L. G. Fierro, Metal oxides: chemistry and applications, Taylor & Francis, 2006.

65. R. D. Gonzalez, T. Lopez, R. Gomez, Catalysis Today 35 (1997) 293-317.

66. P. Francesco, Catalysis Today 41 (1998) 129-137.

67. A. M. Raspolli Galletti, C. Antonetti, I. Longo, G. Capannelli, A. M. Venezia, Applied Catalysis A: General 350 (2008) 46-52.

68. Y. Chen, J. Wang, H. Liu, R. Li, X. Sun, S. Ye, S. Knights, Electrochemistry Communications 11 (2009) 2071-2076.

69. P. H. Matter, E. Wang, M. Arias, E. J. Biddinger, U. S. Ozkan, Journal of Molecular Catalysis A: Chemical 264 (2007) 73-81.

70. J. Chen, Z. H. Zhu, S. Wang, Q. Ma, V. Rudolph, G. Q. Lu, Chemical Engineering Journal 156 (2010) 404-410.

71. F. R. García-García, J. Álvarez-Rodríguez, I. Rodríguez-Ramos, A. Guerrero-Ruiz, Carbon 48 (2010) 267-276.

72. S. Jiang, L. Zhu, Y. Ma, X. Wang, J. Liu, J. Zhu, Y. Fan, Z. Zou, Z. Hu, Journal of Power Sources 195 (2010) 7578-7582.

73. R. Chetty, S. Kundu, W. Xia, M. Bron, W. Schuhmann, V. Chirila, W. Brandl, T. Reinecke, M. Muhler, Electrochimica Acta 54 (2009) 4208-4215.

74. T. Maiyalagan, Applied Catalysis B: Environmental 80 (2008) 286-295.

75. H. Y. Du, C. H. Wang, H. C. Hsu, S. T. Chang, U. S. Chen, S. C. Yen, L. C. Chen, H. C. Shih, K. H. Chen, Diamond and Related Materials 17 (2008) 535-541.

76. Z. Zhu, J. Wang, A. Munir, H. S. Zhou, Electrochimica Acta 55 (2010) 8517-8520.

77. M. S. Saha, R. Li, X. Sun, S. Ye, Electrochemistry Communications 11 (2009) 438-441.

78. Y. G. Lin, Y. K. Hsu, C. T. Wu, S. Y. Chen, K. H. Chen, L. C. Chen, Diamond and Related Materials 18 (2009) 433-437.

79.	H. Li, H. Liu, Z. Jong, W. Qu, D. Geng, X. Sun, H. Wang, International Journal of Hydrogen Energy 36 (2010) 2258-2265.

80.	Z. Chen, D. Higgins, Z. Chen, Electrochimica Acta 55 (2010) 4799-4804.

81.	T. C. Nagaiah, S. Kundu, M. Bron, M. Muhler, W. Schuhmann, Electrochemistry Communications 12 (2009) 338-341.

82.	K. Gong, F. Du, Z. Xia, M. Durstock, L. Dai, Science 323 (2009) 760-764.

83.	D. Geng, H. Liu, Y. Chen, R. Li, X. Sun, S. Ye, S. Knights, Journal of Power Sources 196 (2010) 1795-1801.

Section A:

Synthesis of nanomaterials

CHAPTER 3

SYNTHESIS OF NITROGEN-DOPED: CARBON NANOTUBES USING TWO STAGE THERMAL CVD

3.1   Introduction

Nano-structured carbon based materials, such as carbon nanotubes (CNTs) have received interest due to their fascinating physical and chemical properties [1,2,3,4]. Carbon nanotubes (CNTs) have electronic behaviour ranging from metallic to semiconducting that depends on their structure, composition, chirality and tube diameter. Control of these properties is still a challenge [5]. The doping of the CNTs with other elements offers one practical path to tailor both the physical and chemical properties of CNTs by creating new chemical states that modify their electronic structure [4,6]. Boron (B) and nitrogen (N) are among the most effective dopants used in the literature for the preparation of doped CNTs because of their small atomic size which is relatively similar to carbon atom. This allows both boron and nitrogen to enter the CNT lattice space, thus modifying the physico-chemical structural properties of carbon [7,8,9,10,11]. Significant changes in hardness, electrically conductivity and chemical reactivity of the CNTs have been theoretically predicted and experimentally observed with substitutional doping of CNTs by nitrogen. As a result nitrogen doping in CNTs has received focused attention [12]. The additional lone pairs of electrons on the nitrogen, atom with respect to the delocalised π-system of a graphite-like hexagonal framework, enhances the electron conducting properties of the CNTs [13,14,15,16,17].

Depending on the synthesis conditions used (temperature, type of active metal catalyst, nitrogen source and carbon-nitrogen) various N-CNTs with different microstructures can be synthesized [18,19]. Various experimental methods such as chemical vapour deposition (CVD), high-temperature and high pressure reactions, solvothermal synthesis, solid reactions and gas-solid reactions of amorphous carbon with NH_3 at high temperature have been utilised to produce N-CNTs [20,21].

A CVD method offers the simplest technique towards the formation of doped CNTs [8]. In this chapter the synthesis of N-CNTs using a two stage thermal CVD method is described. The studies showed that the growth of CNTs depends on different parameters such as flow rate, type of carrier gas, and catalyst.

Numerous carbon-containing compounds such as alcohols have proven to be efficient carbon precursors for CNT formation. The feasibility to produce a carbon material using an alcohol as the carbon precursor was established in 1968. Since then many alcohol, have been used with ethanol being the most used alcohol [22,23,24,25,26]. Alcohol not only provide carbon atoms for the CNT formation but alcohol molecules also yield OH radicals upon decomposition, this can further participate in the etching reactions aiding in the CNT purification process. Therefore alcohols have been found to produce cleaner carbon nanotubes which contain less amorphous carbon and other impurities than CNTs produced using alkanes and alkenes [27,28]. In this study cyclohexanol is used as a carbon source. It was previously used by Musso and co-workers [29]. The choice of this alcohol was suggested as it contains a benzene structure and boiling point which is similar to aniline. Additionally, it is a good solvent for ferrocene and this allows the generation of a homogeneous solution [29].

3.2   Experimental

3.2.1   Materials and Reagents

Cyclohexanol, ferrocene and aniline, all analytical grade, were obtained from Sigma Aldrich and used as purchased.

3.2.2   N-CNT synthesis using a two stage furnace thermal-CVD

Undoped and nitrogen doped CNTs were synthesised using a thermal-CVD method in a two stage horizontal split-tube furnace. The reactions were carried out in a horizontal tubular quartz reactor (800 mm X 28 mm) in atmospherc pressure. Cyclohexanol was used as carbon source, aniline as a nitrogen source and ferrocene as catalyst. A mixture (3 g) of cyclohexanol-anilline-ferrocene with different ratios was placed in a quartz boat (120 mm X 15 mm) that was directly introduced into the centre of the first furnace and vaporised at 280°C. The resultant vapours were transferred to the second furnace where the carbon materials were grown at a temperature of 800 - 950 °C under a nitrogen or argon carrier gas flow rate of 100 mL/min measured with MKS mass flow controller (Multi gas controller 647C). The temperature inside the furnaces determined by means of a thermocouple positioned in the middle of the furnace. The reaction was maintained until there was no longer vapour visible in the tube; the furnace was cooled down under the inert gas atmosphere. The black soot was then collected from the inner wall of the quartz tube for characterisation. In the reaction +/- 2.5 g of reactants were consumed. Elemental composition and structural characterisation studies were performed using the instruments below.

3.2.3   Characterisation

The morphology of the as-prepared and purified CNTs was evaluated using a LEO 1525 FE-SEM. The TEM analysis was performed by using a

Philips CM 200 electon microscope with beam energies of 120 kV. TEM was used to analyse the particle size and morphology of the as-prepared CNTs. The presence of the amorphous carbon and residual catalyst particles on the CNTs can be observed by the TEM technique. The samples for analysis were prepared by sonicating about 0.5 mg of CNTs in 5 ml methanol for 5 min. One drop of the resulting suspension was dropped on a copper grid.

Elemental analysis was carried out using XPS. An Electronic Quantum 2000 analyser with resolution of 0.1 at. % using a vacuum operating with Al (K_α) radiation was used.

Simultaneous thermogravimetric-differential analysis was performed using a TA Q500 instrument. CNT samples (5 mg) were analysed in platinum pans at a heating rate of 10 °C/min to 950 °C in an atmosphere of air flowing at 50 ml/min.

Raman spectra were collected before and after purification of CNTs using a Horiba Jobin Yvon T64000 Raman spectrometer. The spectra was recorded from 150 - 3000 cm^{-1} with a 514.5 nm excitation with an energy spectrometer setting 1.2 mW from a Coherent Innova model 308 Ar ion laser in measured backscattering geometry with a cooled charge-coupled device array detector.

3.3   Results

Nitrogen doped CNTs were grown in a two stage furnace using different carrier gas (Ar-5%H_2 or N_2), temperature and nitrogen concentrations with the catalyst concentration kept constant. Ferrocene was used as the catalyst for the CNTs growth. The first furnace at 280 °C was to vaporise the reactants; cyclohexanol, ferrocene and aniline while the second furnace at higher temperature was for the formation of carbon materials. N-CNTs were produced when aniline was introduced into the reaction

mixture. The results of the conditions used to make the N-CNTs are summarised in Table 3.1. The samples were named according to the mass ratio of aniline used and a carrier gas used, for instance, $Anil_N5$ is when 5 mass ratio of aniline was used with nitrogen as a carrier gas and $Anil_{AR}9$ is when 9 mass ratio of aniline was used with argon as a carrier gas.

Table 3.1. Growth conditions of the carbon nanotubes

Sample code	Carrier Gas	Temp (^{o}C)	Fch:Aniline: Cylohexanol (Mass ratio)mg	Flow rate (mL/min)	Yield (mg)	Tubes/ amorphous carbon/fibers ±%
$Anil_{AR}0$	Ar	800	1:0:39	100	-	-
$Anil_{AR}0$	Ar	850	1:0:39	100	-	-
$Anil_{AR}0$	Ar	900	1:0:39	100	490	90cC, 10aC
$Anil_{AR}5$	Ar	800	1:5:34	100	-	-
$Anil_{AR}5$	Ar	850	1:5:34	100	-	-
$Anil_{AR}5$	Ar	900	1:5:34	100	270	80cC, 20aC
$Anil_{AR}2$	Ar	900	1:2:37	100	300	80NT, 15aC,5cC
$Anil_{AR}5$	Ar	900	1:5:34	100	270	90NT, 10aC
$Anil_{AR}9$	Ar	900	1:9:30	100	130	95NT, 5aC
$Anil_N0$	N_2	800	1:0:39	100	90	80F, 20aC
$Anil_N0$	N_2	850	1:0:39	100	280	80T, 20aC
$Anil_N0$	N_2	900	1:0:39	100	960	90cC, 10aC
$Anil_N5$	N_2	800	1:5:34	100	-	-
$Anil_N5$	N_2	850	1:5:34	100	-	-
$Anil_N5$	N_2	900	1:5:34	100	450	90NT, 10aC
$Anil_N2$	N_2	900	1:2:37	100	810	80NT, 15aC,5cC
$Anil_N5$	N_2	900	1:5:34	100	450	90NT, 10aC
$Anil_N9$	N_2	900	1:9:30	100	310	95NT, 5aC

T: Nanotubes (CNTs), NT: Nitrogen-doped CNTs, F: Nanofibers, aC: Amorphous carbon and cC: Conical stacking graphene sheets

3.3.1 TEM and SEM analysis

3.3.1.1 Effect of the carrier gas

Ar-5%H_2 or N_2 were used as carrier gases for synthesis of CNTs materials. The Ar-5%H_2 produced carbon material showed lower yields when compared to the N_2 synthesised CNTs material (Table 3.1). The results indicated the material only formed at reaction temperatures above 850 ^{o}C when Ar-5%H_2 was used as the carrier gas. In contrast, for the synthesis of CNTs using N_2 as carrier gas, a substantial amount of carbon material formed even at temperatures of 800 ^{o}C. FIB-SEM images of sample Anil$_{AR}$9 and Anil$_N$9 produced at 900 ^{o}C for both Ar-5%H_2 and N_2 carrier gases are shown in Table 3.1.
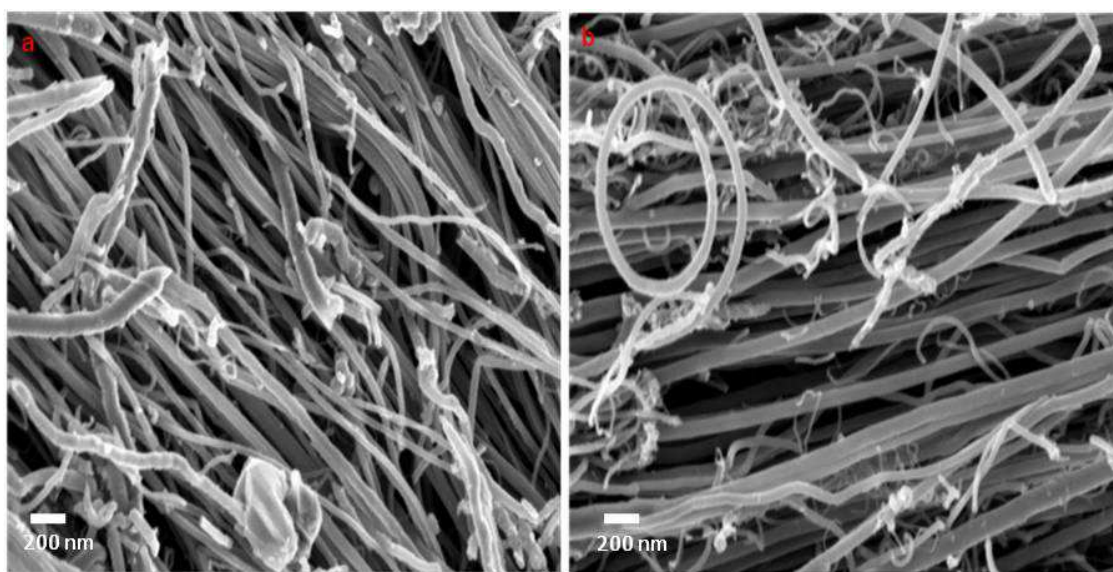
Figure 3.1. FIB-SEM images of the CNTs grown under a) Nitrogen b) argon with 5% hydrogen. Synthesis conditions: 3g of ferrocene-anilline-cyclohexanol mixture with ratio 1:5:34. Flow rate 100 mL/min, temp=900 °C.

The material produced using Ar-5%H_2 has tubes with outer diameter in a range of 20 - 80 nm, while the nitrogen carrier gas produced tubes that had a 30 - 110 nm diameter range. The hydrogen in the argon carrier gas is playing a major role in the diameter of the material formed during synthesis. Hydrogen cleans the outer surface of the tube which leads to

48

the smaller diameters and lower yield of the CNTs. Wasal et al. have carried out a study on the CVD synthesis of MWCNTs and they investigated the role of hydrogen on CNT synthesis using ferrocene as a catalyst and xylene as the carbon source [30]. The study revealed that hydrogen caused a competition between the formation of different compounds (soot, carbon fibers and CNTs) and it also reduced the rate of carbon production by dehydrogenation.

3.3.1.2 Effect of temperature

The yield of the carbon material was observed to increase with an increase of temperature as shown in Table 3.1. Figure 3.2 illustrates the high resolution TEM images of the as-synthesised materials at: 800, 850 and 900 ^{o}C. In addition, Figure 3.3 shows the low resolution TEM images.
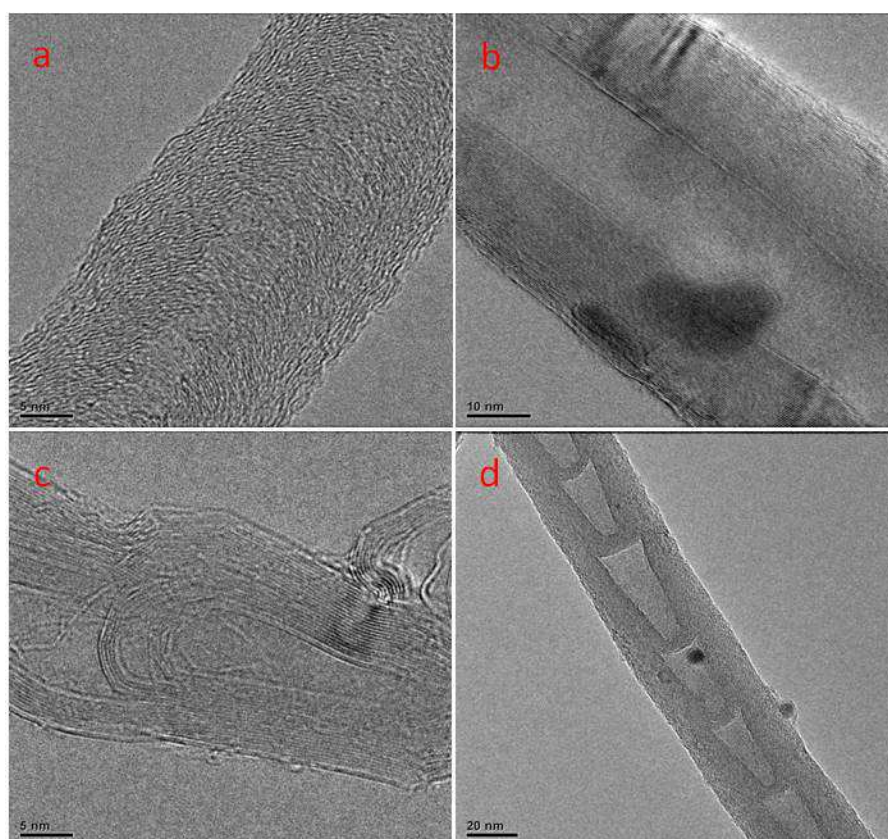
Figure 3.2. TEM images of the carbon material grown at (a) 800 ^{o}C, (b) 850 ^{o}C, (c) 900 ^{o}C and N-CNTs (d) 900 ^{o}C. Synthesis conditions: 3g of ferrocene-anilline-cyclohexanol mixture with ratio 1:5:34. Flow rate 100 mL/min, N$_2$ carrier gas.

In Figure 3.2a, at 800 ^{o}C, a carbon nanofibers material with helical-like morphology and "herringbone" structure is produced. Ismagilov et.al., [31] reported similar morphology formation before.

Regular CNTs with hollow tube where obtained at the temperature of 850 ^{o}C with a narrow diameter range of 35 - 100 nm (Figure 3.2b). At 900 ^{o}C, morphology with a conical stacking of graphene sheets with intermittent hollow regions is observed (Figure 3.2c).
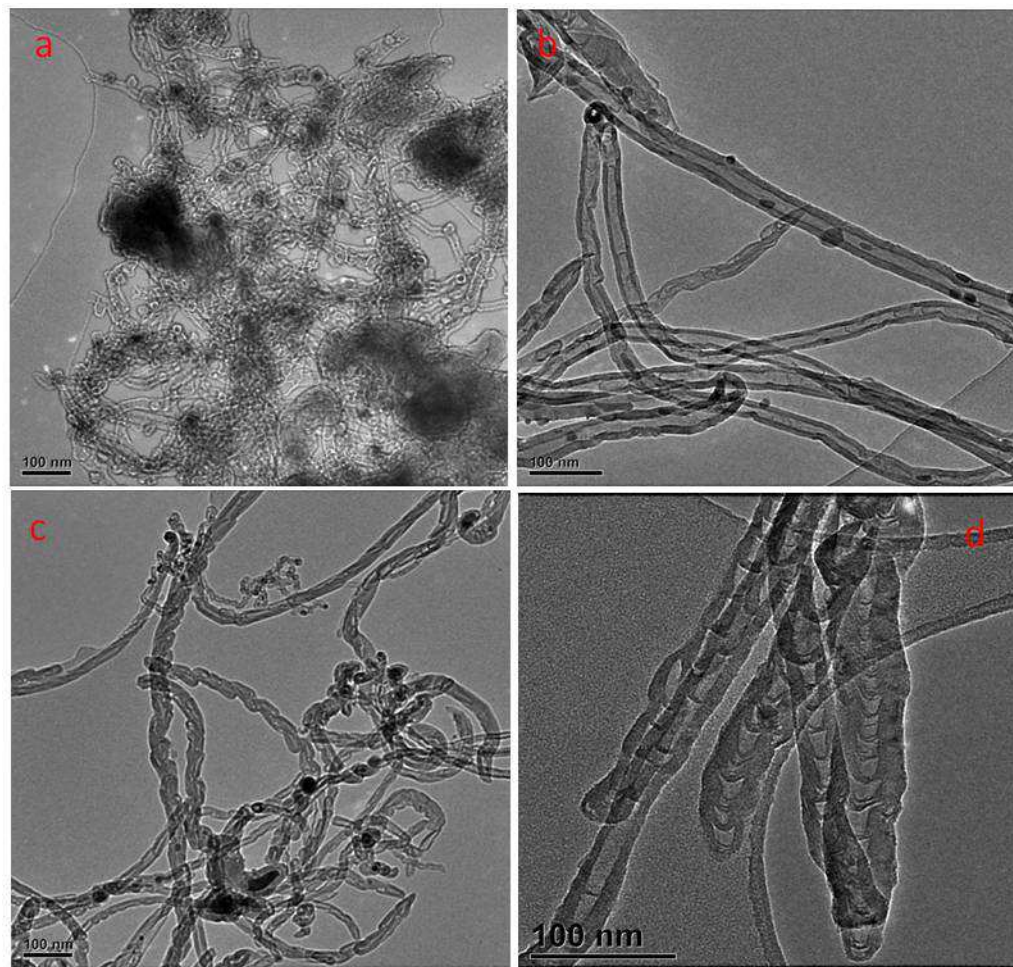
Figure 3.3. TEM images of the carbon material grown at (a) 800 ^{o}C, (b) 850 ^{o}C (c) 900 ^{o}C (d) and N-CNTs at 900 ^{o}C. Synthesis conditions: 3g of ferrocene-anilline-cyclohexanol mixture with ratio 1:5:34. Flow rate 100 mL/min, N_2 carrier gas.

The structure of the carbon material depends on the ratio between the diffusion rate of carbon through the catalyst and on its surface [32]. The diffusion rate in turn depends on temperature. At 800 ^{o}C the diffusion rate of Fe catalyst and C was too low for the CNTs to nucleate and completely grow into hollow tubes and it resulted in carbon nanofibers. At 900 ^{o}C diffusion rate was too high, which led to irregular/distorted morphology. It does not seem to match the growth kinetics of the fine nanotube [33].The suitable diffusion rate for CNTs was at 850 ^{o}C. Ar-5%H_2 carrier gas is able to form carbon material at 900 ^{o}C only. However, the materials synthesized under Ar-5%H_2 carrier gas do not give hollow tube CNTs (Figure 3.4) and the yield is low. For this reason the material produced under the N_2 carrier gas will be discussed in more details.

When aniline was introduced as a reactant together with ferrocene and cyclohexanol no carbon materials were produced at a temperature below 900 ^{o}C. This shows that the surface diffusion rate of Fe and C was affected by the introduction of the aniline in the solution. Shalagina et al, [32] reported that nitrogen changes the ratio of diffusion rate by hampering the bulk diffusion or facilitating the surface diffusion rates. Hence, N-CNTs were formed at a higher temperature as compared to the undoped CNTs which were formed at a lower temperature of 850 ^{o}C (Figure 3.3b). The CNTs formed had a fairly crystalline structure, constituted by a periodical bamboo like structure instead of a hollow channel found for CNTs formed without aniline as shown in Figure 3.2d. The formation of the bamboo was attributed to the incorporation of nitrogen dopant atoms. Nitrogen atoms generate pentagons in the graphite network of the tube by interrupting the precipitation of the graphite shells leading to the bamboo shape structure [13,34,35,36,37].
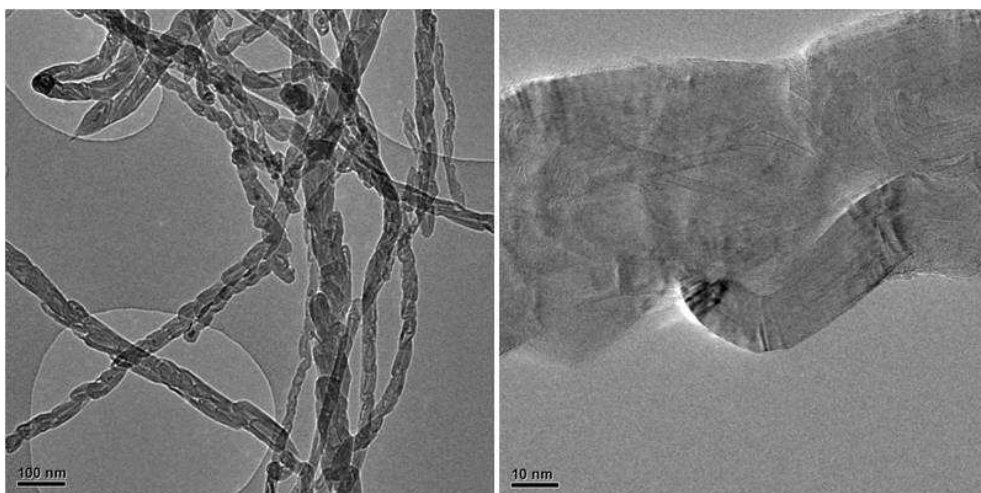
Figure 3.4. TEM images of the carbon material grown at 100 ml/min flow rate of Ar at 900 $^{\circ}$C.

Even though the nitrogen doped CNTs were obtained, it is difficult to control the reaction process. Three compounds (cyclohexanol, ferrocene, aniline) with different vapour pressure are introduced at 280 $^{\circ}$C and they are vapourise at different rate. Therefore, it is not easy to control the synthesis process.

3.3.2   Raman spectroscopy analysis of synthesised carbon

Raman spectroscopy measurements were conducted to evaluate the graphitization and crystalinity of the as-prepared samples as a function of temperature is illustrated in Figure 3.5. All spectra show mainly two bands; a D-band at 1330 cm^{-1} and a G-band at 1580 cm^{-1}. The D-band is attributed to a disorder-induced feature due to lattice distortion. The G-band originates from the in plane stretching vibration mode, E_{2g}, of a single crystal graphite [38].The intensities give information about structural change characteristics of the carbon materials resulting from a change in morphology. The I_d/I_g of Anil$_N$0 - 800 $^{\circ}$C, Anil$_N$0 - 850 $^{\circ}$C, Anil$_N$0 - 900 $^{\circ}$C and Anil$_N$5 - 900 $^{\circ}$C were 1.08, 0.52, 0.65 and 0.56 respectively as shown in Table 3.2.
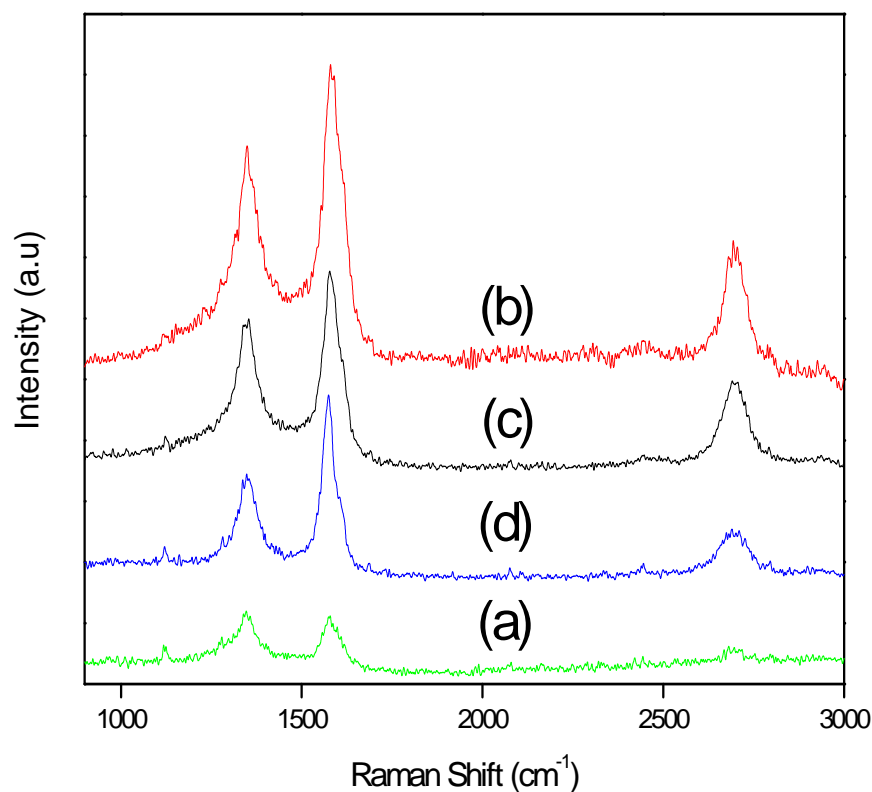
Figure 3.5. Raman spectra of the CNTs grown (a) 800 ^{o}C, (b) 850 ^{o}C (c) 900 ^{o}C and (d) $Anil_N5$ at 900 ^{o}C. Synthesis conditions: 3g of ferrocene-anilline-cyclohexanol mixture with ratio 1:0:39. Flow rate 100 mL/min, N_2 carrier gas.

Table 3.2. I_d/I_g of CNTs at different temperatures

Sample	Temp (^{o}C)	D-band (cm^{-1})	G-band(cm^{-1})	I_d/I_g
Anil$_N$0	800	1349	1578	1.08,
Anil$_N$0	850	1349	1578	0.52
Anil$_N$0	900	1349	1578	0.65
Anil$_N$5	900	1348	1572	0.56

The I_d/I_g is strongly dependent on the defect fraction originating from use of different temperatures and it could be considered as measure of the crystallinity [39]. The ratio of 0.52 for tubes formed at 850 ^{o}C showed the

crystalline order of graphene to be higher when compared to carbon material prepared at 800 and 900 ^{o}C. The herringbone nanofibers formed at 800 ^{o}C appeared to have poor crystallinity and these results are in agreement with TEM results.

With the incorporation of N there was a down-shift of the G-band with 6 cm^{-1} and this is probably due to the new type of disorder with nitrogen doping. This shift is ascribed to the C-C expansion or contraction and the electronic structure changes [40]. For that reason, the down-shifts of the G-band with introduction of nitrogen implies an enhanced electron transfer between valence and conduction bands [17]. The peak at 2702 cm-1 represents a second order G' band; an overtone mode of the D-band which corresponds to two-phonon processes and its appearance does not need defects. The most pronounced difference between the Raman spectra of CNTs (Figure 3.5b) and N-CNTs (Figure 3.5d) nanotubes is the strong decrease in the G′ band intensity with nitrogen doping. Although the origin of the G′ band is independent of the structural defects, Raman spectra showed that the intensity, of this band is sensitive to nitrogen incorporation in CNTs [41].

3.3.2.1 Effect of the aniline

Figure 3.6a shows the SEM images of the CNTs without aniline. The tubes have bends and twists. Additions of N results in straighten tubes though the reasons for the behavior are not yet known (Figure 3.6b-d). The increase of aniline in a reaction mixture also leads to a decrease in the yield of the as-prepared material (see Table 3.1). This might be due to the fact that yield depends on the amount of carbon that deposit to form the solid material; CNTs. Therefore with the increase of aniline there is more nitrogen substitution and less carbon deposit.
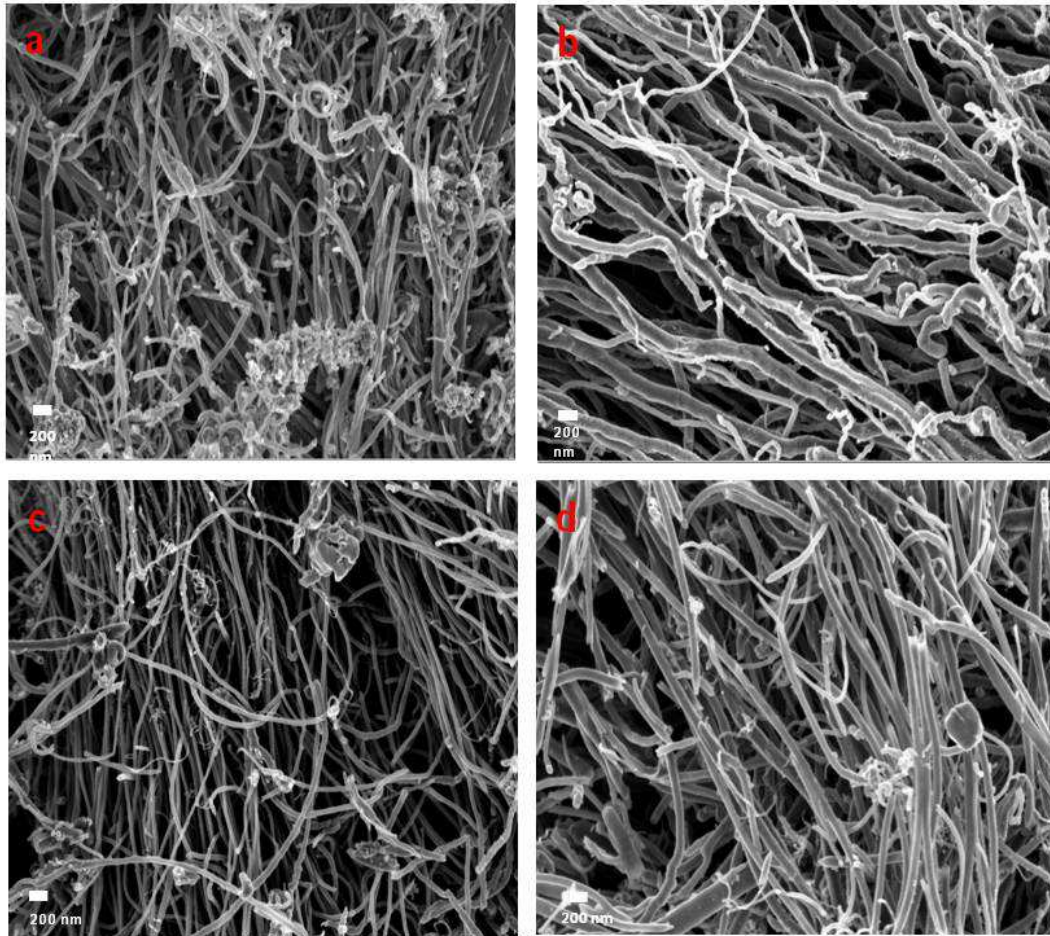
Figure 3.6. FIB-SEM images of the CNTs with nitrogen carrier gas with different ratios of FcH: Anil:Cyc (a) Anil$_N$0 (b) Anil$_N$2 (c) Anil$_N$5 (d) Anil$_N$9

3.3.3　XPS analys of N-CNTs

Figure 3.7 illustrates the XPS characterisation of as-prepared N-CNTs (*Anil$_N$5)*. It shows the full spectra of the material. The C1 peak positions at 284.9 eV is due to the delocalised sp^2-hybridized carbon or graphite-like C - C bonding [17,42].
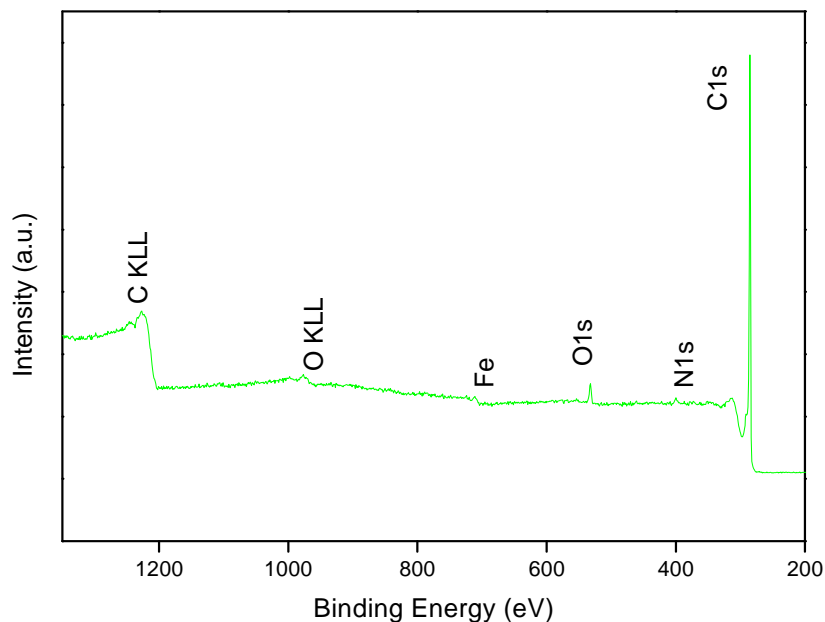
Figure 3.7. XPS N1s spectra of N-CNTs

The other C1 peak at 286.6 eV corresponds to the sp^2 and sp^3 hybridized bonding geometry between nitrogen and carbon [17,42]. However, the C1s signal is not considered to be the best evidence in supporting nitrogen doping into CNTs [43].

XPS also detected the presence of nitrogen. Figure 3.8 shows a narrow scan of the N1s at region 360 - 410 eV. The N1s signals were masked by the high noise/signal ratio, due to the low content of nitrogen in the sample [44].The percentage (atomic) nitrogen contents presents in the N-CNTs are shown in Table 3.3. The nitrogen concentration in the doped N-CNTs varied from 0.2 to 1.3 at. % as the aniline in the reaction mixture increased. The maximum nitrogen atomic percentage that was able to be doped on the CNTs is 1.3 at. %. XPS also detected very low atomic percentage of Fe (< 0.2 at. %) at 710 eV due to the synthesis catalyst, formed from ferrocene.
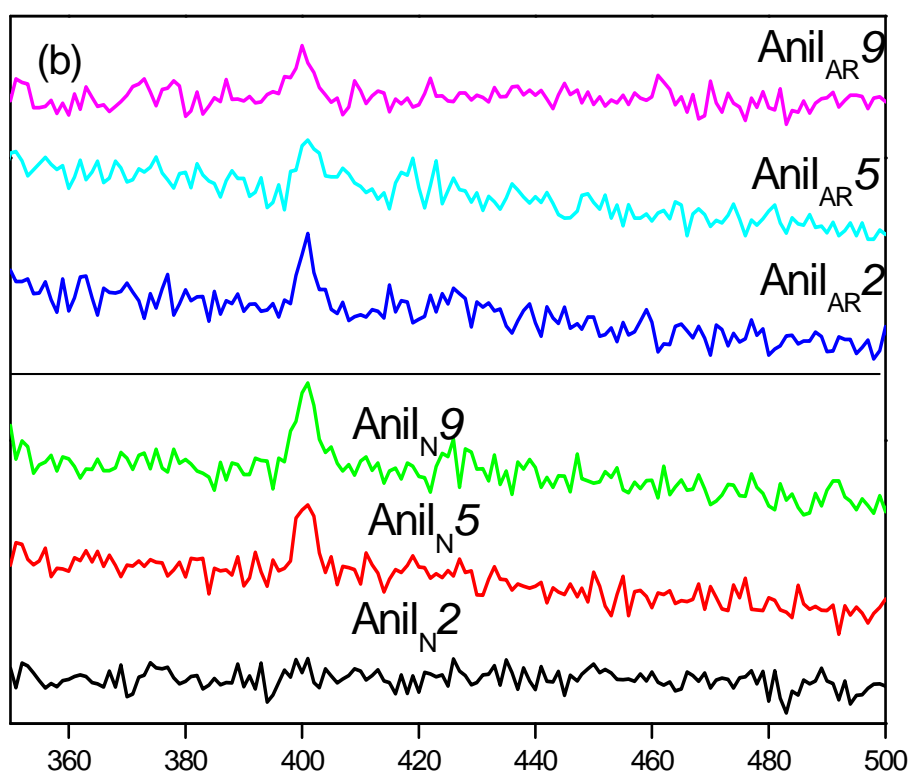
Figure 3.8. Normalised XPS N1s spectra of N-CNTs

Table 3.3. XPS elemental compositon of N-CNTs synthesised with various gas with different ratios.

Postion (ev)		400	298	532	701
Sample Name		N at.%	C (at.%)	O (at.%)	Fe (at.%)
Nitrogen gas					
1:2:37	$Anil_N2$*	0.2	96	3.1	0.2
1:5:34	$Anil_N5$	0.8	95.7	3.2	0.3
1:9:30	$Anil_N9$*	1.3	95.1	3.0	0.4
Argon/5% H_2 gas					
1:2:37	$Anil_{AR}2$	1.0	96.6	2.3	0.1
1:5:34	$Anil_{AR}5$	1.3	96.4	2.1	0.2
1:9:30	$Anil_{AR}9$*	1.3	95.7	2.5	0.4

*The XPS detected < 0.1 % silicon which was obtained when scrapping out carbon material from quartz tube. Error bar=+/- 0.1

3.3.4 TGA analysis

Thermogravimetric analysis (TGA), coupled with a derivative curve of the weight loss (DTG), is often used to investigate the thermal stability as well as the composition and purity of carbons. It is an effective way to quantitatively evaluate CNTs, in particular, the content of residual metal. It is easy to obtain the residual metal content using this technique by simply oxidising the CNT samples in air. The TGA and corresponding DTG curves of the carbon nanotubes are shown in Figure 3.9 and Figure 3.10 respectively. From the analysis it shows gradual weight loss for all samples in the range from 100 – 370 ^{o}C. This weight loss is due to readily removed volatile compounds, moisture, and adsorbed gas molecule [8,45]. There is no significant weight loss before 500 ^{o}C in the as-prepared CNTs, thus ruling out the presence of a significant amount of amorphous carbon.
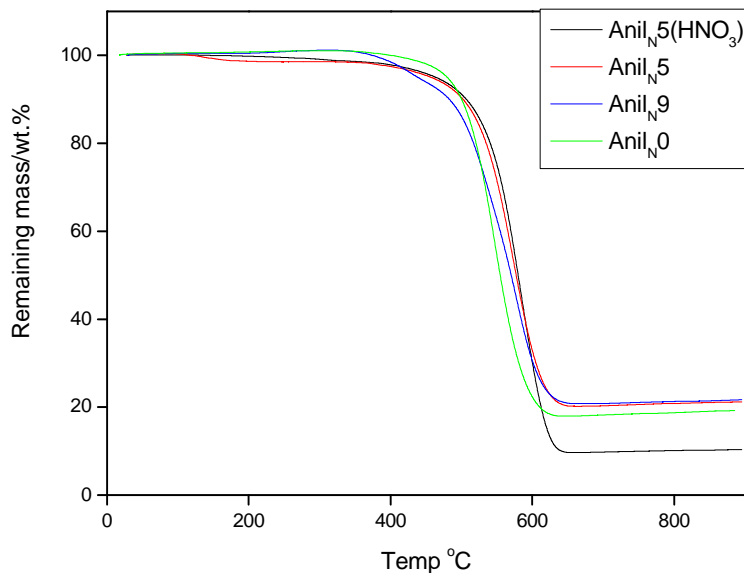
Figure 3.9. TGA of the CNTs grown at 900 ^{o}C, 100 ml/min flow rate of nitrogen with different ratios of FcH: Anl:Cyc

The material produced without aniline, *Anil$_N$0* had the lowest decomposition temperature of 553 ^{o}C, associated with the irregularities of

the stacking of graphene sheets. The decomposition temperatures for *Anil$_N$5* and *Anil$_N$9* were 573 and 537 ^{o}C respectively. *Anil$_N$5* had a better thermal stability than *Anil$_N$9*. The thermal stability of the N-CNTs shifts to slightly lower temperature as the nitrogen content increases. This is credited to more structural disorder when the aniline in the mixture is increased and hence the N content of the CNTs. Increase in presence of nitrogen atoms, create localized defects that are energetically less stable than the pure carbon lattice [46]. About 20 % residue is due to the Fe metal impurities as Fe_2O_3 from the ferrocene catalyst.
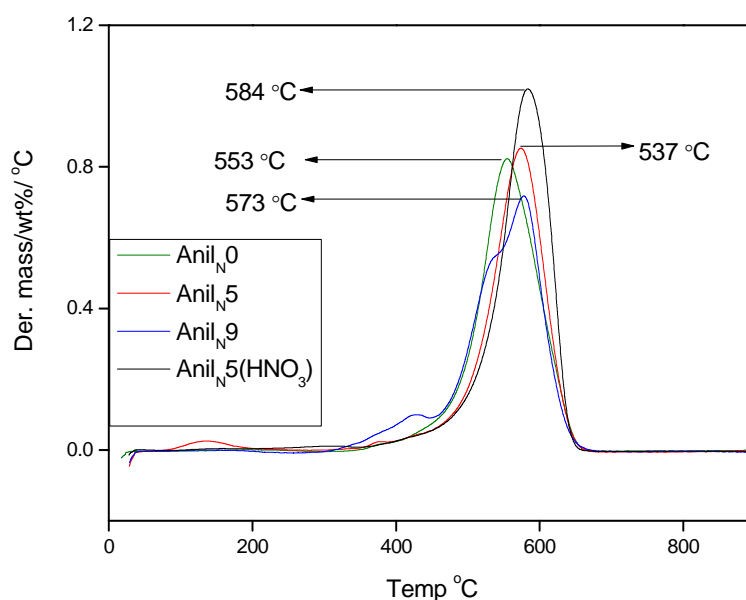
Figure 3.10. Derivative graph (DTA) of the CNTs grown with different ratios of FcH:Anl:Cyc. Synthesis conditions: 3g of ferrocene-anilline-cyclohexanol mixture. Flow rate 100 mL/min, N_2 carrier gas, temp = 900 °C.

In order to purify the N-CNTs, *Anil$_N$5* were stirred in 30 % nitric acid (HNO$_3$) solution for 2 h at 110 ^{o}C and then washed with distilled water. TGA revealed that the residue decreased from 20 to 5 %. The remaining residue might be due to the Fe particles that are located inside the tubes. The stability of the *Anil$_N$5 (HNO$_3$)* material slightly increases from 573 to

584 °C after the removal of the impurities. This improvement is attributed to the removal of catalyst which is known to aid the oxidation of carbon.

3.3.4.1 Raman analysis of N-CNTs

The Raman spectra of the N-CNTs are shown in Figure 3.11 and three peaks can be observed. The first peak around 1350 cm^{-1} corresponds to the disorder-induced band (D-band), the second peak around 1580 cm^{-1} corresponds to the tangential mode (G-band) and the last peak G' occurring at 2700 cm^{-1} is an overtone mode of the D-band. The I_d/I_g ratio was used to investigate the extent of disorder in the graphitic carbon [40]. Table 3.4 shows the positioning of the G-and the D-bands, the I_d/I_g ratio as well as the nitrogen content for N-CNTs of the N-CNTs grown from the different ratio of aniline to cyclohexanol.

The high I_d/I_g of $Anil_N0$ was due to defects from unusual morphology with a conical stacking of graphene sheets with intermittent hollow region. The spectra show that the I_d/I_g ratio significantly increases with increasing nitrogen content up to $Anil_N5$. In $Anil_N9$, the I_d/I_g ratio was found to slightly increase. These results suggest that increasing the aniline mass ratio in mixture reduces the disorder of the carbon. There is a loss in ordering in the graphene layers as more nitrogen is incorporated into the CNTs. These results are in agreement with TEM and TGA data. It is also observed from the Raman data (Table 3.4) that increasing the N content leads to down-shift of the D-band. The down-shift of D-band by 5 cm^{-1} for the N-CNTs indicates the appearance of new types of disorder in N-CNTs relative to that of pure carbon material synthesised with same conditions. The position of the G-band is also shifted. However, the G-band is not related to the structural defects and a modification in the electronic structure of CNTs with nitrogen doping could be the reason for the observed shift [41].
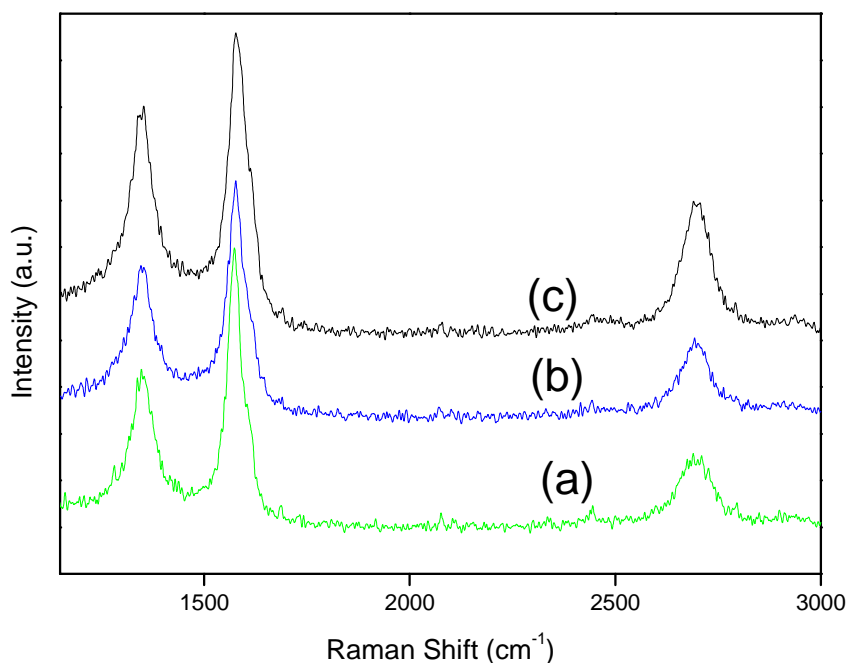
Figure 3.11. Raman spectra of the N-CNTs with different ratios of FcH:Anl:Cyc (a) $Anil_N5$, (b) $Anil_N9$ and (c) $Anil_N0$. Synthesis conditions: 3g of ferrocene-anilline-cyclohexanol mixture. Flow rate 100 mL/min, N_2 carrier gas, temp = 900 °C.

Table 3.4. Raman data for the N- CNT

Sample	N-content (at. %)	D-band (cm^{-1})	G-band (cm^{-1})	I_d/I_g
$Anil_N0$	0	1350	1581	1.08
$Anil_N5$	0.8	1345	1572	0.56
$Anil_N9$	1.3	1345	1576	0.59

3.4   Conclusion

Nitrogen doped carbon nanotubes with nitrogen content of up to 1.3 at. % were effectively produced using a two stage thermal CVD. Both carrier gases, Argon/5% H_2 and N_2 contributed to production of N-CNTs when aniline was introduced. The Argon/5% H_2 produced N-CNTs with smaller tubes diameters in a range of 20 - 80 nm and lower yields when compared

to N-CNTs produced with nitrogen carrier gas which showed better yields with tubes diameters of 35 - 100 nm. The regular CNTs with hollow tube where obtained at the temperature of 850 ^{o}C, while the N-CNTs were obtained at 900 ^{o}C. The optimum parameters to obtain N-CNTs are when nitrogen is used as a carrier gas at 900 ^{o}C. Even though the N-CNTs were obtained it is not easy to control the synthesis due to compounds with different vapour pressure. The next step of this series will be to deposit the metal particles on the N-CNTs with specific focus on catalytic activity.

References

1. A. Nieto-Márquez, J. C. Lazo, A. Romero, J. L. Valverde, Chemical Engineering Journal 144 (2008) 518-530.

2. K. Chizari, I. Janowska, M. Houllé, I. Florea, O. Ersen, T. Romero, P. Bernhardt, M. J. Ledoux, C. Pham-Huu, Applied Catalysis A: General 380 (2010) 72-80.

3 Y. Tang, B. L. Allen, D. R. Kauffman, A. Star, Journal of the American Chemical Society 131 (2009) 13200-13201.

4. E. Cruz-Silva, D. A. Cullen, L. Gu, J. M. Romo-Herrera, E. MuÃoz-Sandoval, F. LÃpez-UrÃas, B. G. Sumpter, V. Meunier, J.-C. Charlier, D. J. Smith, H. Terrones, M. Terrones, ACS Nano 2 (2008) 441-448.

5. X. Y. Tao, X. B. Zhang, F. Y. Sun, J. P. Cheng, F. Liu, Z. Q. Luo, Diamond and Related Materials 16 (2007) 425-430.

6. E. N. Nxumalo, V. P. Chabalala, V. O. Nyamori, M. J. Witcomb, N. J. Coville, Journal of Organometallic Chemistry 695 (2010) 1451-1457.

7. A. A. Koós, F. Dillon, E. A. Obraztsova, A. Crossley, N. Grobert, Carbon 48 (2010) 3033-3041.

8. P. Ghosh, T. Soga, K. Ghosh, R. A. Afre, T. Jimbo, Y. Ando, Journal of Non-Crystalline Solids 354 (2008) 4101-4106.

9. Y.-H. Li, T.-H. Hung, C.-W. Chen, Carbon 47 (2009) 850-855.

10. B. G. Sumpter, V. Meunier, J. M. Romo-Herrera, E. Cruz-Silva, D. A. Cullen, H. Terrones, D. J. Smith, M. Terrones, ACS Nano 1 (2007) 369-375.

11. F. Villalpando-Paez, A. Zamudio, A. L. Elias, H. Son, E. B. Barros, S. G. Chou, Y. A. Kim, H. Muramatsu, T. Hayashi, J. Kong, H. Terrones, G. Dresselhaus, M. Endo, M. Terrones, M. S. Dresselhaus, Chemical Physics Letters 424 (2006) 345-352.

12. S. Maldonado, S. Morin, K. J. Stevenson, Carbon 44 (2006) 1429-1437.

13. P. Ghosh, M. Tanemura, T. Soga, M. Zamri, T. Jimbo, Solid State Communications 147 (2008) 15-19.

14.   P. H. Matter, E. Wang, M. Arias, E. J. Biddinger, U. S. Ozkan, Journal of Molecular Catalysis A: Chemical 264 (2007) 73-81.

15.   C. Tang, Y. Bando, D. Golberg, F. Xu, Carbon 42 (2004) 2625-2633.

16.   R. Chetty, S. Kundu, W. Xia, M. Bron, W. Schuhmann, V. Chirila, W. Brandl, T. Reinecke, M. Muhler, Electrochimica Acta 54 (2009) 4208-4215.

17.   H. Liu, Y. Zhang, R. Li, X. Sun, S. Désilets, H. Abou-Rachid, M. Jaidann, L.-S. Lussier, Carbon 48 (2010) 1498-1507.

18.   J. Amadou, K. Chizari, M. Houllé, I. Janowska, O. Ersen, D. Bégin, C. Pham-Huu, Catalysis Today 138 (2008) 62-68.

19.   A. A. Koós, M. Dowling, K. Jurkschat, A. Crossley, N. Grobert, Carbon 47 (2009) 30-37.

20.   Y. Zhong, M. Jaidann, Y. Zhang, G. Zhang, H. Liu, M. Ioan Ionescu, R. Li, X. Sun, H. Abou-Rachid, L.-S. Lussier, Journal of Physics and Chemistry of Solids 71 (2010) 134-139.

21.   H. Li, H. Liu, Z. Jong, W. Qu, D. Geng, X. Sun, H. Wang, International Journal of Hydrogen Energy 36 (2010) 2258-2265.

22.   P. Ramesh, T. Okazaki, T. Sugai, J. Kimura, N. Kishi, K. Sato, Y. Ozeki, H. Shinohara, Chemical Physics Letters 418 (2006) 408-412.

23.   S. Maruyama, E. Einarsson, Y. Murakami, T. Edamura, Chemical Physics Letters 403 (2005) 320-323.

24.   A.S. Botello-MÃndez, J. Campos-Delgado, A. n. Morelos-GÃmez, J. M. Romo-Herrera, Ã. n. G. RodrÃ-guez, H. Navarro, M. A. Vidal, H. Terrones, M. Terrones, Chemical Physics Letters 453 (2008) 55-61.

25.   K. B. Kouravelou, S. V. Sotirchos, X. E. Verykios, Surface and Coatings Technology 201 (2007) 9226-9231.

26.   T. Okazaki, H. Shinohara, Chemical Physics Letters 376 (2003) 606-611.

27.   A. Nasibulin, A. Moisala, H. Jiang, E. Kauppinen, Journal of Nanoparticle Research 8 (2006) 465-475.

28.   L. M. Cele, N. J. Coville, Carbon 47 (2009) 1824-1832.

29.   S. Musso, G. Fanchini, A. Tagliaferro, Diamond and Related Materials 14 (2005) 784-789.

30   W. Wasel, K. Kuwana, P. T. A. Reilly, K. Saito, Carbon 45 (2007) 833-838

31.   Z. R. Ismagilov, A. E. Shalagina, O. Y. Podyacheva, A. V. Ischenko, L. S. Kibis, A. I. Boronin, Y. A. Chesalov, D. I. Kochubey, A. I. Romanenko, O. B. Anikeeva, T. I. Buryakov, E. N. Tkachev, Carbon 47 (2009) 1922-1929

32.   A. E. Shalagina, Z. R. Ismagilov, O. Y. Podyacheva, R. I. Kvon, V. A. Ushakov, Carbon 45 (2007) 1808-1820.

33.   A. Hussain, Nanotechnology **14** (2003) 925-930.

34.   Z. Chen, D. Higgins, Z. Chen, Electrochimica Acta 55 (2010) 4799-4804

35.   D. Higgins, Z. Chen, Z. Chen, Electrochimica Acta 56 (2010) 1570-1575

36.   Y.-L. Li, F. Hou, Z.-T. Yang, J.-M. Feng, X.-H. Zhong, J.-Y. Li, Materials Science and Engineering: B 158 (2009) 69-74.

37.   Y. Shao, J. Sui, G. Yin, Y. Gao, Applied Catalysis B: Environmental 79 (2008) 89-99.

38.   E. Xu, J. Wei, K. Wang, Z. Li, X. Gui, Y. Jia, H. Zhu, D. Wu, Carbon 48 (2010) 3097-3102.

39.   R. Yadav, P. Dobal, T. Shripathi, R. Katiyar, O. Srivastava, Nanoscale Research Letters 4 (2009) 197-203.

40.   R. I. Jafri, N. Rajalakshmi, S. Ramaprabhu, Journal of Power Sources 195 (2010) 8080-8083.

41.   L. G. Bulusheva, A. V. Okotrub, I. A. Kinloch, I. P. Asanov, A. G. Kurenya, A. G. Kudashov, X. Chen, H. Song, physica status solidi (b) 245 (2008) 1971-1974.

42.   Y. G. Lin, Y. K. Hsu, C. T. Wu, S. Y. Chen, K. H. Chen, L. C. Chen, Diamond and Related Materials 18 (2009) 433-437.

43.   Z. Chen, D. Higgins, Z. Chen, Carbon 48 (2010) 3057-3065.

44.   J. Chen, Z. H. Zhu, S. Wang, Q. Ma, V. Rudolph, G. Q. Lu, Chemical Engineering Journal 156 (2010) 404-410.

45.   E. N. Nxumalo, V. O. Nyamori, N. J. Coville, Journal of Organometallic Chemistry 693 (2008) 2942-2948.

46.   C.P. Ewels, M. Glerup, Journal of Nanoscience and Nanotechnology 5 (2005) 1345.

CHAPTER 4

THE EFFECT OF MICROWAVE IRRADIATION ON THE SYNTHESIS OF RUTHENIUM/NITROGEN-DOPED CARBON NANOTUBES

4.1   Introduction

Advances in the catalysis field have shown that nanoparticles with nanostructured surfaces as compared to larger particles enhance the catalytic activity in most reactions [1,2]. The challenges for catalyst improvement are the design of structural factors such as morphology, nanoparticle size and metal inter-particle distance [3].

Intensive research has been conducted in order to develop new catalyst supports which can modify the catalytic activity and the selectivity of a catalytically active phase. The interaction of nanoparticles with a support plays an important role in the design of the catalyst [4]. Carbon based nanostructures (e.g. carbon nanotubes, carbon spheres, carbon fibers, etc.) have been found to be good supports for metal nanoparticles [4,5]. Studies have shown that doping carbon nanostructures with nitrogen generates n-type semi conductors, which have greater electron mobility than the corresponding undoped carbon nanostructures [6,7,8]. Nitrogen introduces chemically active sites that are required for anchoring of nanoparticles during deposition [9]. Therefore, it is proposed that the improved catalytic activity of nitrogen containing carbon nanostructures is due to the higher dispersion of metals and good interaction between the support and the metal particles [10]. In addition, nitrogen is able to generate defects on carbon, which increases the edge plane exposure and as a result enhances the catalytic activity [11].

The dispersion of a metal on a support is still largely based on conventional catalyst preparation techniques, such as wet impregnation followed by chemical reduction. These approaches often lack fine control of structural factors. In addition, use of these processes can be time consuming since they include multiple steps such as long ageing, drying and calcination of the samples. Hence, there is an interest in using alternative techniques to synthesise a catalyst using microwave irradiation [12,13]. In this chapter, we report on the deposition on ruthenium (Ru) nanoparticles on nitrogen doped carbon nanotubes (N-CNTs) using a microwave polyol assisted deposition method.

4.2   Experimental

4.2.1   Materials and Reagents

$RuCl_3.xH_2O$, ethylene glycol (EG), HNO_3 and pristine CNTs with inner diameter of 5-10 nm and outer diameter of 40 - 80 nm were obtained from Sigma Aldrich. Pristine CNTs were functionalised with 30 % HNO_3 at 110°C for 2 h and dried in an oven at 110°C for overnight.

4.2.2   N-CNT synthesis using thermal-chemical vapour deposition (CVD)

N-CNTs were synthesised using a thermal-CVD method in a horizontal split-tube furnace. The reactions were carried out in a tubular quartz reactor (800 X 28 mm). Cyclohexanol was used as carbon source, aniline as a nitrogen source and ferrocene as catalyst. A mixture of cyclohexanol-aniline-ferrocene in a 1:5:34 ratio was placed in a quartz boat (120 mm X 15 mm) that was directly introduced into the centre of the first furnace and vaporised at 280°C. The resultant vapours were transferred to the second furnace where the N-CNTs were grown at a temperature of 900°C under the nitrogen carrier gas flow. The gas flow rate of 100 mL/min measured with MKS mass flow controller (Multi gas controller 647C). The

temperature inside the furnaces determined by means of a thermocouple positioned in the middle of the furnace. The reaction was maintained until there was no longer vapour visible in the tube (ca. 6 min). The furnace was then cooled down under the carrier gas atmosphere. The black soot was then collected from the inner wall of the quartz tube. The soot was then purified and functionalised with 30 % HNO3 at 110°C for 2 h and was dried in an oven at 110°C overnight.

4.2.3   Deposition of Ru nanoparticles on CNTs

Ru nanoparticles were deposited on acid functionalised CNTs and N-CNTs using both microwave assisted polyol and conventional reflux polyol methods. In a microwave teflon vessel, 50 mg of CNTs and 10 mg $RuCl_3.xH_2O$ were mixed with 80 ml ethylene glycol (EG) and sonicated for 10 min to afford a homogenous suspension. The suspension was then placed in a microwave reactor (Anton-Paar Multiwave 3000). The microwave composed of internal temperature sensor, which is able to measure the temperature of individual vessel. The suspension was heated to 200°C and kept at the temperature for 5 min at various power settings: 350, 500, 800 and 1000 W. When the vessels reach the set temperature the power switched off and it switches on if the temperature decreases till end of 5 min.   For conventional method, the same, $RuCl_3.xH_2O$/CNTs/EG mixture described above (50 mg of CNTs, 10 mg $RuCl_3.xH_2O$ and 80 ml ethylene glycol) was placed in a conical flask and refluxed in an oil bath, while stirring for 24 h at 200°C at atmospheric pressure. The colour of the mixture changed from brown to clear solution. After the reactions the resulting suspensions, from both microwave and conventional heated reactions were filtered and the residue was washed with 50 mL acetone and then with 200 mL deionised water and dried at 110°C overnight.

4.2.4   Characterisation

Transmission electron microscopy (TEM) analysis was performed by using a JEOL2100 microscope with beam energy of 200 kV. TEM was used to analyse the particle size and morphology of the as-prepared CNTs. The samples for analysis were prepared by sonicating about 0.5 mg of CNTs in 5 ml methanol for 5 min. One drop of the resulting suspension was dropped on a copper grid. Raman spectra were collected before and after synthesis using a Horiba Jobin Yvon T64000 Raman spectrometer. The spectra was recorded from 150 - 3000 cm^{-1} with a 514.5 nm excitation with energy setting 1.2 mW from a Coherent Innova model 308 Ar-ion laser in measured backscattering geometry with a cooled charge-coupled device array detector. The morphology of the CNTs was evaluated using a LEO 1525 FE-SEM. The SEM was equipped with an energy dispersive spectroscopy (EDS) facility, which was used for elemental analysis of the CNTs. XRD patterns were collected in air at room temperature on a X'Pert Pro PANalytical X-ray diffractometer using Cu Kα radiation (λ = 0.15418) in the 2θ range of 10 to 80 º with a scanning rate of 5 °. Thermal analyses were performed by simultaneous thermogravimetric-differential procedures using a TA Q500 thermal instrument. CNT samples (5 mg) were analysed in platinum pans at a heating rate of 10 °C/min to 950 °C in an atmosphere of air flowing at 50 mL/min.

4.3   Results and discussion

Nitrogen doped CNTs were synthesised according to the procedure outlined in the experimental **section 4.2.2**. A mixture of cyclohexanol-aniline-ferrocene in a 1:5:34 ratio was used due to higher yield, thermal stability and better quality as compared to other ratios. The material was washed with acid (HNO_3) prior to characterisation to remove the impurities and add to fuctional groups.

4.3.1 SEM and TEM analysis of CNTs

Figure 4.1a shows the SEM images of pristine CNTs. The acid-functionalised MWCNTs were entangled together because of their high surface area and the van der Waals attraction between them [14,15]. The TEM (Figure 4.1b) shows the CNT with a hollow tube and crystalline layers. The pristine CNTs have an outer diameter of 20 - 80 nm and inner diameter ranged between 7 - 15 nm.
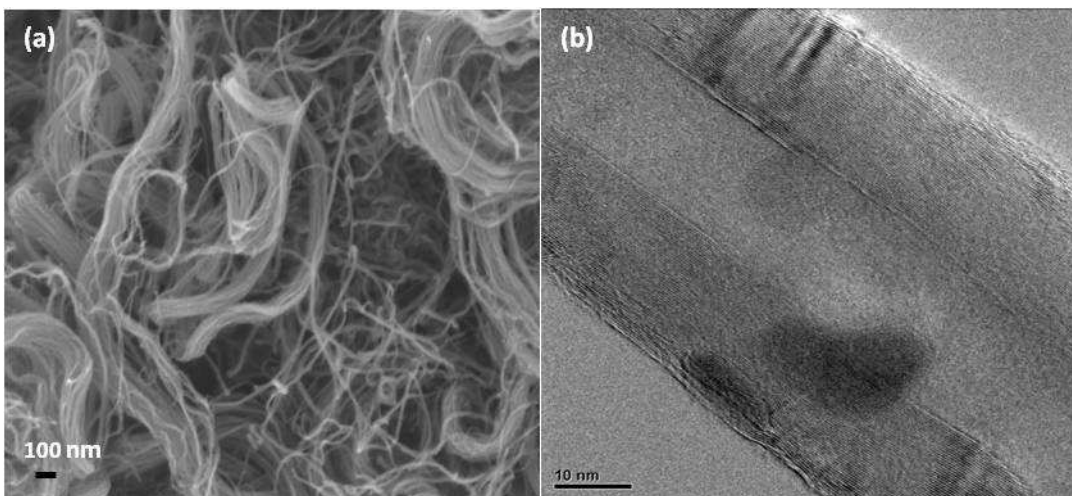
Figure 4.1. SEM and TEM images of the pristine CNTs

The EDS was used to determine elemental composition of the CNTs material as shown in Figure 4.2. Carbon, Molybdenum and Magnesium were identified. The carbon is from the CNTs, Mo and Mg might be due to the catalyst used for the growth of the CNTs.
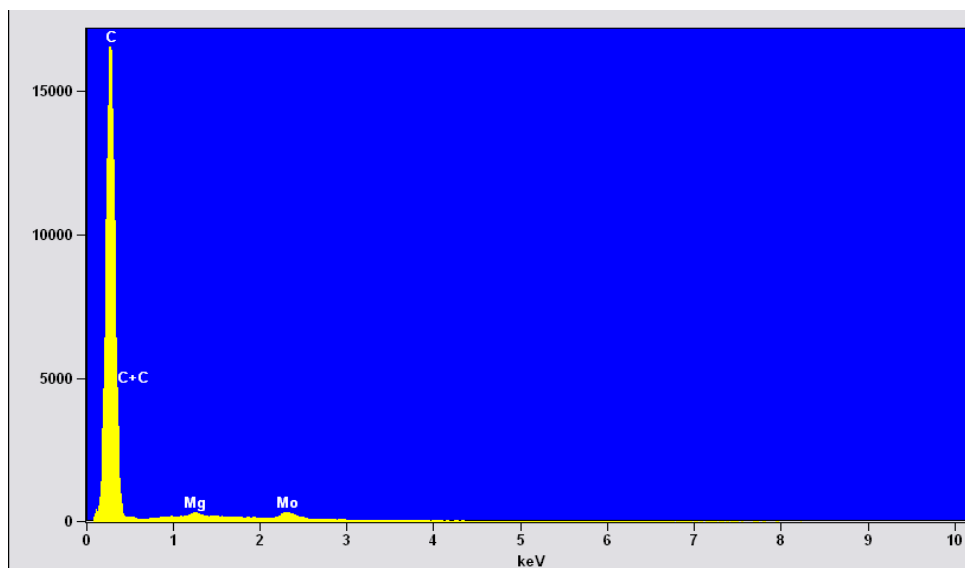
Figure 4.2. EDS of the CNTs

4.3.2   Raman of CNTs

Raman spectroscopy was used to measure the graphitisation and the degree of defect formation (Figure 4.3). The CNTs show the disorder peak around 1350 cm^{-1} corresponding to a *D*-band and a *G*-vibration modes peak at 1580 cm^{-1}.
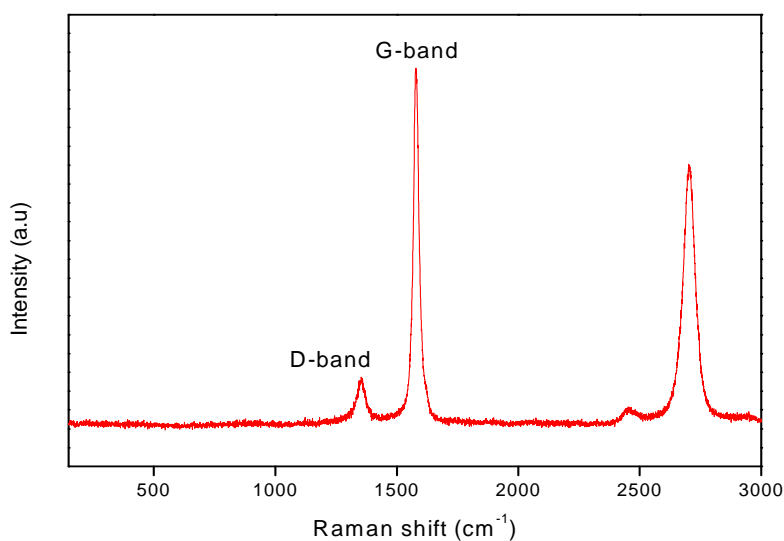
Figure 4.3. Raman spectrum of the functionalised CNTs

The D-band is attributed to the disorder-induced feature due to the lattice distortion, while the G-band originates from the in plane stretching vibration E_{2g} mode of a single crystal graphite structure [16].The peak at 2702 cm^{-1} represents the second order G' band, an overtone mode of the D-band which correspond to two-phonon processes and its appearance does not relate to disorder [17]. There was no signature of RBM at lower frequencies which implies that there were no SWCNTs in the material. The low I_D/I_G ratio of 0.15, an indicator of structural disorder in CNTs indicates that the MWCNTs are of high quality, with few defects and high crystalinity.

4.3.3 TEM analysis of Ru/CNTs

The TEM analysis of the Ru/CNTs prepared using different microwave power settings is shown in Figure 4.4. The images show the effect of microwave power on a series of samples that were prepared by heating the CNTs and Ru solutions to 200 ^{o}C at power 350, 500, 800 and 1000 W respectively. As the power was increased above 500 W, the particles formed agglomerates with an uneven distribution. Moreover, there are large agglomerates of nanoparticles separated from the Ru-decorated CNTs, indicating that some of the reduction reactions randomly occurred throughout the EG suspension. At a power setting of 350 W the particles were not homogenously dispersed on the surface of the CNTs. After the reduction of ruthenium chloride in EG solution, at power setting of 500 W was found to be optimum as it gave ultra-fine metallic Ru nanoparticles homogenously dispersed on the surface of the CNTs with diameter ranging from 5 – 8 nm (Figure 4.4b). The time to reach the 200 °C was decreasing with power increase; the time to reach 350, 500, 800 and 1000 W was 25, 17, 9 and 6 min respectively.
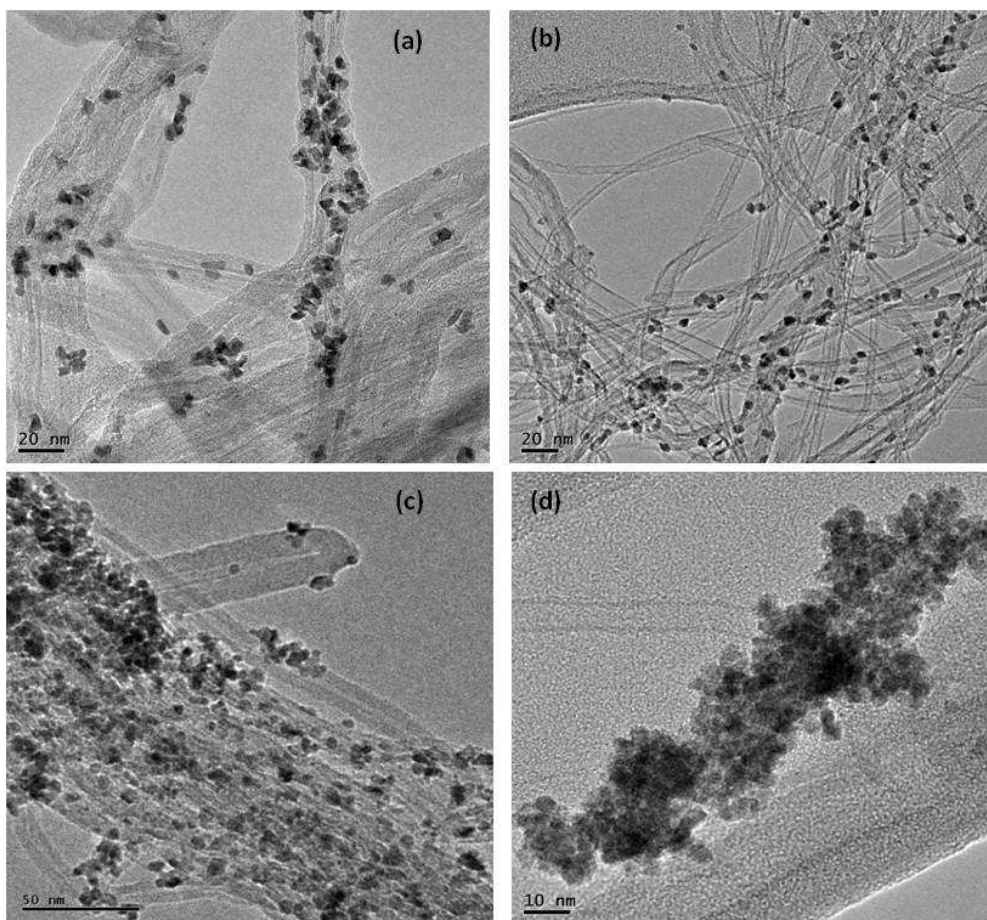
Figure 4.4. TEM images of Ru/CNTs prepared at different microwave power settings. (a) 350 W; (b) 500 W; (c) 800 W; (d) 1000 W. Synthesis conditions: EG 80 ml, t= 200 °C.

The agglomeration of the particles is attributed to the rapid heating rate of the reaction solution, which does not provide sufficient time for the reduction of the metal ions when high power is used. In addition, it was difficult to determine the size of particles prepared at high power.

The Ru particle size distribution histogram of the Ru/CNTs is shown in Figure 4.5. The histogram was done by counting 250 particles on TEM photograph. The average diameter of the Ru particles on CNTs is 6.2 nm when the power setting of 500 W was used.
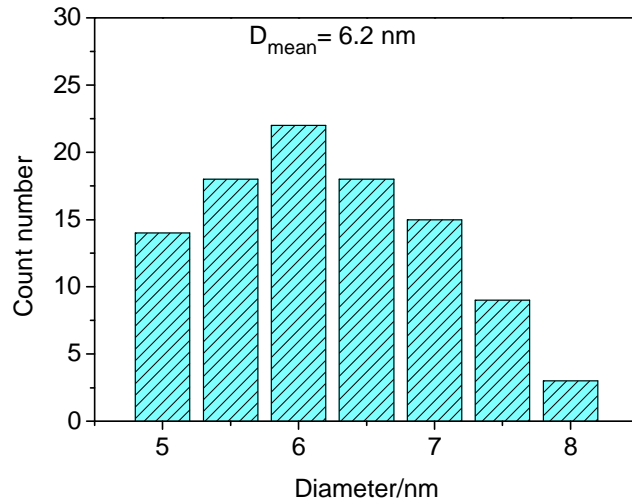
Figure 4.5. Particle size distribution histogram of Ru/CNTs prepared with 500 W.

4.3.4 XRD of Ru/CNTs

The XRD patterns of the Ru on CNTs are shown Figure 4.6. The diffraction peaks at around $2\theta = 26°$, $54°$ and $78°$ are associated with the (002), (004) and (110) planes of carbon [18,19,20]. The other four peaks at 2θ of about $38°$, $43°$, $59°$ and $69°$ are characteristics of the hexagonal crystalline Ru. The Ru crystallite sizes were determined using the Scherrer equation and the line broadening of the peak at $2\theta = 38°$ since it corresponds to the Ru most intense peak.

Using the Scherrer equation,

$$D = \frac{0.89\ \lambda}{\beta \text{Cos}\ \theta}$$

where D is the average crystallite size, λ is the wavelength (0.154 nm), β is the full width at half maximum, and θ is the Bragg diffraction angle. The crystallite size of Ru could be estimated to be 6.5 nm [21]. However, the considerable broadening and overlapping of diffraction peaks from different components make it difficult to calculate the size of other ruthenium nanoparticles from the XRD profile of Ru-decorated CNTs.
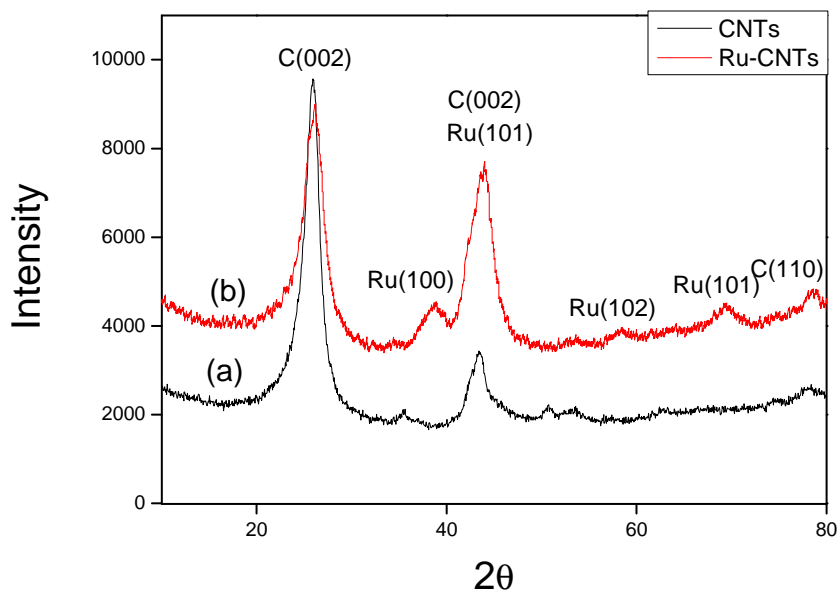
Figure 4.6. XRD patterns of pristine CNTs (a) and (b) Ru-CNTs prepared at 500W.

4.3.5   SEM and TEM analysis of N-CNTs

SEM image of the N-CNTs with outer diameter of 30-100 nm and length of 13 µm are shown in Figure 4.7a. The TEM image of N-CNTs, Figure 4.7b exhibits the typical 'bamboo like' compartments which are promoted by the presence of nitrogen [22,23].
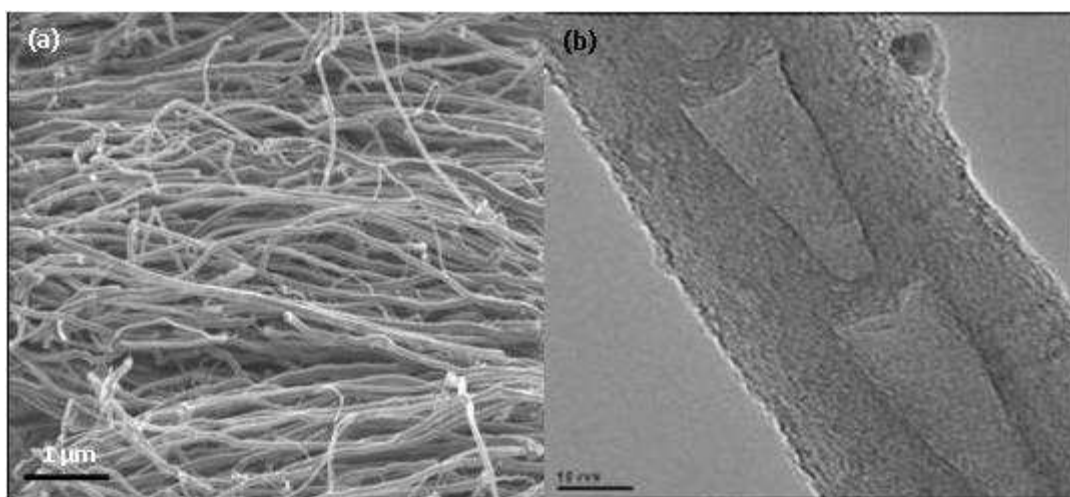
Figure 4.7. SEM and TEM images of N-CNTs

4.3.6   Raman of N-CNTs

The N-CNTs produced were subjected to 30 % HNO_3 treatment to remove the Fe particles and other impurities. The Raman spectra of the purified and as-prepared N-CNTs are shown in Figure 4.8 and three main peaks can be observed. The first peak at 1350 cm^{-1} corresponds to the disorder-induced band (D-band), the second peak at ~ 1590 cm^{-1} corresponds to the tangential mode (G-band) and the last peak G' occurring at ~ 2700 cm^{-1} is an overtone mode of the D-band [24].

After acid treatment, a significant increase in the intensity of a D-band can be observed in Raman spectra in Figure 4.8 I_d/I_g ratio of acid-treated N-CNTs of 0.63 in comparison with 0.52 ratio of the untreated N-CNTs. This suggests the two-dimensional graphitization is altered to a more disordered structure due to the damage of the wall when amorphous material is removed as the walls reacted with acid group.
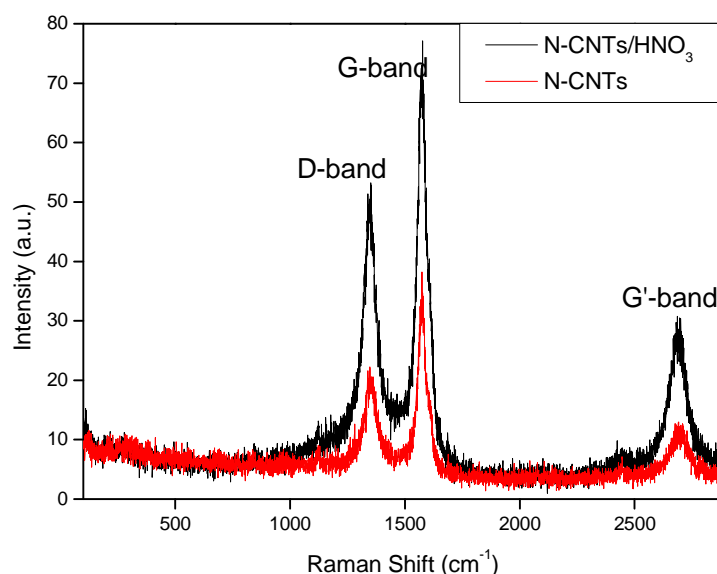
Figure 4.8. Raman of N-CNTs before and after treatment with 30 % HNO_3.

4.3.7 TGA of N-CNTs

Different structural forms of carbon exhibit different thermal oxidation behaviour. The presence of structural imperfections (defects or impurities) in the CNTs can lead to a decrease in the oxidative stability of these materials. These defects sites become more reactive to oxygen at elevated temperatures [25].

A TGA and DTG graph (insets) for the as-prepared and acid treated N-CNTs are presented in Figure 4.9. For as-prepared N-CNTs, two combustion regions are observed which correspond to two stepwise weight losses. The initial combustion around 350 °C was due to the oxidation of amorphous carbon and the second due to the combustion of CNTs at about 537 °C [26].
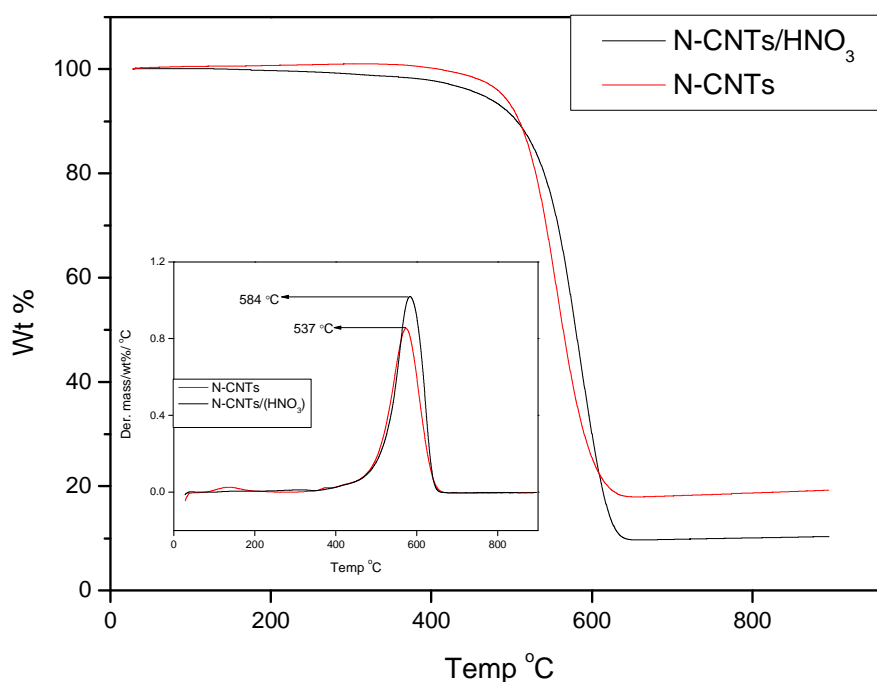
Figure 4.9. TGA of N-CNTs before and after treatment with 30 % HNO_3. Insets: DTG profile

Results also showed that there was a removal of impurities by the acid with a slight increase of thermal stability of 584 °C. The lower decomposition before acid treatment was because the presence of iron catalyses the oxidation of the CNTs.There was less than 10 wt. % residue left after treatment with acid; initially there was 20 wt. % impurities. The remaining residue might be the Fe_2O_3 metal particles trapped inside the tubes which are not easy to remove.

4.3.8   TEM of microwave and conventional method Ru/N-CNTs

Figure 4.10 and Figure 4.11 shows the TEM micrographs, histogram and the selected area electron diffraction (SAED) patterns (insets) of the Ru deposited on the N-CNTs.
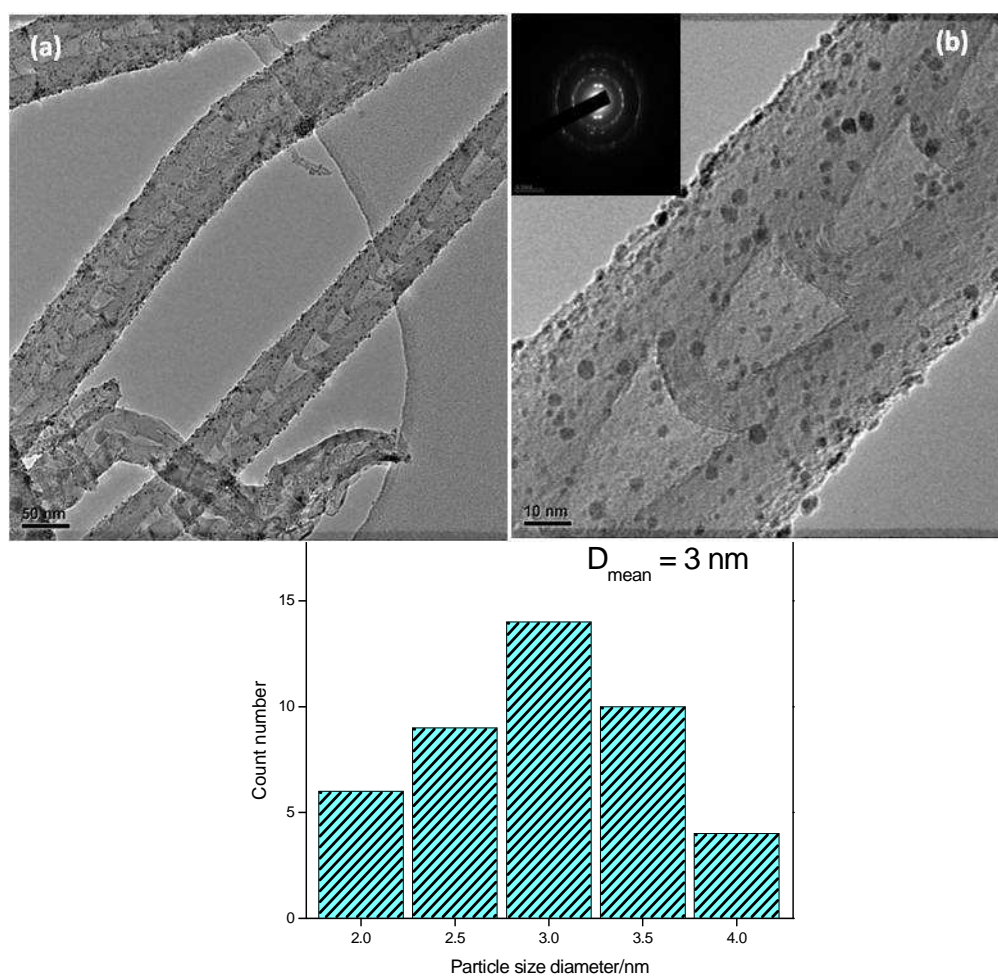
Figure 4.10. TEM images and histogram of Ru deposited on N-CNTs using microwave irradiation.

The SAED of nanoparticles shows continuous rings corresponding to the semicrystalline CNTs, collectively with some spots, which are due to the characteristics of a crystalline hexagonal Ru.

$D_{mean} = 3.5 \, nm$
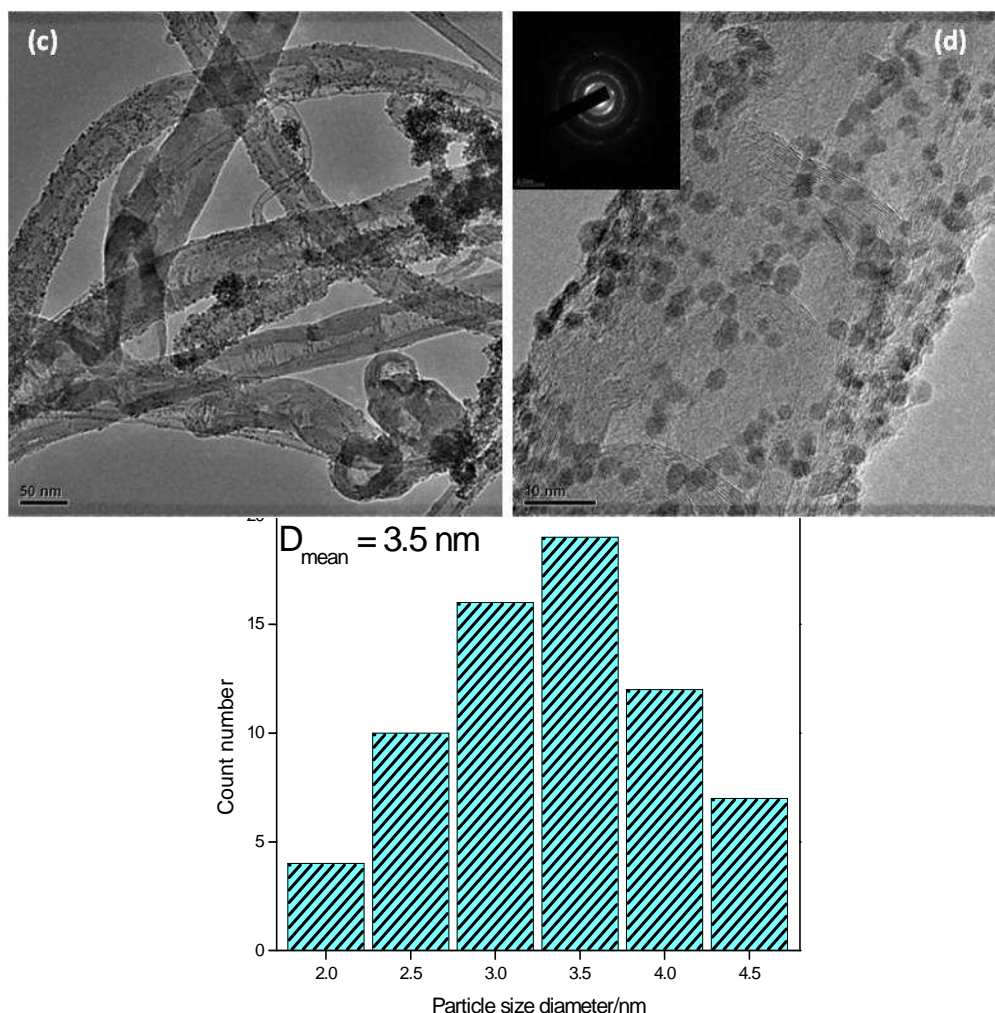
Figure 4.11. TEM images and histogram of Ru deposited on N-CNTs using conventional heating.

It is clear from the TEM image that homogenously highly dispersed particles were attached to the surface of the support with narrow size distribution ranging from 2 - 4 nm when microwave heating was used. Conventional heating also gave a good dispersion of Ru particles with a slightly bigger particle size distribution of 2 - 4.5 nm and with formation of minor metal aggregates. The average particle sizes derived from the TEM

images are 3 nm for microwave irradiation and 3.5 nm for conventional heating.

Microwave is operated under pressure. Therefore, its process is faster in comparison to conventional heating. It is accepted that the rate of reduction determines the size of the metal particle. These contribute to smaller particles without clusters. The high dielectric constant of EG also contributed to the rapid heating under microwave irradiation [13,27,28]. At the same time, good dispersion is due to the contribution of the nitrogen atoms on the network structure of the nanotubes. Nitrogen atoms entering the graphene sheets as substitutes for carbon modify the adsorption strength of the nanotube towards foreign elements which in turn, will greatly modify the overall catalytic activity as well as catalytic selectivity [18,29].

4.3.9   XRD of Ru/N-CNTs

The XRD was used to determine the presence of Ru particles for both conventional and microwave prepared Ru/N-CNTs (Figure 4.12 and Figure 4.11). The XRD pattern of N-CNTs only shows the diffraction lines of carbon at $2\theta = 26.6^o$, 54.2^o and 78.1^o which corresponds to (002), (004) and (110) plane [30]. The pattern looks similar as that of the Ru/N-CNT XRD pattern. This suggests that the sizes of the metallic Ru formed are below 4 nm or their crystal planes have becomes broader [31,32]. The average crystallite size for the Ru/N-CNT catalyst could not be measured using XRD possibly because the crystallite size in this catalyst is below the detection limit of the XRD. Or else, three reflections at around $2\theta = 38°(100)$, $42°(002)$, and $43°$ (101) assigned to the hexagonal structure of ruthenium are overlapped by the diffraction peaks of carbon at 43°.
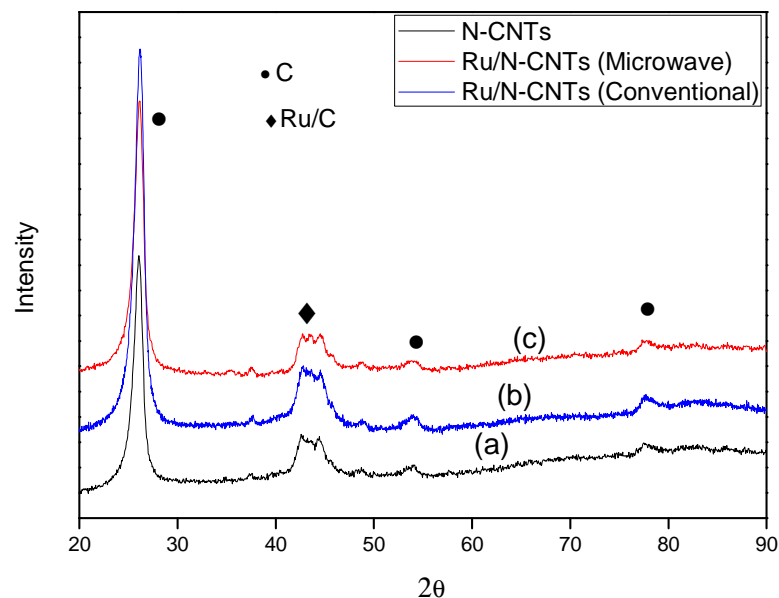
Figure 4.12. X-ray diffraction patterns for (a) N-CNTs, (b) 5Ru/N-CNTs (Conventional) and (c) Ru/N-CNTs (microwave)

The presence of Ru in the bulk of the catalyst was confirmed by EDS as presented in Figure 4.12. The Fe detected was due to the residue left during growth of the N-CNTs. Peak at 2θ of 33 and 49° indicated the presence of hematite (Fe_2O_3) phase [33].
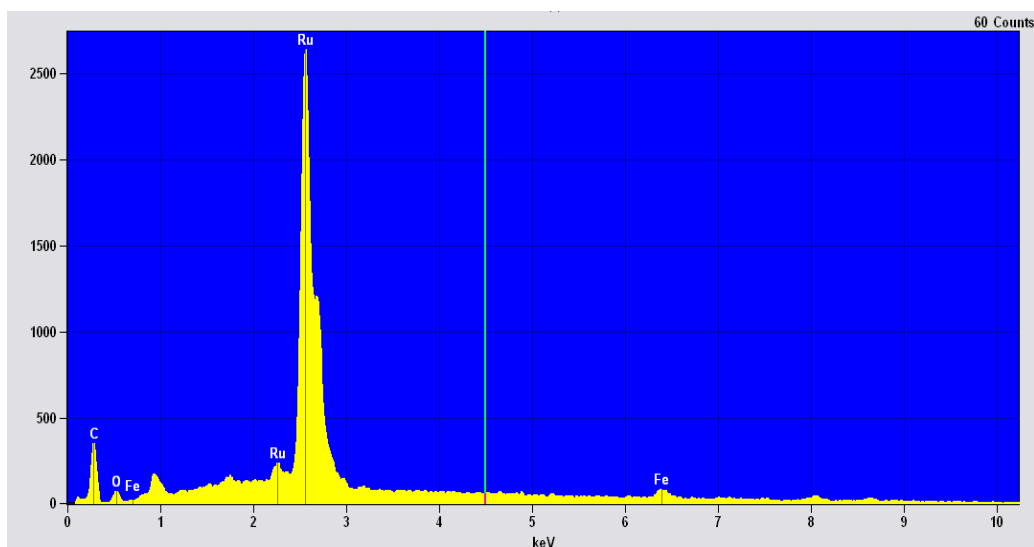
Figure 4.13. X-ray energy dispersive spectrum of 5Ru/N-CNTs.

4.4   Conclusions

The microwave-assisted reaction of $RuCl_3$ and CNTs in EG has promoted the formation and homogenous dispersion of Ru nanoparticles with very narrow size distribution and small particle size with an average diameter of 2.5, 3 and 6.2 nm for N-CNTs prepared with microwave, conventional heating and for pristine CNTs respectively. Microwave irradiation is faster and more efficient than the conventional heating as the conventional heating produced particles slightly bigger and fewer clusters are formed. The sizes of nanoparticles were optimized by varying the microwave heating power and conventional heating time. In conclusion N-CNTs are excellent supports when coupled with an efficient method of deposition.

References

1. S. Martínez-Méndez, Y. Henríquez, O. Domínguez, L. D'Ornelas, H. Krentzien, Journal of Molecular Catalysis A: Chemical 252 (2006) 226-234.

2. K. Patel, S. Kapoor, D. Dave, T. Mukherjee, Journal of Chemical Sciences 117 (2005) 53-60.

3. G.Y. Gao, D.J. Guo, H.L. Li, Journal of Power Sources 162 (2006) 1094-1098.

4. M.J. Ledoux, C. Pham-Huu, Catalysis Today 102-103 (2005) 2-14.

5. M. Sakthivel, A. Schlange, U. Kunz, T. Turek, Journal of Power Sources 195 (2010) 7083-7089.

6. A. A. Koós, M. Dowling, K. Jurkschat, A. Crossley, N. Grobert, Carbon 47 (2009) 30-37.

7. J. L. Figueiredo, M. F. R. Pereira, Catalysis Today 150 2-7.

8. M. S. Saha, R. Li, X. Sun, S. Ye, Electrochemistry Communications 11 (2009) 438-441.

9. R. I. Jafri, N. Rajalakshmi, S. Ramaprabhu, Journal of Power Sources 195 (2010) 8080-8083.

10. K. Chizari, I. Janowska, M. Houllé, I. Florea, O. Ersen, T. Romero, P. Bernhardt, M. J. Ledoux, C. Pham-Huu, Applied Catalysis A: General 380 (2010) 72-80.

11. T. C. Nagaiah, S. Kundu, M. Bron, M. Muhler, W. Schuhmann, Electrochemistry Communications 12 (2009) 338-341.

12. J.Y. Kim, K.H. Kim, S.H. Park, K.B. Kim, Electrochimica Acta 55 (2010) 8056-8061.

13. X. Li, W.X. Chen, J. Zhao, W. Xing, Z.D. Xu, Carbon 43 (2005) 2168-2174.

14 J. LU, Carbon 45 (2007). 1599-1605.

15. J. Shen, W. Huang, L. Wu, Y. Hu, M. Ye, Composites Science and Technology 67 (2007) 3041-305

16.	E. Xu, J. Wei, K. Wang, Z. Li, X. Gui, Y. Jia, H. Zhu, D. Wu, Carbon 48 (2010) 3097-3102.

17.	L. G. Bulusheva, A. V. Okotrub, I. A. Kinloch, I. P. Asanov, A. G. Kurenya, A. G. Kudashov, X. Chen, H. Song, physica status solidi (b) 245 (2008) 1971-1974.

18.	R. Chetty, S. Kundu, W. Xia, M. Bron, W. Schuhmann, V. Chirila, W. Brandl, T. Reinecke, M. Muhler, Electrochimica Acta 54 (2009) 4208-4215.

19.	B. Li, C. Wang, G. Yi, H. Lin, Y. Yuan, Catalysis Today 164 74-79.

20.	D.J. Guo, Journal of Power Sources 195 (2010) 7234-7237.

21.	S. Qiu, S. J. Kalita, Materials Science and Engineering: A (2006) 327-332.

22.	K. Ghosh, M. Kumar, T. Maruyama, Y. Ando, Carbon 48 (2010) 191-200.

23.	P. H. Matter, E. Wang, U. S. Ozkan, Journal of Catalysis 243 (2006) 395-403.

24	R. Saito, A. Grüneis, G.G. Samsonidze, V.W. Brar, G. Dresselhaus, M.S. Dresselhaus, A. Jorio, L.G. Cançado, C. Fantini, M.A. Pimenta, New Journal of Physics 5 (2003) 157.

25.	H. Li, N. Zhao, C. He, C. Shi, X. Du, J. Li, Materials Science and Engineering: A 473 (2008) 355-359.

26.	P. Ramesh, T. Okazaki, T. Sugai, J. Kimura, N. Kishi, K. Sato, Y. Ozeki, H. Shinohara, Chemical Physics Letters 418 (2006) 408-412.

27.	D. M. Han, Z. P. Guo, R. Zeng, C. J. Kim, Y. Z. Meng, H. K. Liu, International Journal of Hydrogen Energy 34 (2009) 2426-2434.

28.	W.-X. Chen, J. Y. Lee, Z. Liu, Materials Letters 58 (2004) 3166-3169.

29.	J. Amadou, K. Chizari, M. Houllé, I. Janowska, O. Ersen, D. Bégin, C. Pham-Huu, Catalysis Today 138 (2008) 62-68.

30.	R. I. Zhao, Y. Ma, J. Zhang, F. Li, W. Liu, Q. Cui, Materials Science-Poland 28 (2010).

31.   H.-B. Pan, C. M. Wai, The Journal of Physical Chemistry C 114 (2010) 11364-11369.

32.   Q.-C. Xu, J.-D. Lin, J. Li, X.-Z. Fu, Y. Liang, D.-W. Liao, Catalysis Communications 8 (2007) 1881-1885.

33.   R. M. M. Abbaslou, J. Soltan, A. K. Dalai, Applied Catalysis A: General 379 (2010) 129-134.

Section B: PART A

The catalyst performance in oxygen reaction reduction (ORR)

CHAPTER 5

RU SUPPORTED ON NITROGEN-DOPED CARBON NANOTUBES FOR THE OXYGEN REDUCTION REACTION IN ALKALINE MEDIA

5.1   Introduction

The study of fuel cells is dominated by their potential for use in portable, transport and stationary power supplies [1,2,3]. A fuel cell is a galvanic cell, in which a free energy of a chemical reaction is converted into electrical energy via an electric current. Fuel cells are mostly classified by the electrolyte used in the cell with an exception to direct methanol fuel cell (DMFC). In the DMFC methanol is electrochemically oxidised directly in the fuel cell. Fuel cell can also grouped by the operating temperature used; low temperature cells operate ≤ 500 °C and high temperature cells operate from 500 - 1000 °C (Table 5.1) [4,5].

Table 5.1. The types of fuel cells

Low temperature
Alkaline fuel cells (AFC)
Proton exchange membrane fuell cells (PEMFC)
direct methanol fuel cell (DMFC)
Phosphoric acid fuel cell (PAFC)
High temperature
Molten carbonate fuel cell (MCFC)
Solid oxide fuel cell (SOFC)

Fuel cell consists of anode where the hydrogen reaction occurs and a cathode where the oxygen reduction occurs [6]. Figure 5.1 shows a typical hydrogen/oxygen fuel cell.

Cathode: $O_2 + 2H_2O + 4e^- \rightarrow 4OH^-$

Anode: $2H_2 + 4OH^- + 4e^-$

Overall: $O_2 + H_2 \rightarrow 2H_2O$
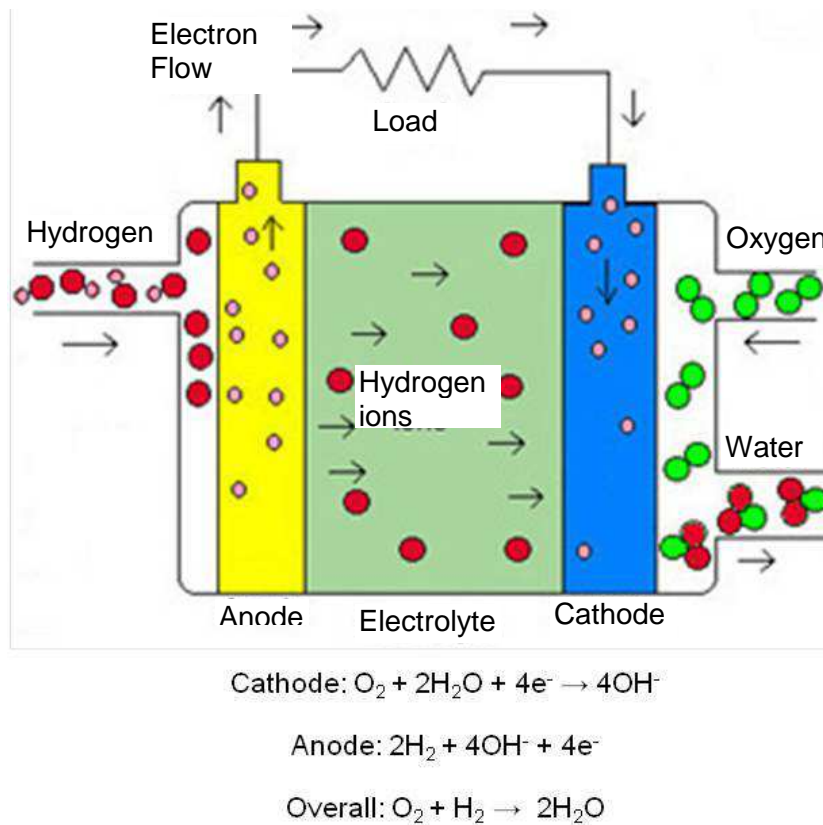
Figure 5.1. Diagram showing the fundamentals of a fuel cell [6]

The oxygen reduction reaction (ORR) at the cathode in the fuel cells plays an important role in controlling the performance of a fuel cell but the poor kinetics of the ORR hinders this performance. The catalytic ORR has attracted increasing attention in alkaline media due to faster kinetics than found in acidic media [3,7,8,9,10]. Another benefit is the improved materials stability afforded by the use of alkaline electrolytes. Very few electrode materials are stable in strongly acidic conditions, especially under the strongly oxidizing conditions found at oxygen cathodes. On the

contrary, a wider range of materials is stable in alkaline solutions, including some less expensive materials [11].

In alkaline media, the ORR proceeds by two different pathways: the oxygen within the solution can diffuse to the surface of the electrode and react to form a hydroxyl ion through a four-electron reaction,

$$O_2 + 2H_2O + 4e^- \leftrightarrow 4OH^- \tag{1}$$

The reaction can also produce H_2O_2 through a less efficient two-electron transfer pathway as illustrated in reactions (2) to (4). The oxygen is first reduced to H_2O_2 (as HO_2^-),

$$O_2 + H_2O + 2e^- \leftrightarrow HO_2^- + OH^- \tag{2}$$
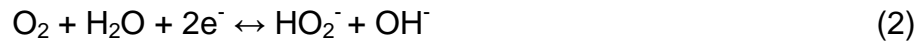
and followed by reaction

$$HO_2^- + H_2O + 2e^- \leftrightarrow 3OH^- \tag{3}$$

or the decomposition reaction

$$2HO_2^- \leftrightarrow 2OH^- + O_2 \tag{4}$$

The H_2O_2 is responsible for the deterioration of electrode performance over time as it destroys the active sites. H_2O_2 also produces the reactive intermediates that can further convert to harmful free radical species [7,12,13,14,15,16,17].

Currently platinum-based metals are the best electrocatalysts for ORR. However, due to the high cost of platinum, the large-scale synthesis and commercialisation of this electrocatalyst is problematic [3,18,19,20,21] Apart from its high cost, the Pt-based electrode also suffers from its

susceptibility to time dependent drift and CO deactivation and it is unselective [15]. For these reasons many research groups are developing non-platinum electrocatalysts that are more active, stable, and more economical [18,19,22]. This includes the development of a catalyst that can enhance effectiveness and reduce the required metal loading, and the use of a support that can increase efficiency and electrocatalytic use [23]. The support chosen for the catalyst plays an important role in fuel cell performance owing to metal support interactions and the surface reactivity [24. Recently, several researchers have shown that nitrogen modified carbon nanotubes (CNTs) are good electrocatalyst supports and that they enhance the electrocatalytic activity for the ORR [3,18,20,25,26].

Model simulations have shown that nitrogen incorporation on the CNTs provides an additional valence electron that could improve the electron donation process of graphite to oxygen, enhancing the oxygen reduction reaction efficiency [3]. The nitrogen modified CNTs are conventionally synthesised by chemical vapour deposition (CVD), laser ablation and arc discharge. The CVD method is the most commercially viable technique used to synthesise N-CNTs. This method has the advantage of high yields, and controllable growth conditions and reveals that scalability is not a problem [27]. When this support is used, generally well-dispersed metal nanoparticles with a small size distribution can be achieved [23]. The catalyst preparation conditions affect the size and the distribution of particles on the support [28,29]. A microwave-assisted polyol reduction technique shows promise for preparation of the nanoparticles on a support. Microwave irradiation allows uniform heating of metal precursors to a high temperature within a few seconds, leading to shorter crystallization times and more homogenous nucleation when compared to conventional preparation methods [30,31].

Due to the influence of N-CNTS on the ORR activities [32,33], in this study the N-CNTS have been used as support for Ru nanoparticles for improvement of the ORR activity in alkaline medium. Ruthenium as metal

electrode is known to predominately catalyse ORR to H_2O_2 rather than to H_2O [12].

The use of nitrogen modified CNTs as a support for Ru nanoparticles for the ORR in alkaline media has not been reported previously. In this chapter N-CNTs were synthesised using CVD and used as a support material for a Ru nanocatalyst. The ORR in alkaline medium was then investigated after deposition of different loadings of Ru on N-CNTs by the microwave method. These nanocatalysts showed promising results towards ORR in alkaline medium.

5.2 Experimental

5.2.1 Materials and Reagents

Cyclohexanol, ferrocene, aniline, $RuCl_3.xH_2O$, ethylene glycol (EG), HNO_3, nafion solution, and KOH, all analytical grade, were obtained from Sigma Aldrich. The N-CNTs used, with inner diameters of 5 - 10 nm and outer diameters of 30 -100 nm, were synthesised in-house (Chapter 3).

5.2.2 Synthesis of N-CNTs Synthesis

N-CNTs were synthesised using a CVD process involving a two stage furnace with cyclohexanol as the carbon source, aniline as the nitrogen source, and ferrocene as the catalyst. A mixture of ferrocene-anilline-cyclohexanol in 1:5:34 ratio (3 g) was placed in a quartz boat and directly introduced in the centre of the first furnace and vaporised at 280 °C. The resultant vapours were transferred to the second furnace where the N-CNTs were grown at a temperature of 900 °C under a nitrogen flow. The reaction was maintained at 900 °C until there was no reactant left in the tube. The furnaces were switched off and cooled down under the inert gas atmosphere. The black soot of about (ca 450 mg) was then collected from the inner wall of the quartz tube for characterisation. The collected

material was treated with 30 % (v/v) HNO$_3$ at 110 °C for 2 h, washed with acetone, then water, and was then dried in an oven at 110 °C overnight.

5.2.3   Preparation of Ru Nanocatalysts Supported on N-CNTs

Ru nanoparticles were deposited on N-CNTs using microwave assisted polyol methods. In a microwave teflon vessel, 50 mg N-CNTs and (2, 5 and 10 mg) RuCl$_3$.xH$_2$O were mixed with 80 mL EG and sonicated for 10 min to afford a homogenous suspension. Ru/N-CNT samples were thus made with different wt. % of Ru on N-CNTs and the samples were named according to the amount of Ru expected viz. 2Ru/N-CNTs, 5Ru/N-CNTs, 10Ru/N-CNTs. The suspension was then placed in a microwave reactor (Anton-Paar Multiwave 3000). The suspension was heated to 200 °C and kept at this temperature for 5 min at 500 W. The resulting suspension was filtered and the residue was washed with 20 mL acetone, then with 50 mL deionised water and dried at 110 °C overnight.

5.2.4   Characterization of Ru/N-CNTs Nanocatalysts

The transmission electron microscopy (TEM) analysis was performed using a JEOL 2100 microscope with beam energies of 200 kV. TEM was used to analyse the particle size and distribution of the prepared catalysts. The presence of the amorphous carbon and residual catalyst particles on the N-CNTs was also observed with the TEM technique. The samples for TEM analysis were prepared by sonicating about 0.5 mg of CNTs in 5 mL methanol for 5 min. A drop of the suspension was cast onto the carbon film covered Cu grid for analysis. The morphology of the N-CNTs was observed using a LEO 1525 FE-SEM. The scanning electron microscope (SEM) was equipped with energy dispersive spectroscopy (EDS) attachment, which was used for elemental analysis. The amount of Ru supported on the N-CNTs was quantified using inductively coupling plasma (ICP) spectroscopy (Spectro-Acros). A PANalytical X'PERT-PRO diffractometer with a Cu-Kα (λ =0.15405 nm) radiation source operated at

40 kV and 50 mA at 0.026 step size was utilized to study the crystallinity of the prepared catalysts.

5.2.5 Electrocatalytic Evaluation of Ru/N-CNTs Nanocatalysts

A nanocatalyst ink was prepared by ultrasonically dispersing 0.025 g of the nanocatalyst powder in 2.5 mL deionized water to which 0.25 mL of 5 wt% Nafion solution was added. After 30 min, 2 μL of the ink was pipetted onto a polished glassy carbon (GC) disk electrode with an area of 0.0314 cm^2, air dried for 30 min, and then heated at 95 °C for 15 min to remove the solvents. The electrocatalytic activity of as prepared catalyst for oxygen reduction was performed in a 0.5 M KOH oxygen saturated solution using a standard three-electrochemical cell at 25 ^{o}C. The cell was composed of a double junction Ag/AgCl reference electrode, platinum rod as counter electrode and glassy carbon modified with the catalyst as the working electrode. The potential of the working electrode was varied from -1.0 to 0.2 V vs. Ag/AgCl with a potential sweep rate of 10 mV/s. Using an Autolab potentiostat PGSTAT 302 (Eco Chemie, Utrecht, Netherlands) driven by General Purpose Electrochemical Systems data processing software (GPES) and FRA software version 4.9. Electrocatalytic activity was assessed using a rotating disk electrode (RDE) at different speed rotations. The solution was purged through the cell with nitrogen gas (99.99 %, Air Liquide) for 60 min and thereafter it was saturated with oxygen (99.99%, Air Liquide). All solutions were prepared with deionised water of resistivity not less than 18.2 MΩ cm.

5.3 Results and discussion

5.3.1 Structural characterization

Figure 5.2 shows the SEM and TEM images of the N-CNTs produced by the CVD method. The TEM images in different spots were used to estimate the average percentage of N-CNTs and armophous carbon in bulk material. The material produced was composed of an average of 90 % N-CNTs and 10 % amorphous carbon.
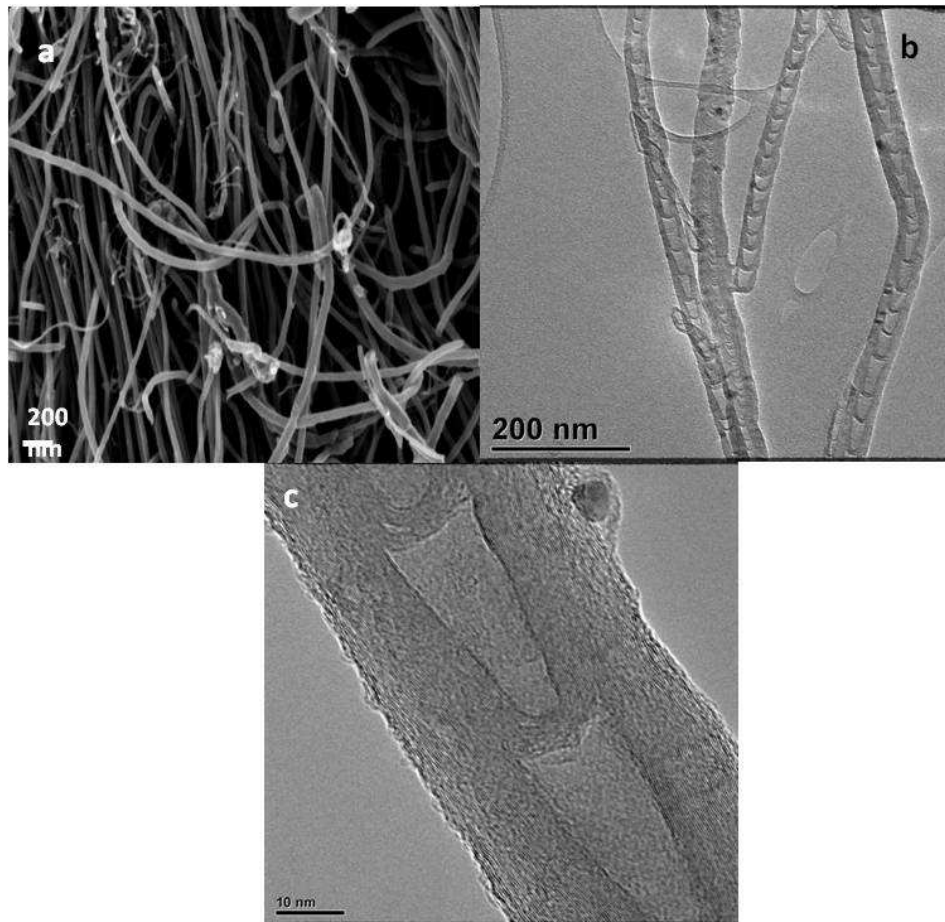
Figure 5.2. (a) Scanning electron microscope image of the N-CNTs, (b) and (c) high-resolution transmission electron microscope images of the N-CNTs at two different magnifications

The diameters of the tubes were in the range 30 - 100 nm with approximate lengths of 17 µm. The TEM image displays the characteristic bamboo-like morphology of N-CNTs commonly reported in the literature [26,34].

The formation of the compartment resulted from the pentagon structures in the graphite network due to the presence of nitrogen [20]. Nitrogen incorporated in the graphite network is not only important for the ORR activity but also for the attachment of the metal particles to the surface of the support. The nitrogen atom has an extra electron compared to carbon and the surface of the N-CNTs is expected to be more electronegative than the CNT surface [30]. This results in N-CNTs possessing high surface nucleation sites, which allow for the anchorage and high dispersion of the metal active phase on the support surface. The Ru/N-CNT catalysts were prepared using the polyol method in a microwave oven. The advantage of the microwave technique is that the resulting Ru nanoparticle size is small and the distribution is narrow and uniform.

The TEM images of the 2 - 10 wt. % Ru deposited on N-CNTs and the selected area electron diffraction (SAED) pattern (insets) are shown in Figure 5.2. The SAED of nanoparticles shows continuous rings corresponding to the semicrystalline CNTs, collectively with some spots, which are due to the characteristics of a crystalline Ru hexagonal structure. It follows from Stoe & Cie [35], (IPDS Software) that the lattice spacing 2.08 Å corresponds to the (101), and the lattice spacing 1.24 Å is diffraction line of (103) Ru. While 3.43 Å is due to the (002) carbon plane. Selected areas of the SAED electron diffraction patterns in Fig 5.3 confirm the presence of hexagonal Ru phase and carbon.
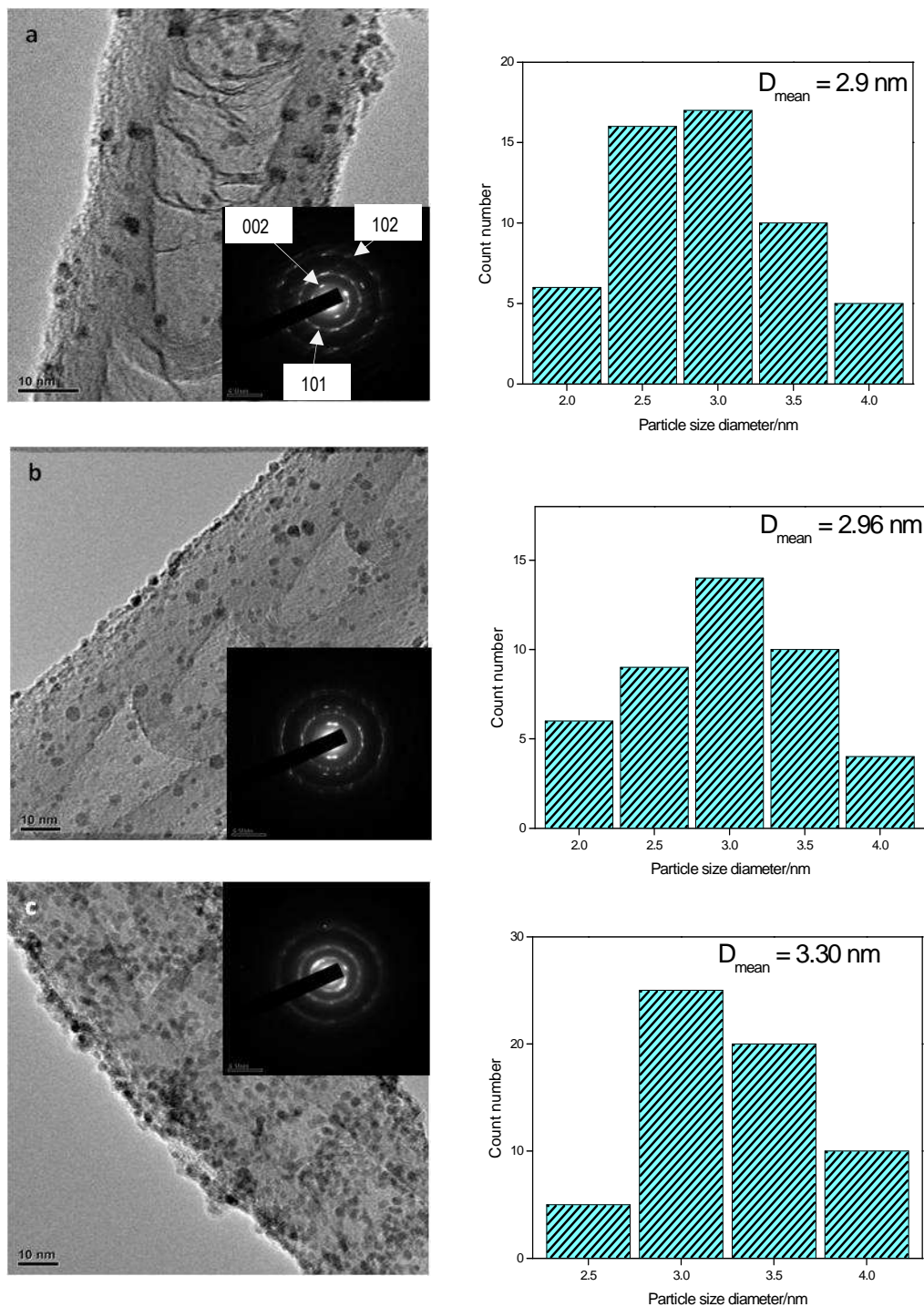
Figure 5.3. Transmission electron microscopic images and corresponding diameter histogram of (a) 2Ru/N-CNTs, (b) 5Ru/N-CNTs, and (c) 10Ru/N-CNTs. Insets shows the selected area electron diffraction.

TEM images reveal a good dispersion of nanoparticles on the surface of the N-CNTs which could be attributed to the combination of preparation technique and the active sites created by nitrogen doping [36,25]. Although the metal loading varied from 2 - 10 wt. % the particle sizes were between 2 - 4 nm for all the loadings. The histograms express a slight shift of particle sizes to a bigger particle size with the increase in Ru loading. The Ru nanoparticles show the mean sizes of 2.9 (Figure 5.3a), 3.0 (Figure 5.3b) and 3.3 nm (Figure 5.3c) for 2, 5, and 10 wt. % loading, respectively. Moreover, Ru particles on the wall surface of the N-CNTs also increased with the increase of the loading. ICP was used to determine the amount of metals in the material (Table 5.2). The Fe (< 0.2 %) is due to the catalyst, formed from ferrocene. The Ru loading obtained from ICP agrees with the loading used in the preparation method.

Table 5.2. Metal loading on the N-CNTs obtained using ICP

Catalyst	Ru loading wt.%	Fe %
2Ru/N-CNTs	2.13	< 0.2
5Ru/N-CNTs	5.20	< 0.2
10Ru/N-CNTs	9.97	< 0.2

Error= 0.1

XRD was used to determine the crystalline nature of the catalyst as shown in Figure 5.4. The XRD pattern only shows the diffraction lines of carbon at $2\theta = 26.6^{o}$, 54.2^{o} and 78.1^{o} which corresponds to (002), (004) and (110) plane. The spectra looked the same irrespective of the amount of Ru deposited on the N-CNTs; no signals were observed for Ru due to the small size of the metallic Ru formed (below 4 nm) [37]. The sizes of the ruthenium particles are very small and are outside the detection limit of the diffractometer. XRD detects the sizes above 4 nm. Moreover, there is little amount of ruthenium on N-CNTs. The combination of small amount and

small size of Ru particles contributed to no signal. Further, the Ru (101) is approximately at $2\theta = 43$ and it overlaps with the C peak [38].
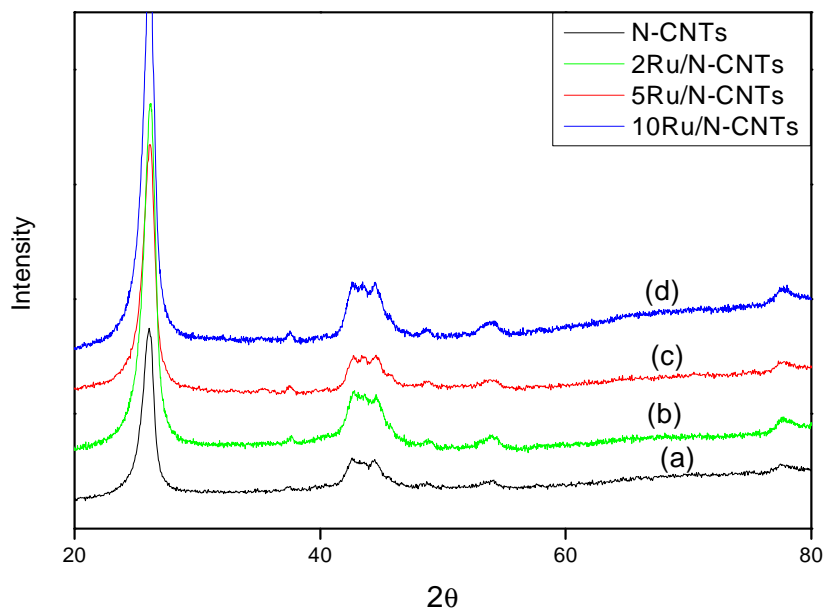
Figure 5.4. X-ray diffraction patterns for (a) N-CNTs, (b) 2Ru/N-CNTs (c) 5Ru/N-CNTs and (d) 10Ru/N-CNTs

The presence of Ru in the bulk of the catalyst was confirmed by EDS as presented in Figure 5.5.
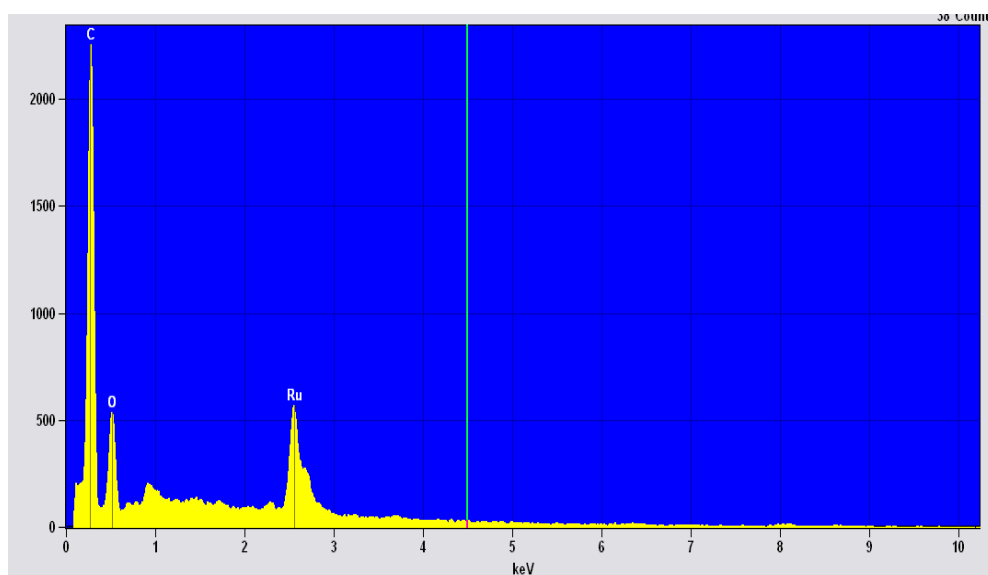
Figure 5.5. X-ray energy dispersive spectrum of 5Ru/N-CNTs

5.3.2   Electrochemical Evaluation

Cyclic voltammograms (CV) measured for glassy carbon, N-CNTs, 2Ru/N-CNTs, 5Ru/N-CNTs and 10Ru/N-CNTs in nitrogen, are shown in Figure 5.6.
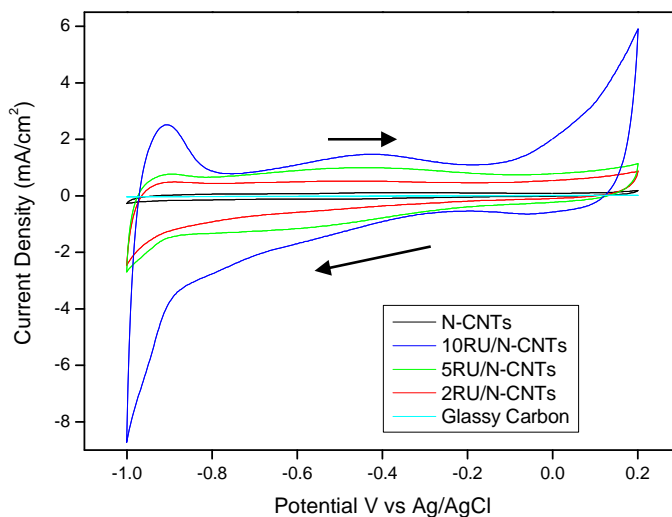
Figure 5.6. Cyclic voltammograms of the Ru/N-CNT catalysts in nitrogen saturated 0.5 M KOH solution. Scan rate 10 mV/s.

The CV data gave the expected signatures of Ru in alkaline medium. There are no signals from the glassy carbon which confirms that there is no activity from the glassy carbon. There are also no clear redox features observed with the N-CNTs which suggest that any metal catalyst residue that remained from the CVD synthesis had no effect on the activity of Ru [19]. The current density of the Ru/N-CNTs increased with an increase in Ru content.

5.3.3   Oxygen reduction reaction

Rotating Disk Electrode (RDE) experiments were conducted at six different rotation speeds: 500, 1000, 1500, 2000, 2500, and 3000 rpm in alkaline medium. The activity of the prepared N-CNTs towards the reduction of oxygen in alkaline electrolyte was compared to that of commercial CNTs without N using the onset potential at 1500 rpm. The onset potential of commercial CNTs was more negative at -0.184 V while that of N-CNTs

was more positive at -0.144 V thus indicating improved ORR kinetics on N-CNTs than on the commercial CNTs. For this reason the study focused on the activity of a range of Ru/N-CNTs materials. Figure 5.7 compares the linear sweep voltammetry (LSV) data for the N-CNTs, 2Ru/N-CNTs, 5Ru/N-CNTs and 10Ru/N-CNTs in an oxygen saturated solution at 1500 rpm. The addition of Ru on the N-CNTs slightly shifted the onset potential to more positive values. The glassy carbon current density was close to 0 mA/cm^2 which confirms that glassy carbon is not contributing to the activity in ORR. The current density of 3.57 mA/cm^2 was observed for the N-CNTs. A current density plateau was attained when the Ru loading on the N-CNTs was between 2 and 10 wt %. All the catalysts were active towards the ORR in alkaline electrolyte. The current density was higher at 8.03 mA/cm^2 on 2Ru/N-CNTs and decreased to 7.53 and 4.79 mA/cm^2 for 5Ru/N-CNTs and 10Ru/N-CNTs, respectively.
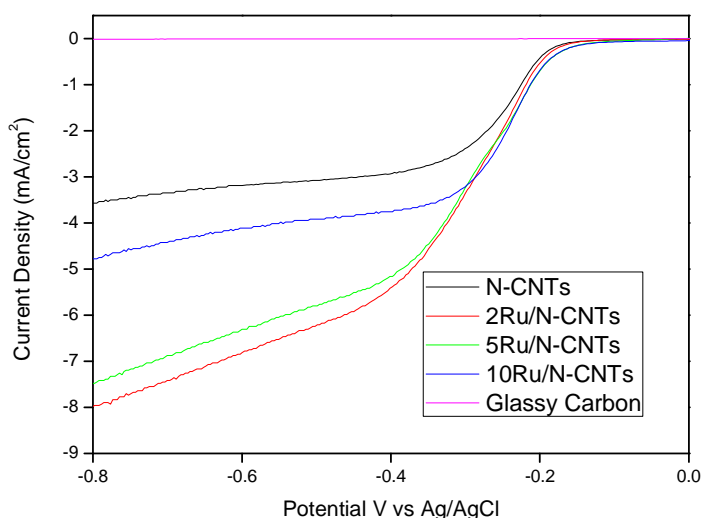
Figure 5.7. Rotating disk electrode (RDE) linear sweep voltammograms of the Ru/N-CNT catalysts in oxygen-saturated 0.5 M KOH solution. Scan rate 10 mV/s at 1500 rpm.

The diffusion limitation of oxygen from the electrolyte to the electrode surface area played a role in the system. The decrease in the current density with an increase in Ru content suggested that besides the external

diffusion limitation of oxygen from the bulk electrolyte to the electrode surface, a second mass transfer limitation within the catalyst layer is involved. This mass transfer within the catalyst layer, results in a higher hindrance effect with an increase in Ru loading [39].

Figure 5.8 shows the potentiodynamic ORR curves and the polarisation curves of the prepared nanocatalysts at different rotation rates (500 - 3000 rpm). Three distinct characteristic regions of ORR processes that take place on the surface of the catalyst can be seen: 1) the kinetic region (E > -0.25), where the current is independent of the rotation velocity; 2) the mixed control region (-0.45< E < -0.25), where kinetics and the diffusion processes determine the behaviour; 3) the mass transfer region (E < -0.45), where the diffusion current is a function of the rotation velocity [9,40]. The cathodic current increase is due to the increase of the oxygen available at the surface of the electrode due to the rotation. The current density increased with an increase in the rotation speed; and the onset potential remained the same for all rotations.

The (Koutecky–Levich) K-L plots obtained from the polarisation curves were used to calculate the number of electrons exchanged per oxygen molecule. The first-order Koutecky–Levich expression, shown below, was used:

$$\frac{1}{i} = \frac{1}{i_k} + \frac{1}{i_d} \tag{5}$$

where i_k is the kinetic current density, i the observed current density and i_d is the diffusion limiting current density controlled by the mass transfer of oxygen in the solution as expressed in equation 6:

$$\frac{I_d}{A} = i_d = 0.21 nFD_{O_2}^{2/3} \upsilon^{-1/6} C_{O_2} \omega^{1/2} \tag{6}$$

where n is the number of electrons transferred, F is the Faraday constant (96485 C mol^{-1}), D_O is the diffusion coefficient of O_2 (1.68 x 10^{-5} cm^2.s^{-1}) [7], v is the kinematic viscosity of the electrolyte solution (1.1 x 10^{-2} cm^2.s^{-1}), C_O is the dissolved oxygen concentration in the electrolyte solution (1.031 x 10^{-6} mol.L^{-1}) and ω is the rotation rate in rpm [7,10,41,42].
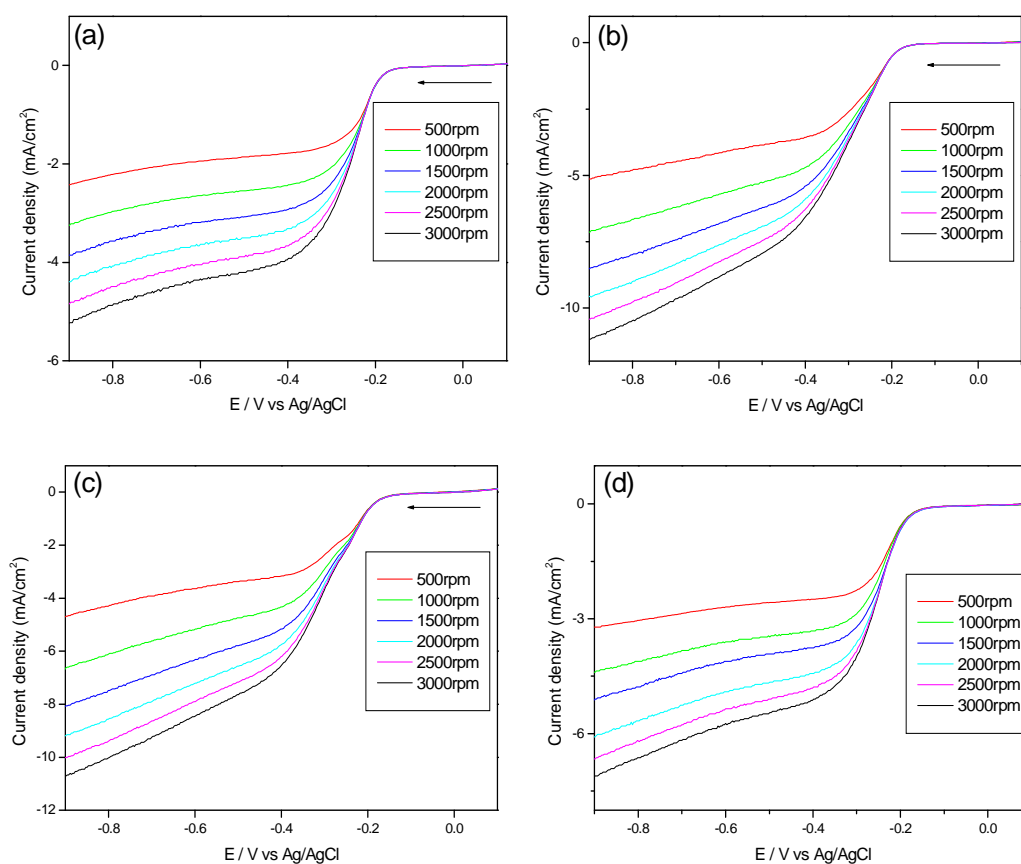
Figure 5.8. Rotating disk electrode (RDE) polarization curves at different rotation rates for (a) N-CNTs), (b) 2Ru/CNTs, (c) 5Ru/N-CNTs, and (d) 10 Ru/N-CNTs

The K-L plots of the N-CNTs, 2Ru/N-CNTs, 5Ru/N-CNTs and 10Ru/N-CNTs samples are shown in Figure 5.9. They all have similar slopes which is an indication of first-order reaction kinetics for the ORR

[41]. The linearity of the K-L slope also shows that the reaction order was unity for the electrode with respect to O_2 [43].
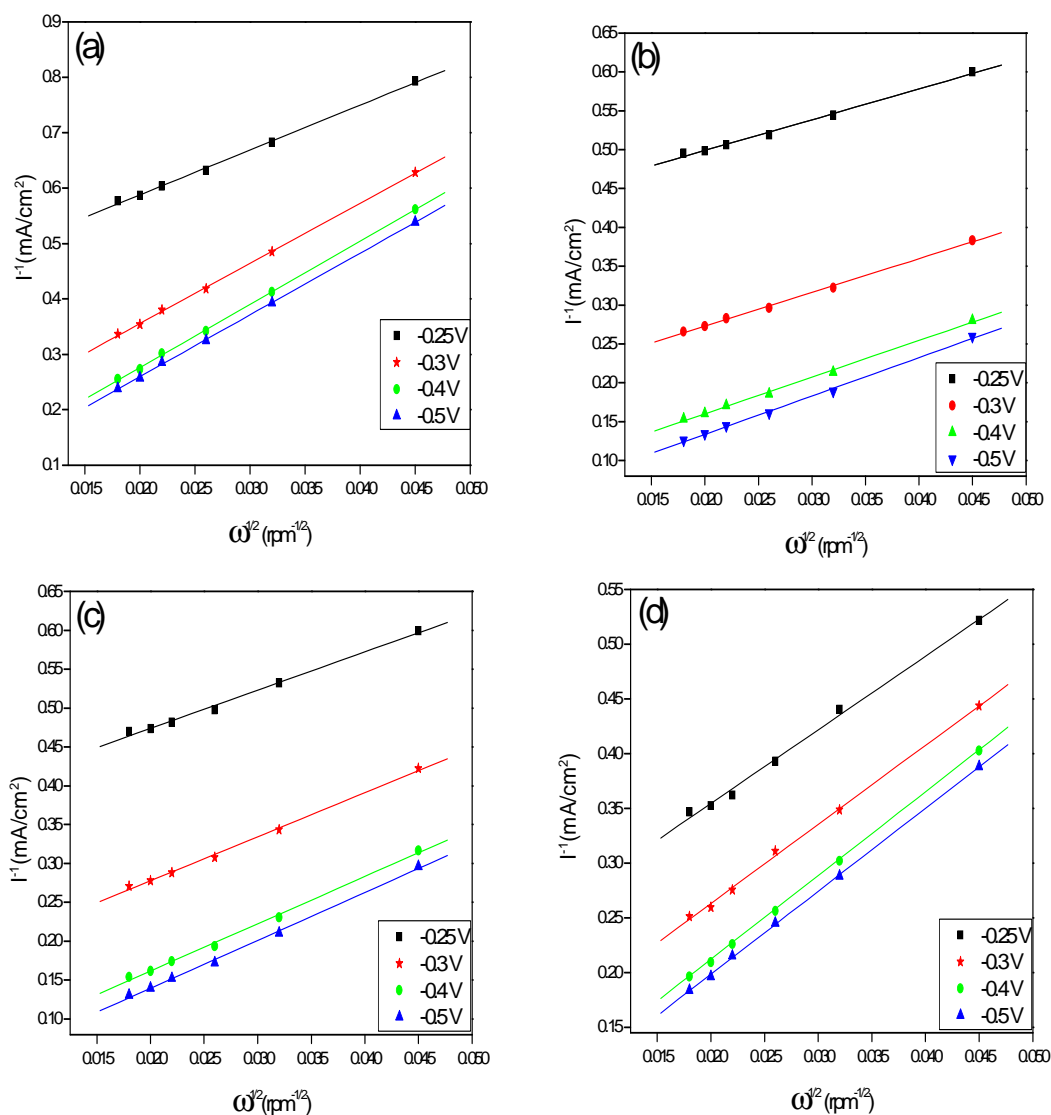
Figure 5.9. Koutecky-Levich plots for: (a) N-CNT, (b) 2Ru/CNT, (c) 5Ru/N-CNT, and (d) 10Ru/N-CNT.

From the slope of the K-L equation, and using equation 6, the number of electrons transferred per oxygen molecule was calculated (Table 5.3).

Table 5.3. Summary of the important activity indicator of ORR

Electrode	Onset potential V	No of electron transferred at (1500 rpm, -0.30V)	Limiting current density (mA/cm^2)
N-CNTs	-0.166	2.4	-2.95
2Ru/N-CNTs	-0.158	3.9	-4.76
5Ru/N-CNTs	-0.153	3.7	-4.54
10Ru/N-CNTs	-0.148	3.2	-3.66

The n value of 2.4 and 3.2 for N-CNTs and 10Ru/N-CNTs respectively, lies between 2 and 4, which indicates that the electrocatalytic ORR on the nanocatalyst surface involves mixed 2e- and 4e- reduction processes [44]. 2Ru/N-CNTs and 5Ru/N-CNTs nanocatalysts showed the oxygen within the solution diffuse to the surface of the electrode and react to form a hydroxyl ion through a four-electron reaction. With the increase of the loadings from 2 - 5 and 10 wt. % the n value decreases to 3.7 and 3.2, respectively. This might be due to the formation of the isolated metallic Ru particles, since isolated 3d transition metals tend to produce H_2O_2, thereby causing a low n value [9]. The ORR activity thus appears to depend on the concentration of the ruthenium on the support. The higher the concentration the more the particles and the closer they get to each other as seen in the TEM image in Figure. 5.3. Thus might create a hindrance effect that will affect the interaction of the oxygen with the ruthenium.

5.4   Conclusions

In this study the electrochemical activity of ruthenium deposited on N-CNT nanocatalysts, prepared *via* a CVD technique associated with a microwave assisted deposition, was examined. The Ru nanoparticles of mean diameter of 2.9 - 3.3 nm were uniformly distributed on the N-CNT surface. Due to their increased nanocatalyst activity N-CNTs appear to be a promising potential support material for Ru nanoparticles for ORR in

alkaline media. The 4 electron reaction of ORR was found to be more favourable on 2Ru/N-CNTs and 5Ru/N-CNTs. The lower loading of Ru metal nanoparticles on the 2Ru/N-CNT catalyst proved to give a better catalyst, which makes it a potential material for the ORR catalysis in fuel cells in alkaline media.

References

1.   M. Simões, S. Baranton, C. Coutanceau, Applied Catalysis B: Environmental 93 (2009) 354-362.

2.   B. Li, J. Prakash, Electrochemistry Communications 11 (2009) 1162-1165.

3.   Z. Chen, D. Higgins, Z. Chen, Electrochimica Acta 55 (2010) 4799-4804.

4   L. Carrette, K. A. Friedrich, and U. Stimming, Fuel Cells 1 (2001) 5

5   L. Carrette, K. A. Friedrich, and U. Stimming, ChemPhysChem 1 (2000) 162.

6.   F. Bidault, D. J. L. Brett, P. H. Middleton, N. P. Brandon, Journal of Power Sources 187 (2009) 39-48.

7.   H. Li, H. Liu, Z. Jong, W. Qu, D. Geng, X. Sun, H. Wang, International Journal of Hydrogen Energy 36 (2010) 2258-2265.

8.   K. Scott, E. Yu, G. Vlachogiannopoulos, M. Shivare, N. Duteanu, Journal of Power Sources 175 (2008) 452-457.

9.   Q. He, X. Yang, X. Ren, B. E. Koel, N. Ramaswamy, S. Mukerjee, R. Kostecki, Journal of Power Sources 196 (2011) 7404-7410.

10.   J. Kim, T. Momma, T. Osaka, Journal of Power Sources 189 (2009) 909-915.

11.   L. Jiang, A. Hsu, D. Chu, R. Chen, Journal of Electroanalytical Chemistry 629 (2009) 87-93.

12.   J.-W. Lee, B. Popov, Journal of Solid State Electrochemistry 11 (2007) 1355-1364.

13.   B. Wang, Journal of Power Sources 152 (2005) 1-15.

14.   P. A. Christensen, A. Hamnett, D. Linares-Moya, Physical Chemistry Chemical Physics 13 (2010) 5206-5214.

15.   K. Gong, F. Du, Z. Xia, M. Durstock, L. Dai, Science 323 (2009) 760-764.

16.   W. Jin, H. Du, S. Zheng, H. Xu, Y. Zhang, The Journal of Physical Chemistry B 114 (2010) 6542-6548.

17. F. Wang, S. Hu, Journal of Electroanalytical Chemistry 580 (2005) 68-77.

18. S. A. Mamuru, K. I. Ozoemena, Electrochemistry Communications 12 (2010) 1539-1542.

19. T. C. Nagaiah, S. Kundu, M. Bron, M. Muhler, W. Schuhmann, Electrochemistry Communications 12 (2009) 338-341.

20 Z. Chen, D. Higgins, Z. Chen, Carbon 48 (2010) 3057-3065.

21. A. Altamirano-Gutiérrez, O. Jiménez-Sandoval, J. Uribe-Godínez, R. H. Castellanos, E. Borja-Arco, J. M. Olivares-Ramírez, International Journal of Hydrogen Energy 34 (2009) 7983-7994.

22. G. Liu, H. Zhang, J. Hu, Electrochemistry Communications 9 (2007) 2643-2648.

23. S.-Y. Ang, D. A. Walsh, Journal of Power Sources 195 (2010) 2557-2563.

24. V. Selvaraj, M. Vinoba, M. Alagar, Journal of Colloid and Interface Science 322 (2008) 537-544.

25. Y. Chen, J. Wang, H. Liu, R. Li, X. Sun, S. Ye, S. Knights, Electrochemistry Communications 11 (2009) 2071-2076.

26. D. Higgins, Z. Chen, Z. Chen, Electrochimica Acta 56 (2010) 1570-1575.

27. L. Mabena, S. Sinha Ray, S. Mhlanga, N. Coville, Applied Nanoscience 1 (2011) 67-77.

28. A. N. Golikand, M. Asgari, E. Lohrasbi, International Journal of Hydrogen Energy 36 (2011) 13317-13324.

29. A. B. Kashyout, A. B. A. A. Nassr, L. Giorgi, T. Maiyalagan, B. A. B. Youssef, International Journal of electrochemical science 6 (2011) 379 - 393.

30. Y.-Y. Chu, Z.-B. Wang, D.-M. Gu, G.-P. Yin, Journal of Power Sources 195 (2010) 1799-1804.

31. Z. Guo, Y. Chen, L. Li, X. Wang, G. L. Haller, Y. Yang, Journal of Catalysis 276 (2010) 314-326.

32.   J. D. Wiggins-Camacho, K. J. Stevenson, Environmental Science & Technology 45 (2011) 3650-3656.

33.   Z. Zhu, J. Wang, A. Munir, H. S. Zhou, Electrochimica Acta 55 (2010) 8517-8520.

34.   E. N. Nxumalo, P. J. Letsoalo, L. M. Cele, N. J. Coville, Journal of Organometallic Chemistry 695 (2010) 2596-2602.

35   Stoe & Cie. IPDS Software. Stoe & Cie GmbH, (2000) Darmstadt, Germany.

36.   P. Ayala, R. Arenal, M. Rümmeli, A. Rubio, T. Pichler, Carbon 48 (2009) 575-586.

37.   H.B. Pan, C. M. Wai, The Journal of Physical Chemistry C 114 (2010) 11364-11369.

38.   Q.C. Xu, J.D. Lin, J. Li, X.Z. Fu, Y. Liang, D.W. Liao, Catalysis Communications 8 (2007) 1881-1885.

39.   D. Geng, H. Liu, Y. Chen, R. Li, X. Sun, S. Ye, S. Knights, Journal of Power Sources 196 (2010) 1795-1801.

40.   E. Borja-Arco, O. J. Sandoval, J. Escalante-García, A. Sandoval-González, P. J. Sebastian, International Journal of Hydrogen Energy 36 (2011) 103-110.

41.   Z. Chen, D. Higgins, H. Tao, R. S. Hsu, Z. Chen, The Journal of Physical Chemistry C 113 (2009) 21008-21013.

42.   C N. W. Maxakato, S. A. Mamuru, K. I. Ozoemena Electroanalysis 23 (2010) 325-329.

43.   S. A. Mamuru, K. I. Ozoemena, Electroanalysis 22 (2010) 985-994.

44.   M. Maye, N. Kariuki, J. Luo, L. Han, P. Njoki, L. Wang, Y. Lin, H. Naslund, C. Zhong, Gold Bulletin 3-4 (2004) 217-223.

Part B:

Oxidation of styrene and benzyl alcohol

CHAPTER 6

SUPPORTED RUTHENIUM CATALYSTS FOR THE OXIDATION OF STYRENE

6.1   Introduction

Styrene is a molecule that has a terminal olefin linked to an aromatic ring and is used to make polystyrene [1]. An alternative reaction to the styrene polymerisation reaction is the olefin double bond oxidation reaction which gives a substituted benzene product. The products from the oxidation of the double bond have been utilized in industry. As a result there is much interest in the oxidative conversion of styrene to benzaldehyde [2,3,4]. It is known that styrene oxidation at the side chain can lead to various reaction products which depend on the catalysts and reaction conditions [5,6]. For instance, styrene oxide and phenyl acetaldehyde were the main products formed when peroxide is used as oxidant and titanium doped silicate molecular sieves were used as catalyst [7,8]. Benzaldehyde was obtained when niobium and other transition metals were co-doped on mesoporous support materials [3].

Mechanistic studies have suggested that the reaction could occur in a stepwise manner or occur by a stepwise branch pathway with an intermediate that generates by-products. The formation of benzaldehyde can occur via two pathways [2,9] as shown in scheme 1. In the first pathway benzaldehyde is formed by nuleophilic attack of hydrogen peroxide (H_2O_2) on styrene oxide (route 2), followed by cleavage of the intermediate hydroxy-hydroperoxistyrene (route 3). In the second pathway, radical cleavage of the styrene side chain double bond takes place (route 1) [9,10]. Various competing reaction pathways that follow the formation of

the styrene oxide lead to the production of phenylacetaldehyde (route 4), benzoic acid (route 5) and phenylacetic acid (route 6). Phenylacetic acid and benzoic acid are derived via the nucleophilic attack of oxygen atoms at the electron-deficient carbonyl carbon [11].
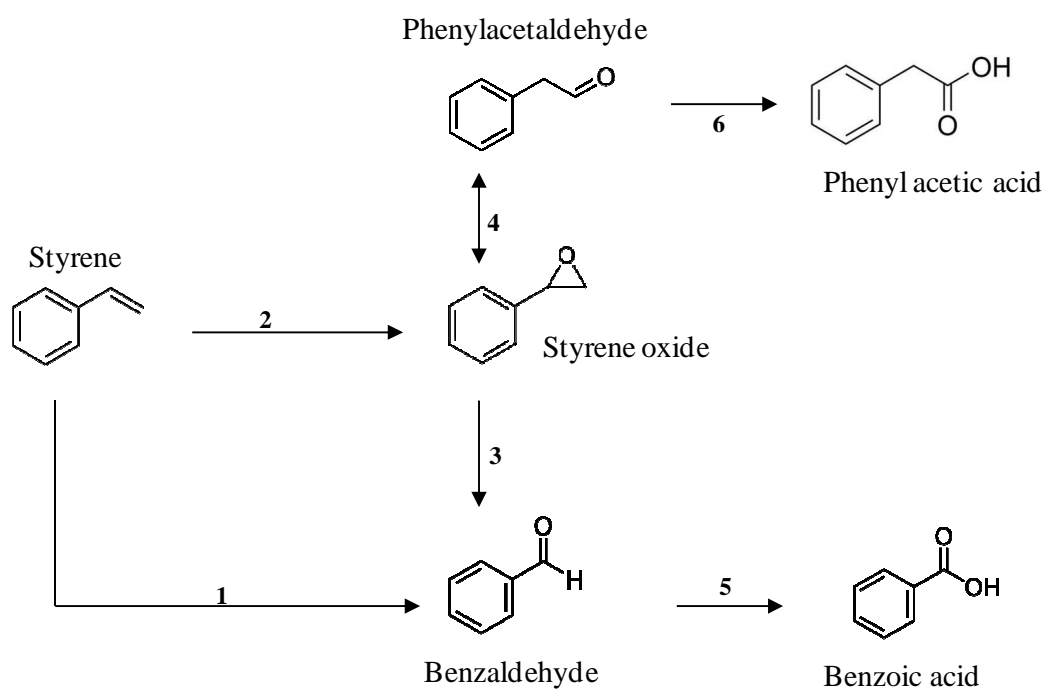
Scheme 6.1. Reaction products obtained in the oxidation of styrene

Traditionally when homogenous catalysts are used styrene is oxidised by peracid and stoichiometric amounts of reactants are used. However, peracids are very expensive, corrosive and dangerous to handle. Even though homogenous catalysts give high yields, the use of homogenous catalysts requires separation of reactants and catalyst from the desired product and separation of the products at the end of the reaction [12,13]. Due to the ease in separation, recovery and recycling, continuous processing of heterogeneous catalysts have advantages over homogenous catalysts. Further, solid supported catalysts

(heterogeneous catalysts) are considerably cheaper and environmentally more friendly [2,14,15]. Organic peroxides and hydrogen peroxide can be used as oxidants for the oxidation of the olefins when heterogeneous catalysts are used [16]. A major goal in this area of catalysis is to use hydrogen peroxide as an oxidising agent in the reaction because it is environmentally acceptable and its by-product is water [17].

The oxidation of styrene has been reported to be carried out using different oxidants over doped transition metals catalysts on different supports; these include: microporous or mesoporous molecular sieves [3,6,18,19] zeolites [20,21,22,] carbon materials [23], and polymers [24]. Silver [25,26,27,28], palladium [29] and gold [13,23,30,31] are the supported transition metals that have been used, mainly for styrene oxidation. Hulea et al., [9] investigated the oxidation of styrene by H_2O_2 over Ti-containing molecular sieves. The product distribution from the styrene oxidation depended on the nature of the catalyst. The selectivity to phenylacetaldehyde was very high for all catalysts with a small pore opening, while benzaldehyde selectivity was high when Ti-containing catalysts had large pores. Ti-containing molecular sieves were earlier used by Laha et al. [32]. In the study by Laha, the results obtained using urea-hydrogen peroxide (UHP) as oxidant were compared with those obtained with H_2O_2 under the same conditions. Styrene oxide was a major product when the UHP oxidant was used while benzaldehyde selectivity was favoured when H_2O_2 was used as oxidant. Zeolites (ZSM-5) showed good performance when modified with a series of transition metals. A chromium on zeolite catalyst was found to be the most active of all the metal-ZSM-5 catalysts evaluated (cobalt, chromium, iron, zinc, manganese, and copper) when hydrogen peroxide was used as oxidant. High benzaldehyde selectivity was obtained [2]

Today carbon nanotubes (CNTs), due to their unique chemical and physical properties, are extensively studied as catalyst supports. Theoretical studies of the CNT supports indicate that a site-specific

support-material interaction can be present, which is the result of the bending of graphene sheets in CNTs. This CNT effect plays an important role in heterogeneous catalysis because it allows tuning of the catalytic properties through use of the structure of the support material [33]. Moreover, CNT properties can be manipulated by functionalisation which also provides chemical attachment of catalysts to CNTs [34]. Gold supported on CNTs have proved to be active in catalysing the oxidation of styrene with a good conversion and high styrene oxide selectivity using tert-butyl hydroperoxide (THBP) as oxidant [30].

Ruthenium metal has been exploited for its electron charge transfer properties; and CNTs are often utilised as electron acceptors due to their extended π-electron conjugation. In addition Ru is a cheap metal relative to other noble metals that have been used [34,35]. Thus, supporting Ru on CNTs will combine the exceptional properties of ruthenium with those originating from CNTs.

To the best of our knowledge there are no literature reports on the study of Ru-CNT catalysts for styrene oxidation in the liquid phase. In practice, the oxidation of styrene can be performed in the liquid or gas phase, depending mainly on the thermal stability and volatility of the reagents and products. Chimentao et al., [36] studied the sensitivity of the styrene oxidation reaction to a silver nanoparticle catalyst in a gas phase reaction. The biggest disadvantage of a gas-phase oxidation is the high reaction temperature, which tends to increase energy consumption, give low selectivity, and leads to more rapid deactivation of catalyst active sites [37]. Thus, in this study the oxidation of styrene, in the presence of hydrogen peroxide, over a ruthenium catalyst deposited on CNTs was investigated. The catalytic activity was evaluated using different reaction conditions.

6.2 Experimental

6.2.1 Materials

Pristine MWCNTs with inner diameter of 5 - 10 nm and outer diameter of 40-80 nm were obtained from Sigma Aldrich. The nitrogen doped CNTs (N-CNTs) (0.8 % nitrogen) with inner diameters of 5 - 10 nm and outer diameters of 30 - 100 nm were synthesised in-house (Chapter 3). Styrene (Aldrich, 99 %), hydrogen peroxide (H_2O_2) (30 % v/v), acetonitrile (Aldrich,), 1,4-dioxane (Aldrich, 99 %), DMF (Aldrich, 99 %) and $RuCl_3.xH_2O$ (Aldrich) were used as received. All chemical reagents were analytical reagents and used without further purification. Microwave teflon vessels were used in the synthesis reactions.

6.2.2 Catalyst preparation

Microwave irradiation was used in this study to make Ru supported CNTs as described in [38]. In the method, 5 wt. % Ru (from $RuCl_3$) was deposited on CNTs and N-CNTs. CNTs or N-CNTs (50 mg) and $RuCl_3.xH_2O$ (10 mg) were mixed in 80 mL ethylene glycol and the brown solution was heated in a microwave oven at 500 W, ramped to 200 ºC in 18 min. The reaction was held for 5 min at 200 ºC before it was cooled to room temperature. A clear solution containing a black precipitate was formed during the reaction. The sample was named according to the expected wt. % Ru loaded onto the CNTs viz. for the above Ru/CNT mixture these samples were named 5Ru/CNTs and 5Ru/N-CNTs as they contained 5 wt. % Ru on the support. The catalysts were filtered, washed with 20 mL acetone and dried at 110 ºC overnight. An ICP analysis was performed to verify the metal loading on the support (4.89 wt. % for Ru/CNTs and 5.16 wt. % for Ru/N-CNTs). The Ru/CNT samples were then calcined in air at 250, 350 and 400 ºC for 2 h.

6.2.3 Characterisation

The morphology and the microstructure of the catalysts were characterised using a JEOL 2100 TEM microscope. XRD patterns were collected in air at room temperature on an X'Pert Pro PANalytical X-ray diffractometer using Cu Kα radiation (λ = 0.15418) operated at 40 kV and 50 mA. The metal content was determined by inductively coupled plasma analysis (ICP-Spectro-Acros).

6.2.4 Catalytic activity

The styrene oxidation reaction was carried out in a 50 mL two-neck round bottomed flask equipped with a magnetic stirrer and a reflux condenser under continuous stirring (1400 rpm), and was heated in an oil bath. The reaction was carried out at different temperatures (80 - 100 ºC), different times (2 - 22 h) and using various solvents (DMF, 1,4-dioxane and acetonitrile) (Table 6.2). After reaction, the catalysts were washed with 20 mL acetone and recovered. The composition of the oxidation products was analysed by a Varian 3700 gas chromatograph equipped with a DBI capillary column (30 m x 0.32 mm x 0.53 μm) and a flame ionisation detector (FID). The injector and the column temperature were kept at 220 ºC and 148 ºC respectively. The column temperature was programmed to ramp at 10 ºC/min. The identification of products was carried out by comparison of their retention time with known standards. The conversion and selectivity data were calculated as follows:

$$\text{Conversion } /\% = \frac{\text{moles of reactant converted}}{\text{moles of reactant in feed}} \text{ x } 100\%$$

$$\text{Selectivit y } /\% = \frac{\text{moles of product formed}}{\text{moles of all products}} \text{ x } 100\%$$

6.3   Results and discussion

Ru/CNTs and Ru/N-CNTs were synthesised with a 5 wt. % Ru content using a microwave irradiation method. The results were discussed in detail in Chapter 4 where the average diameters of the Ru particle size synthesised were 3.5 nm and 6.2 nm for 5Ru/N-CNTs and 5Ru/CNTs respectively. The 5Ru/CNT catalyst was then calcined at different temperatures (250 - 400 ºC) for 2 h. The calcined catalyst was labelled 5RuO$_2$/CNTs. 5RuO$_2$/CNTs was used to obtain the optimum parameters (reaction temp, time, and catalyst amount) which were then used to study the catalytic activity of 5RuO$_2$/N-CNTs.

6.3.1   Characterisation

6.3.1.1 XRD analysis

- **Ru/CNTs**

The calcined and uncalcined Ru/CNT catalysts were characterised by XRD analysis (Figure 6.1). The typical peak located at a 2θ value of about 26° corresponds to the (002) reflection of carbon [39]. The other featured peaks found for the uncalcined Ru/CNT material (Figure 6.1b) at a 2θ of about 38°, 43°, 59°, 69° and 78° were assigned to the (100) (101)(102) and (110) Ru planes respectively. They are assigned to the hexagonal structure of ruthenium [40,41].

It is observed from the XRD patterns that increasing the calcination temperature gave rise to different XRD catalyst patterns. This indicates that the Ru phases present in the catalyst are different or the relative amount of each phase present is different. From the X-ray diffraction analysis of the catalysts shown in Figure 6.1c and Figure 6.1d the formation of RuO$_2$ was detected. In the patterns of the composites heated at 250 °C, the catalyst shows the weak RuO$_2$ diffraction peaks at 35° and 54°. Heating the composites at 400 °C generates XRD patterns that show

typical reflections of crystalline RuO_2. The two major peaks at 28° and 35° in the range of 20 - 40° can be assigned to the diffraction from the (110) and (101) planes of RuO_2 with a tetragonal rutile phase [42].
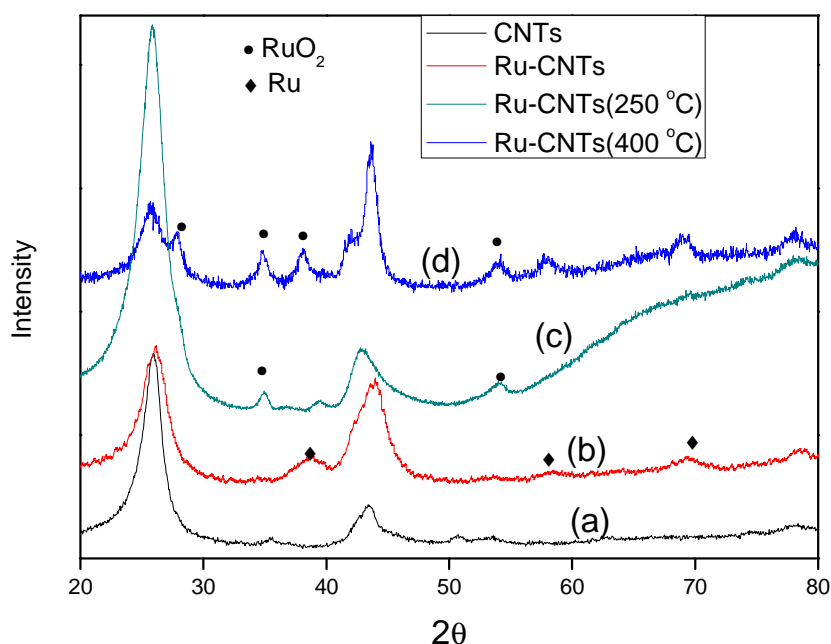
Figure 6.1. XRD patterns of (a) CNTs (b) uncalcined Ru/CNTs (c) calcined Ru/CNTs (250 ºC) and (d) calcined Ru/CNTs (400 ºC).

The Scherrer equation

$$D = \frac{0.89 \ \lambda}{\beta \, \text{Cos} \ \theta}$$

where D is the average crystallite size, λ is the wavelength (0.154 nm), β is the full width at half maximum, and θ is the Bragg diffraction angle was used to quantify the Ru and RuO_2 particle size [43].The crystallite sizes were estimated from the XRD spectra using the Scherrer equation for the uncalcined, 250 and 400 ºC calcined catalysts. The Ru and RuO_2 average crystallite size for the catalysts was measured using the line broadening of the peak at the 2θ value of 38° and 35° respectively.

The peak around $2\theta = 43°$ could not be used because it is a mixture of Ru and carbon phases. Ru crystallites were found to be 6.5 nm for the uncalcined catalyst. The RuO_2 particle size of 250 and 400 ºC calcined catalysts could be estimated and were found to be 7.3 and 9.8 nm respectively. The RuO_2 revealed larger particles at the higher calcination temperature

- **Ru/N-CNTs**

Figure 6.2 shows the XRD patterns of the N-CNTs, $5RuO_2$/N-CNTs sample calcined at 400 °C, (2 h) and the uncalcined 5Ru/N-CNT sample. They exhibit the (002) and (100) basal plane diffraction peaks at 2θ around 26º and 43º in for the hexagonal graphitic carbon structure [44].
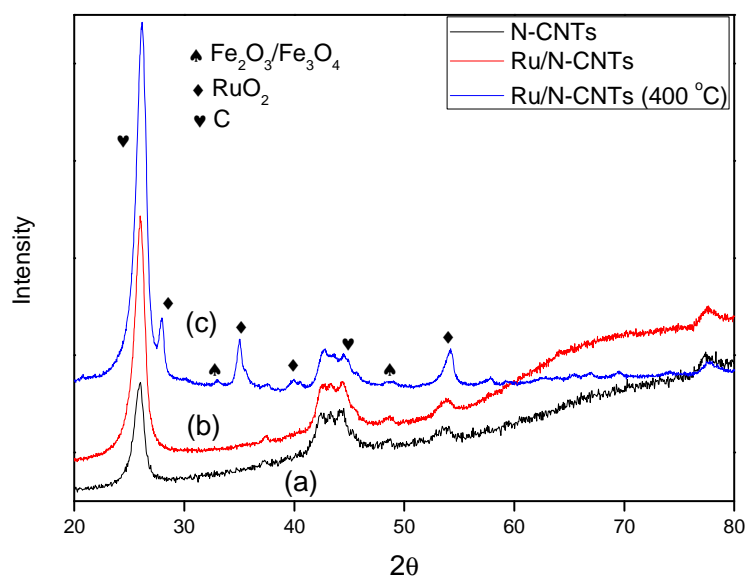
Figure 6.2. XRD pattern of (a) N-CNTs (b) uncalcined and (c) 400 °C calcined $5RuO_2$/N-CNTs

New diffractions at $2\theta = 28°$, $35°$ and $54°$ became evident in the XRD pattern of the thermal-treated sample (Figure 6.2c), which is an evidence of the RuO_2 (101) rutile phase. The peaks at $2\theta = 49°$ indicated the presence of hematite (Fe_2O_3) phase due to Fe residue during N-CNTs growth [45].

6.3.1.2 TEM analysis

TEM micrographs (Figure 6.3) show the morphologies and Ru particle size of Ru/CNTs and Ru/N-CNTs before and after calcination. Figure 6.3a shows an image of the 5Ru/CNT catalyst and Figure 6.3b an image of the 5Ru/CNT catalyst after heat pre-treatment under air at 400 °C. The Ru particle size distributions varied between 5 - 8 nm with an average diameter of 6.2 nm before calcination. Following calcination, TEM studies of the $5RuO_2$/CNTs shows black spots of RuO_2 embedded on the matrix of the carbons and the average particle size diameter distribution increased to 9.2 nm. The TEM image of the Ru/N-CNT catalyst before calcination is shown in Figure 6.3c with the average Ru particle size of ± 3 nm. Figure 6.3d shows an image of the calcined $5RuO_2$/N-CNTs catalyst (400 °C) with average particle size of 5.1 nm. Calcination forms metal oxides. Therefore, the particles obtained after calcination are RuO_2 particles. The presence of Ru on the CNTs was previously determined by EDS and TEM (chapter 5).
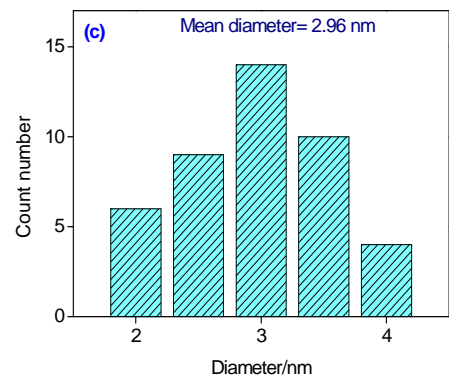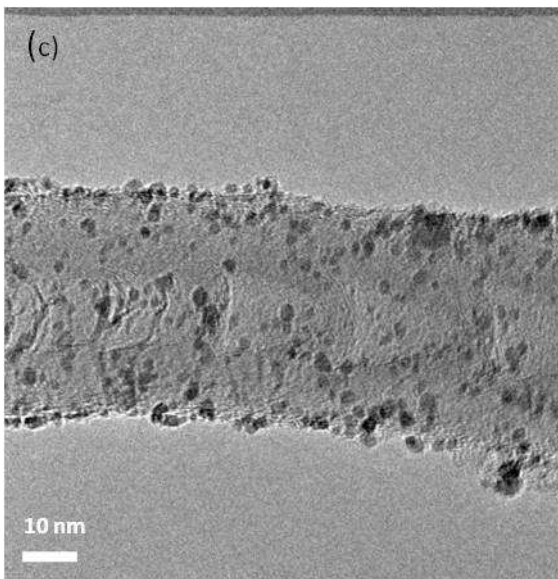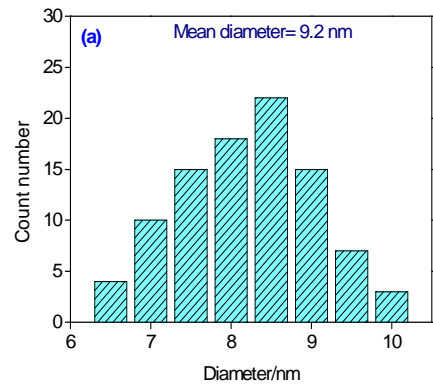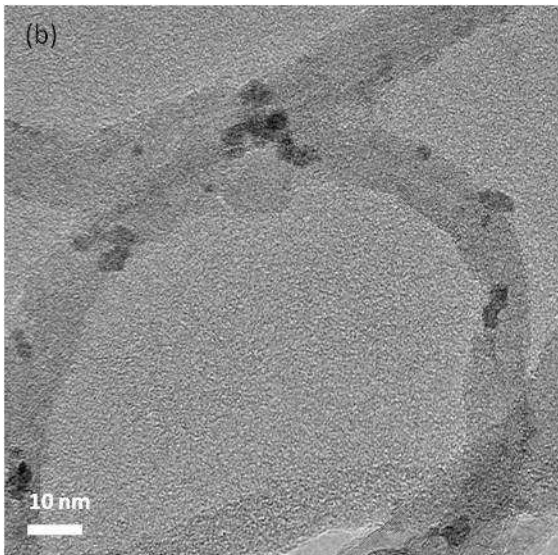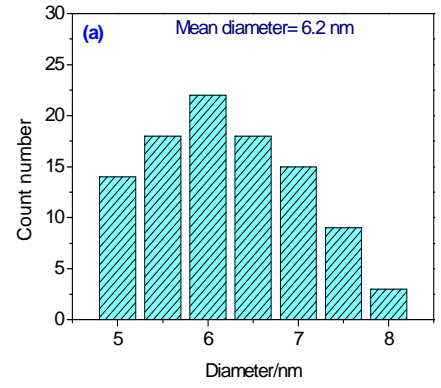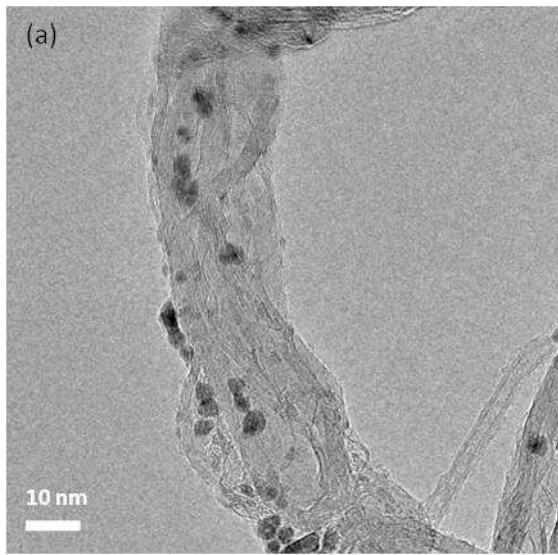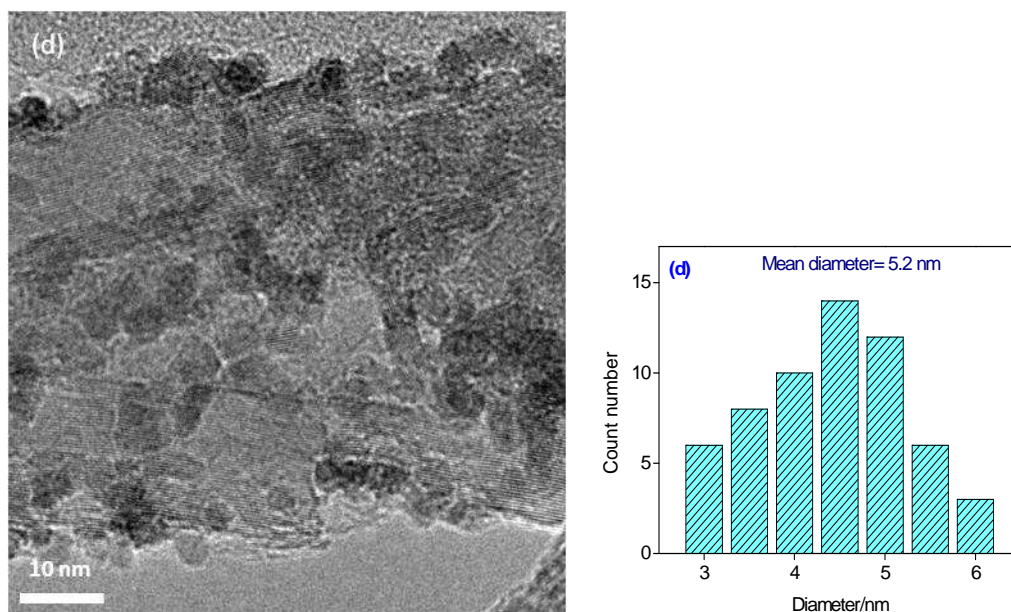
Figure 6.3. TEM images and corresponding histograms of uncalcined (a) 5Ru/CNTs and calcined (400 ºC) (b).5Ru/CNTs. Uncalcined (c) 5Ru/N-CNTs and calcined (d) 5Ru/N-CNTs (400 ºC).

6.3.2   Oxidation of Styrene

The oxidation of styrene in the presence of H_2O_2 by 5Ru/CNTs as a catalyst was investigated. The off-line analysis was carried out using a GC-FID instrument. An approximately 0.2 µL sample was injected into the gc column instrument using a syringe and this sample was used to analyze the products produced during the styrene oxidation reaction. Typical traces produced during oxidation of styrene were recorded using Clarity software (v. 2.5 a Data Apex Chromatograph software package) is shown in Figure 6.4. The peak areas corresponding to each reactant on product detected was taken to correspond to the number of moles of that molecule passing through the detector. Blank experiments were performed to control the experiment; (i) styrene without a catalyst and (ii) styrene over catalyst without oxidant. In the blank experiment performed without catalyst the oxidation occurred at a very low rate (80 ºC) and less than 1 mol % conversion of styrene was obtained after 7 h. Moreover, in a blank

reaction in which styrene was reacted over a catalyst without oxidant the oxidation also occurred at a low rate with 2 mol % conversion after 24 h.
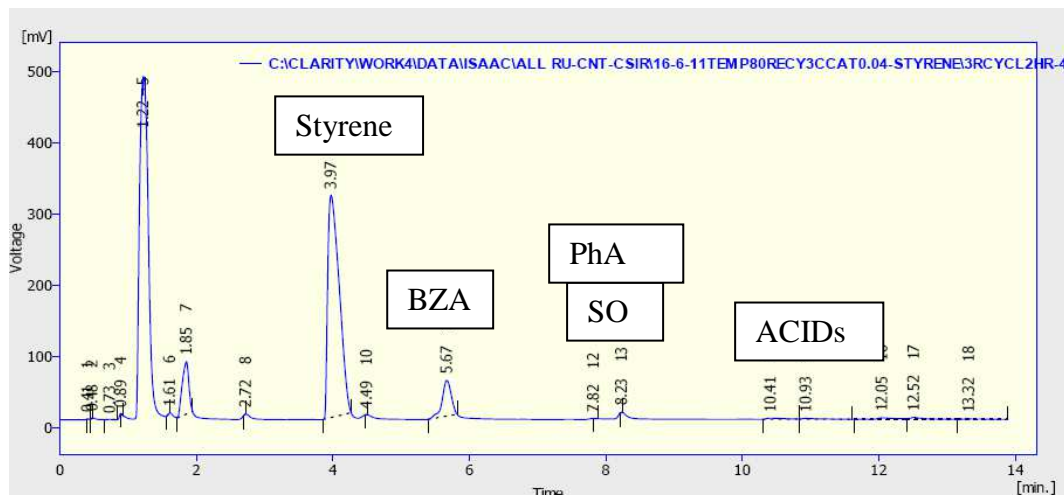
BZA-Benzaldehyde
SO-Styrene oxide
PhA-Phenylacetaldehyde
ACIDs-Phenyl acetic acid (PhAAc) and Benzoic acid (BAc)

Figure 6.4. A typical trace for the styrene oxidation product using GC

The oxygen on the surface of the CNTs aided in low conversion of styrene noted in Ru blank reaction. In the presence of a catalyst and oxidant oxidation of styrene produced benzaldehyde (BZA), trace amounts of styrene oxide (SO), and the by-products; benzoic acid (BAc), and phenyl acetic acid (PhAAc) [3,9,10,26,46].

6.3.2.1 Effect of reaction temperature

The impact of reaction temperature on the oxidation of styrene over $5RuO_2$/CNTs is shown in Figure 6.5. The reaction was carried out in 1,4-dioxane as a solvent with 0.04 g of catalyst at various temperatures for 4 h. The styrene conversion increased from 34 mol % at 70 ºC to 85 mol % at 100 °C. It has been reported in similar studies that this is related to the decomposition of H_2O_2 which increases with an increase of temperature [47]. At lower temperatures (70 °C and 80 °C) benzaldehyde

is the main product. To obtain information on the pathway for the formation of benzaldehyde in the styrene oxidation reaction, styrene oxide was reacted over $5RuO_2$/N-CNTs using peroxide as oxidant. Benzaldehyde is formed in two pathways as shown in Scheme 6.1.
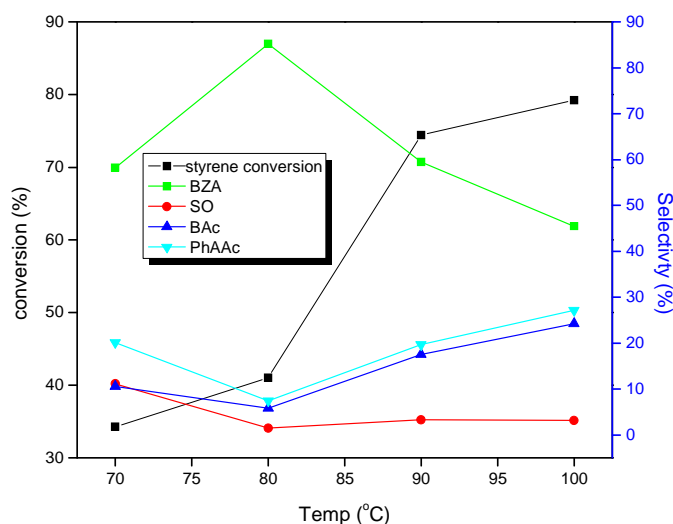
Figure 6.5. Influence of reaction temperature on the oxidation of styrene over $5RuO_2$/CNTs. Reaction conditions: catalyst = 0.04 g, styrene:H_2O_2 = 1:6 1,4-dioxane = 10 ml and t = 4 h.

However, data in Figure 6.6 suggest that the styrene oxide formed in the reaction mostly generates phenylacetic acid. Which implies most of benzaldehyde is formed via the radical cleavage of the side chain of styrene. As the temperature increased, the selectivity to benzoic acid and phenyl acetaldehyde increased at the cost of benzaldehyde. The increase of benzoic acid is due to a secondary oxidation reaction, in which styrene is firstly oxidised into benzaldehyde and then further oxidised to benzoic acid [48,49]. The increase in phenyl acetic acid at higher temperature arises from the epoxidation reaction which competes more favourably with C=C bond cleveage which firstly gave styrene oxide. The styrene oxide then isomerised to phenyl acetaldehyde (route 4), (Scheme 1) [47].

Phenyl acetaldehyde was not observed as it presumably converted, as soon as it is formed, to PhAAc (Route 6). A temperature of 80 °C is thus regarded as an optimal reaction temperature to give the best conditions for the conversion and selectivity for the reaction.
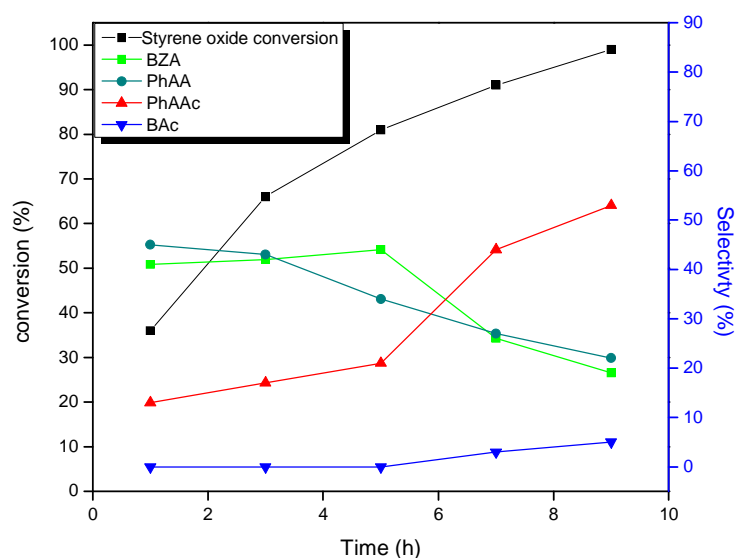
Figure 6.6. Oxidation of styrene oxide Reaction conditions: catalyst = 0.04 g, styrene:H_2O_2 = 1:6 1,4-dioxane = 10 ml and t = 4 h.

6.3.2.2 Effect of reaction time

The impact of the reaction time on the oxidation of styrene at 80 °C is depicted in Figure 6.7. There is an induction period at the beginning of the reaction and after the induction period styrene conversion increases exponentially. The conversion of styrene was observed to increase continuously with time. After 22 h (not shown) the conversion was close to complete (98 %). However, the selectivity to benzaldehyde decreased markedly with prolonged time, while an increase in benzoic acid and phenyl acetic acid took place. This suggests over-oxidation with prolonged time [4]. To gain insight into the reaction mechanism pathways and their relevance on the oxidation, the oxidation of benzaldehyde by 5RuO$_2$/CNTs

catalyst at 80 °C was studied. Benzoic acid was the only product formed as shown in Figure 6.8.
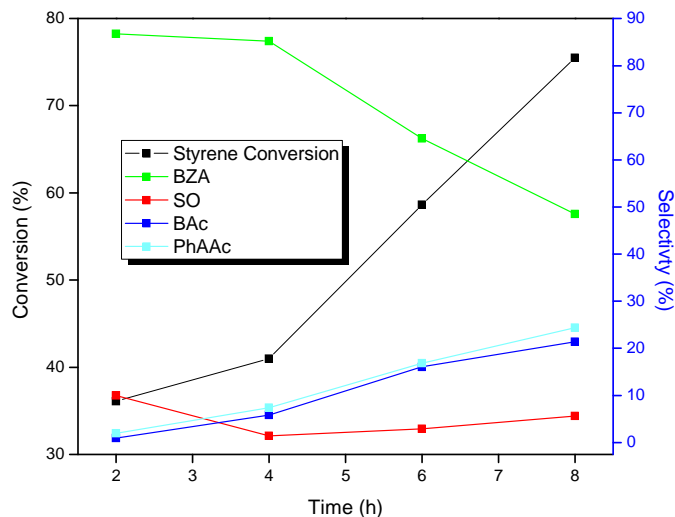
Figure 6.7. Influence of reaction time on the oxidation of styrene over 5Ru/CNTs. Reaction conditions: catalyst = 40 mg, styrene:H_2O_2 = 1:6 1,4-dioxane = 10 ml, and T= 80 ºC.
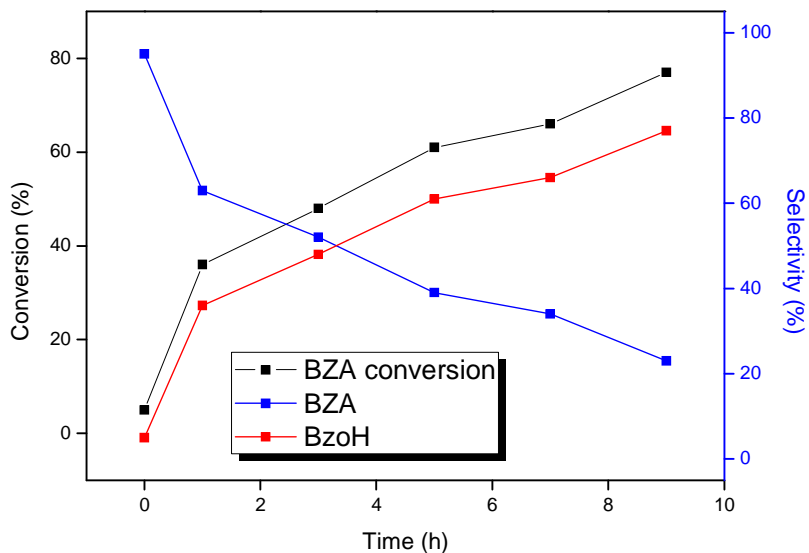
Figure 6.8. The oxidation of benzaldehyde to benzoic acid. Reaction conditions: catalyst = 40 mg, styrene:H_2O_2 = 1:6 1,4-dioxane = 10 ml, and T= 80 ºC.

6.3.2.3 Effect of amount of catalyst

The amount of catalyst used was varied from 0.02 g to 0.08 g and the results are presented in Figure 6.9. When the amount of catalyst was increased from 0.02 to 0.04 g the conversion of styrene also increase from 36 mol % to 41 mol %. At the same time, the selectivity of benzaldehyde slightly increased from 79 to 85 %. This relates to a doubling of the catalyst surface area which produces more active sites. As the amount of catalyst used is increased further, from 0.04 g to 0.08 g, the conversion of styrene increased slightly (41 to 44 %) but the benzaldehyde selectivity decreased (85 to 60 %) with an increase of benzoic acid. This is arises since when a large excess of catalyst is used there is a greater chance of both styrene and benzaldehyde being simultaneously adsorbed on the RuO_2 [47]. In other words the benzaldehyde and styrene compete for the active sites. The activity and styrene conversion using 0.04 g catalyst was investigated in later studies.
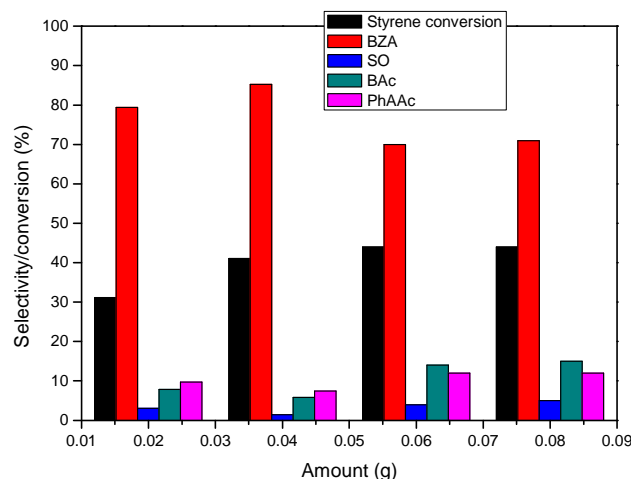
Figure 6.9. Influence of catalyst amount on the oxidation of styrene over 5Ru/CNTs. Reaction conditions: styrene:H_2O_2 = 1:6 1,4-dioxane = 10 ml, T= 80 ⁰C and t = 4 h.

6.3.2.4 Effect of calcination temperature

Table 6.1 summarises the experimental data obtained for the three catalysts after performance in the styrene oxidation reaction. When the calcination temperature was increased to 400 °C, the conversion of the styrene decreased while the selectivity to the benzaldehyde increased. The decrease of the styrene conversion at higher calcination temperature is related to the sintering of Ru particles and formation of bigger particle sizes. The particle size plays an important role in the selectivity; the bigger RuO_2 particle size shows a slightly better selectivity (85 %) to benzaldehyde.

Table 6.1. Influence of calcination temperature on the oxidation of styrene over 5Ru/CNTs.

Calcination (°C)	Ave. RuO_2 particle Size (nm)	Ave.Ru particle Size (nm)	Styrene Conversion (%)	BZA	SO	BAc	PhAAc
Uncalcined	-	6.5	47	79	5	4	12
250	7.3	-	48	78	4	5	11
400	9.8	-	41	85	1	6	7

Reaction conditions: Reaction conditions: catalyst = 0.04 g, styrene:H_2O_2 = 1:6 1,4-dioxane = 10 mL, T= 80 ºC and t = 4 h. Error bar = +/- 1.

6.3.2.5 Effect of H_2O_2 concentration

To determine the effect of the H_2O_2 oxidant on the oxidation of the styrene oxidation, three different styrene:H_2O_2 molar ratios were studied at 80 ºC for 4 h (Figure 6.10). An increase in the oxidant concentration enhanced the styrene oxidation and benzaldehyde selectivity was increased. Styrene oxidation was 17 % and benzaldehyde selectivity was 76 % when a 1:4 styrene:H_2O_2 molar ratio was used. The lower conversion at the 1:4 molar ratio could relate to the H_2O_2 being a limiting reagent in the reaction [50]. A maximum conversion of the styrene (41 %) together with high

benzaldehyde selectivity (85 %) was obtained at a 1:6 molar ratio. Both the catalytic activity and the benzaldehyde selectivity decreased when a molar ratio above 1:6 was used. When excess peroxide is used over oxidation take place. It is also possible that at higher H_2O_2 volumes more water is present which suppresses the catalyst activity [9].
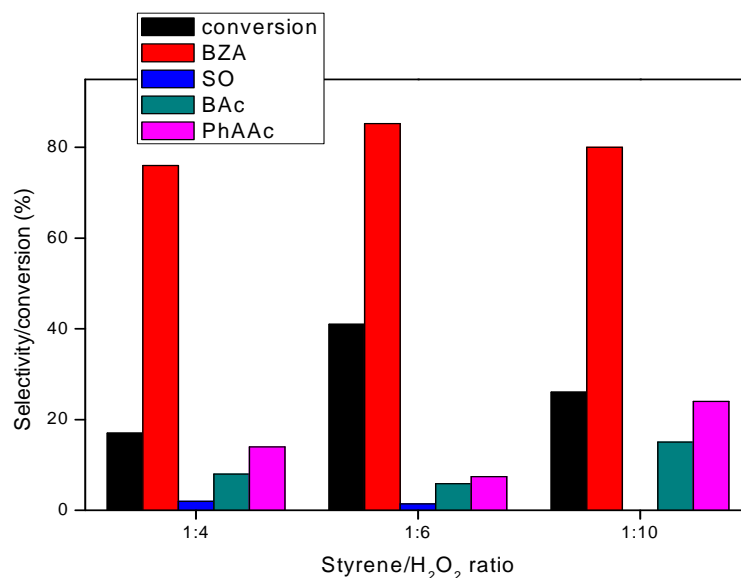
Figure 6.10. Effect of styrene:H_2O_2 ratio. Reaction conditions: catalyst = 40 mg, 1,4-dioxane = 10 ml, T= 80 ⁰C and t = 4 h.

6.3.2.6 Effect of solvent

The nature of the solvent has an important effect on the outcome of a reaction, and affects yields, by-product formation and reaction kinetics [9]. The styrene oxidation reaction was examined using different solvents (4 h, 80 ⁰C) as shown in Table 6.2. The solvents chosen were polar aprotic solvents. The solubility of O_2 in polar aprotic solvents accelerates the oxidation and it benefits the reaction [51]. The 5RuO$_2$/CNT catalyst exhibited the highest catalytic activity when 1,4-dioxane solvent was used. The conversion was 41 % in 1,4-dioxane with a corresponding 85 % selectivity to benzaldehyde. DMF and acetonitrile were also active but gave lower conversion as compared to 1,4-dioxane. The styrene conversions in these two solvents were 17 % and 15 % respectively. This

lower conversion might be explained by the coordination of Ru with the N heteroatom in the solvent molecule [51]. Even though the 1,4-dioxane has a higher activity at 4 h, DMF and acetonitrile have higher selectivity to the two products, benzaldehyde and styrene oxide. However, at equi-conversion (± 15 % styrene conversion) in all solvents, 1,4-dioxane has a high selectivity to benzaldehyde (90 %) and styrene oxide. This conversion occurs after a reaction time of 1 h as compared to 4 h for DMF and acetonitrile. DMF shows a higher selectivity to styrene oxide. This could be due to the rate of isomerisation (route 4) and the priviledge that the nucleophilic attack of styrene is slow in DMF as a solvent.

Table 6.2. Effect of solvent on styrene oxidation[a]

Temp (°C)	Styrene Conversion (%)	Selectivity (%)			
		BZA	SO	BAc	PhAAc
1,4-dioxane	41	85	1	6	7
1,4-dioxane	15[a]	90	10	-	-
Acetonitrile	15	93	7	-	-
DMF	17	75	25	-	-

[a]The conversion of styrene at 1 h.
Reaction conditions: catalyst = 40 mg, styrene:H_2O_2 = 1:6 1,4-dioxane = 10 mL, T= 80 ºC and t = 4 h. Error bar = +/- 1.

6.3.2.7 Effect of recycling

An important factor that has to be taken into consideration is the catalytic stability and durability of a catalyst. It is one of the most important properties of a heterogeneous catalyst. The metallic components can leach out from the support, resulting in either the formation of an active homogenous catalyst or a loss of catalyst activity on subsequent recycling [52,53]. In order to evaluate those effects, reuse of the catalyst was carried out. After an oxidation reaction (6 h), the catalyst was recovered by filtering off the solution from the catalyst. The catalyst was then washed with 20 mL acetone and heated in an oven at 120 ºC for 4 h. The catalyst was then reused in four subsequent consecutive catalytic cycles under the

same reaction conditions used in the first styrene oxidation reaction (80 ºC, 4 h) (Figure 6.11). The recycled catalyst gave a slightly reduced activity with each recycle. Styrene conversion remained nearly constant after the second cycle and there was a small variation in benzaldehyde selectivity when the first cycle, (85 %) was compared with subsequent cycles (~ 80 %) as shown in Figure 6.12.
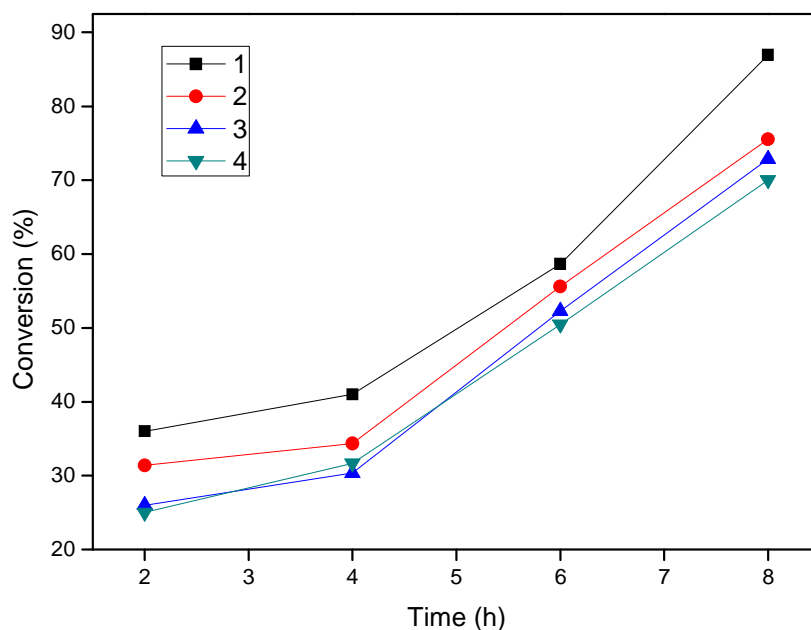
Figure 6.11. Influence of reuse of a catalyst on the oxidation of styrene over 5Ru/CNTs. Reaction conditions: catalyst = 40 mg, styrene:H_2O_2 = 1:6 1,4-dioxane = 10 ml and T= 80 ºC.

ICP was used to confirm the presence and amount of Ru in the catalyst after use and it was found that the Ru content of the used catalyst was 4.91 % for Ru/CNTs, which is similar to that of the fresh catalyst. Further no ruthenium was detected by ICP in the filtrates. The minor changes on the catalyst activity are believed to be from physical losses of catalyst during the recycling process.
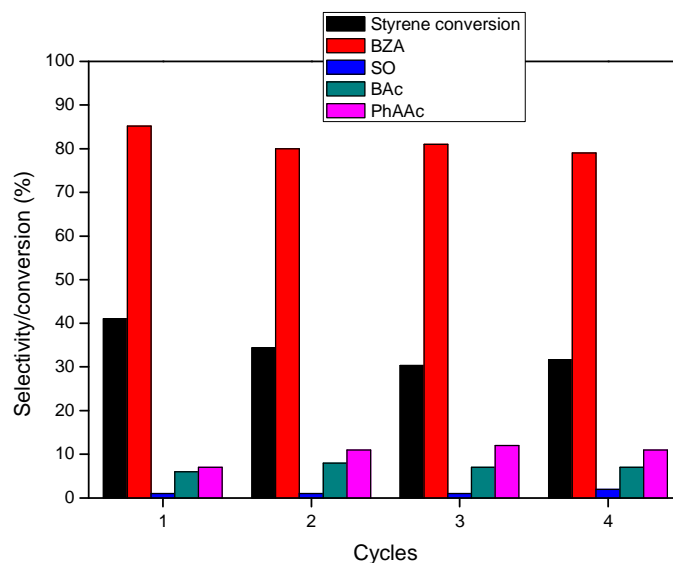
Figure 6.12. Selectivity of recycled catalyst. Reaction conditions: catalyst = 40 mg, styrene:H_2O_2 = 1:6 1,4-dioxane = 10 mL, T= 80 ℃ and t = 4 h.

6.3.2.8 The effect of N-CNTs

Table 6.3 reports the results of the Ru catalyst supported on CNTs and on the N-CNTs for styrene oxidation using peroxide (40 mg catalyst, 80 °C, 1,4-dioxane, 4 h). The support is shown to have an effect on both the conversion and the selectivity of the oxidation reaction. N-CNTs show a better Ru nanoparticle dispersion, with smaller particle sizes as compared to pristine CNTs (Table 6.1). This is due to N-functionalities that are incorporated in the carbon network structure. Additional lone pairs of electrons on N atoms enhance the electronic properties of CNTs [54.]. The nitrogen atoms entering the graphene sheets as a substituent for carbon also modify the adsorption strength of the nanotube towards foreign elements quite significantly [55]. The RuO$_2$/N-CNT catalyst was expected to perform better than the Ru/CNTs. However, the conversion of styrene was 41 % using the CNTs as support and 34 % using the N-CNTs; and the corresponding selectivity was 85 and 87 % respectively. At the equi-conversion of 34 % styrene conversion, RuO$_2$/CNTs gave a better conversion and better selectivity to

132

benzaldehyde with 11 % styrene oxide selectivity. The lower conversion of styrene with RuO_2/N-CNTs might be explained by the RuO_2 nanoparticle size. A similar selectivity trend was found with smaller Ru particles produced on the uncalcined (6.8 nm) and 250 °C RuO_2 calcined catalyst (7.3 nm) as compared to larger particles produced with the 400 °C RuO_2 calcined catalyst (9.8 nm). The results suggest that styrene oxidation reaction depends on the size of the metal nanoparticles. The larger the particles size the better the selectivity.

Table 6.3. Effect of N-CNTs on styrene oxidation

Support	Conversion (%)	Selectivity (%)			
		BZA	SO	BAc	PhAAc
CNTs[a]	41	85	1	6	7
N-CNTs[a]	34	87	3	3	6
CNTs[b]	34	89	11	0	0

Reaction conditions: catalyst = 40 mg, styrene:H_2O_2 = 1:6 1,4-dioxane = 10 mL, T= 80 °C. Error bar = +/- 1.
[a]Conversion at 4 h
[b]Conversion at ± 2 h

6.3.3   Comparison of catalysts with literature data

$5RuO_2$/CNT and $5RuO_2$/N-CNT catalysts were compared with the similar data for styrene oxidation reaction obtained from the literature as shown in Table 6.4. Although there was no data that used ruthenium as catalyst for styrene oxidation, all the reactions were done in a solvent using H_2O_2 as an oxidant and they were highly selective to benzaldehyde. The comparison result shows that both $5RuO_2$/CNT and $5RuO_2$/N-CNT catalysts were also highly selective to benzaldehyde. The VSB-5 catalyst showed a higher selectivity but lower activity. Equi-conversion of the styrene oxidation reaction using $5RuO_2$/CNTs with the catalyst from the literature studies was done in order to compare the activity. Catalysts **A-C** were the only catalysts that showed better selectivity than the $5RuO_2$/CNT catalyst, even though their selectivity was obtained after a longer period.

5RuO$_2$/CNT catalyst showed better selectivity to benzaldehyde than catalysts **D-J**. The prepared 5RuO$_2$/CNT and 5RuO$_2$/N-CNT catalysts may thus have potential utilisation in the selective oxidation of styrene.

Table 6.4. Comparison of catalyst for styrene oxidation reaction with H$_2$O$_2$ as oxidant

Catalyst		Time/ h	Temp/ °C	Solvent	Conv/ %	Sel/ %	Equi-Conv[a]	Ref
5RuO2/CNT	**-**	**4**	**80**	**1,4 - dioxane**	**41**	**85**		**Present work**
5RuO$_2$/N-CNT	**-**	**4**	**80**	**1,4 - dioxane**	**34**	**87**		**Present work**
Ag- ϒ-Zrp	**A**	8	82	MeOH	68	**64**	**55**	[48]
Ag-ϒ-Zrp	**B**	8	82	MeCN	57	**82**	**67**	[48]
Fe-SBA	**C**	4	80	MeCN	66	**73**	**59**	[5]
Ti-SBA	**D**	4	80	MeCN	53	48	**58**	[5]
CoVSB-1	**E**	6	70	Acetone	40	28	**85**	[3]
Cr-ZSM-5	**F**	7	80	MeCN	49	61	**70**	[2]
VSB-5	**G**	6	70	Acetone	28	94	**95**	[3]
7,16diacetyl[Ni{Me$_4$(Bzo)$_2$[14]tetraeneN$_4$}]-NaY	**H**	6	75	MeCN	54	58	**58**	[10]
[Ni{Me$_4$(Bzo)$_2$[14]tetraeneN$_4$}]-NaY	**I**	6	75	MeCN	44	62	**80**	[10]
Cu(II)-NaY	**J**	6	75	MeCN	6.2	78	**100**	[10]

[a]Equi-conversion = equivalent point of conversion

6.4   Conclusion

RuO$_2$/CNT catalysts are active in catalysing the oxidation of styrene with relatively high benzaldehyde selectivity (85 %) using hydrogen peroxide as oxidant. Other products such as benzoic acid, phenyl acetic acid and traces of styrene oxide were obtained with very low selectivity. The best result, styrene conversion of 41 % and benzaldehyde selectivity of 85 %, was obtained by using 1,4-dioxane as the solvent at 80 ⁰C, (0.04 g catalyst calcined in air at 400 ⁰C for 2 h and reaction time 4 h). The 5RuO$_2$/N-CNT catalyst showed a better selectivity to benzaldehyde (88 %) but at lower

conversion (34 %) as compared to undoped $5RuO_2$/CNTs after 4 h reaction. However, at equi-conversion the $5RuO_2$/CNT catalyst appeared to be a better catalyst. This is related to the larger RuO_2 particle size being more selective to benzaldehyde. This catalyst system is also simple to use and separation and recycling proved easy.

Reference

1.   K. Weissermel, H. J. Arpe, Industrial Organic Chemistry, Wiley-VCH, 2003.

2.   C. Saux, L. B. Pierella, Applied Catalysis A: General 400 (2010) 117-121

3.   D. Gao, Q. Gao, Catalysis Communications 8 (2007) 681-685.

4.   V. R. Choudhary, R. Jha, N. K. Chaudhari, P. Jana, Catalysis Communications 8 (2007) 1556-1560.

5.   W. Tanglumlert, T. Imae, T. J. White, S. Wongkasemjit, Catalysis Communications 10 (2009) 1070-1073.

6.   G. Wang, Z. Liu, Y. Liu, G. Liu, M. Xu, L. Wang, Chinese Journal of Catalysis 29 (2008) 1159-1164.

7.   V. Hulea, E. Dumitriu, Applied Catalysis A: General 277 (2004) 99-106.

8.   S. B. Kumar, S. P. Mirajkar, G. C. G. Pais, P. Kumar, R. Kumar, Journal of Catalysis 156 (1995) 163-166.

9.   V. Hulea, E. Dumitriu, Applied Catalysis A: General 277 (2004) 99-106.

10.   V. K. Bansal, P. P. Thankachan, R. Prasad, Applied Catalysis A: General 381(2010) 8-17.

11.   L. Nie, K. K. Xin, W. S. Li, X. P. Zhou, Catalysis Communications 8 (2007) 488-492.

12.   P. J. Miedziak, Q. He, J. K. Edwards, S. H. Taylor, D. W. Knight, B. Tarbit, C. J. Kiely, G. J. Hutchings, Catalysis Today 163 (2011) 47-54.

13.   V. Choudhary, D. Dumbre, Topics in Catalysis 52 (2009) 1677-1687.

14.   K. Yamaguchi, N. Mizuno, Angewandte Chemie International Edition 41 (2002) 4538-4542.

15.   T. Harada, S. Ikeda, F. Hashimoto, T. Sakata, K. Ikeue, T. Torimoto, M. Matsumura, Langmuir 26 (2010) 17720-17725.

16.   J. Jiang, R. Li, H. Wang, Y. Zheng, H. Chen, J. Ma, Catalysis Letters 120 (2008) 221-228.

17.   R. Ramanathan, S. Sugunan, Catalysis Communications 8 (2007) 1521-1526.

18.   S. Mandal, A. SinhaMahapatra, B. Rakesh, R. Kumar, A. Panda, B. Chowdhury, Catalysis Communications 12 (2011) 734-738.

19.   W. Zhan, Y. Guo, Y. Wang, Y. Guo, X. Liu, Y. Wang, Z. Zhang, G. Lu, The Journal of Physical Chemistry C 113 (2009) 7181-7185.

20.   M. Silva, C. Freire, B. de Castro, J. L. Figueiredo, Journal of Molecular Catalysis A: Chemical 258 (2006) 327-333.

21.   J. Zhuang, D. Ma, Z. Yan, X. Liu, X. Han, X. Bao, Y. Zhang, X. Guo, X. Wang, Applied Catalysis A: General 258 (2004) 1-6.

22.   M. A. Uguina, D. P. Serrano, R. Sanz, J. L. G. Fierro, M. LÃ³pez-Granados, R. Mariscal, Catalysis Today 61 (2000) 263-270.

23.   J. Liu, F. Wang, T. Xu, Z. Gu, Catalysis Letters 134 (2010) 51-55.

24.   K. Yogish, N. V. S. Sastri, Industrial & Engineering Chemistry Research 27 (1988) 2214-2217.

25.   R. J. Chimentao, I. Kirm, F. Medina, X. Rodra-guez, Y. Cesteros, P. Salagre, J. E. Sueiras, J. L. G. Fierro, Applied Surface Science 252 (2005) 793-800.

26.   X. Liu, A. Klust, R. J. Madix, C. M. Friend, The Journal of Physical Chemistry C 111 (2007) 3675-3679.

27.   V. Purcar, D. Donescu, C. Petcu, R. Luque, D. J. Macquarrie, Applied Catalysis a-General 363 (2009) 122-128.

28.   L. Zhou, R. J. Madix, Surface Science 603 (2009) 1751-1755.

29.   B. Feng, Z. Hou, X. Wang, Y. Hu, H. Li, Y. Qiao, Green Chemistry 11 (2009) 1446-1452.

30.   Y. Liu, H. Tsunoyama, T. Akita, T. Tsukuda, Chemical Communications 46 (2010) 550-552.

31.   L. Luo, N. Yu, R. Tan, Y. Jin, D. Yin, D. Yin, Catalysis Letters 130 (2009) 489-495.

32.	S. C. Laha, R. Kumar, Journal of Catalysis 204 (2001) 64-70.

33.	H. Friedrich, S. Guo, P. E. de Jongh, X. Pan, X. Bao, K. P. de Jong, ChemSusChem 4 (2011) 957-963.

34.	H. Li, J. Wu, Y. Jeilani, C. Ingram, I. Harruna, Journal of Nanoparticle Research 14 (2011) 1-14.

35.	M. Oubenali, G. Vanucci, B. Machado, M. Kacimi, M. Ziyad, J. Faria, A. Raspolli-Galetti, P. Serp, ChemSusChem 4 (2011) 950-956.

36.	R. J. Chimentao, I. Kirm, F. Medina, X. Rodraguez, Y. Cesteros, P. Salagre, J. E. Sueiras, J. L. G. Fierro, Applied Surface Science 252 (2005) 793-800.

37.	Fan, Y. Dai, Y. Li, N. Zheng, J. Guo, X. Yan, G. D. Stucky, Journal of the American Chemical Society 131 (2009) 15568-15569.

38.	L. F. Mabena, S. S. Ray, N. J. Coville, Ceramic Engineering and Science Proceedings 32 (2011) 33-42.

39.	D.J. Guo, Journal of Power Sources 195 (2010) 7234-7237.

40	J. Lu, Carbon 45 (2007) 1599-1605.

41	A. Nirmala Grace, K. Pandian, Materials Chemistry and Physics 104 (2007) 191-198.

42	R. M. A. Tehrani, S. Ab Ghani, Biosensors and Bioelectronics 38 (2012) 278-283.

43.	S. Qiu, S. J. Kalita, Materials Science and Engineering: A (2006) 327-332.

44.	R. I. Zhao, Y. Ma, J. Zhang, F. Li, W. Liu, Q. Cui, Materials Science-Poland 28 (2010) 189-198.

45	R. M. M. Abbaslou, J. Soltan, A. K. Dalai, Applied Catalysis A: General 379 (2010) 129-134.

46.	L. Zhou, R. J. Madix, The Journal of Physical Chemistry C 112 (2008) 4725-4734.

47.	S. K. Pardeshi, R. Y. Pawar, Materials Research Bulletin 45 (2010) 609-615.

48.   N. Dimitratos, J. A. Lopez-Sanchez, D. Morgan, A. Carley, L. Prati, G. J. Hutchings, Catalysis Today 122 (2007) 317-324.

49.   L. Xinrong, X. Jinyu, L. Huizhang, Y. Bin, J. Songlin, X. Gaoyang, Journal of Molecular Catalysis A: Chemical 161 (2000) 163-169.

50.   L. Jia, S. Zhang, F. Gu, Y. Ping, X. Guo, Z. Zhong, F. Su, Microporous and Mesoporous Materials 149 (2012) 158-165.

51.   H. Zhang, Y. Liu, X. Zhang, Chinese Journal of Catalysis 32 (2011) 1693-1701.

52.   A. Villa, D. Wang, N. Dimitratos, D. Su, V. Trevisan, L. Prati, Catalysis Today 150 (2010) 8-15.

53.   Y. Chen, H. Lim, Q. Tang, Y. Gao, T. Sun, Q. Yan, Y. Yang, Applied Catalysis A: General 380 (2010) 55-65.

54.   P. H. Matter, E. Wang, U. S. Ozkan, Journal of Catalysis 243 (2006) 395-403.

55.   J. Amadou, K. Chizari, M. Houllé, I. Janowska, O. Ersen, D. Bégin, C. Pham-Huu, Catalysis Today 138 (2008) 62-68.

CHAPTER 7

STUDIES ON STYRENE OXIDATION OVER NITROGEN DOPED CARBON NANOTUBE SUPPORTED RUTHENIUM

7.1 Introduction

This chapter is a continuation from chapter 6. In the previous chapter the Ru/N-CNTs were shown to show some activity. To further explore this issue Ru was deposited on nitrogen doped CNTs prepared differently from those in chapter 6. The aim was to understand if the activity of the N-CNTs is dependent on the synthesis procedure. In this study also, nitrogen doped carbon nanotubes (N-CNTs*) synthesized by CVD were used, and the studies of Ru/N-CNTs* on oxidation of styrene was fully investigated. The nitrogen doped carbon nanotubes (N-CNTs*) with 2.2 at.% nitrogen content were synthesized by the catalytic decomposition of acetylene (C_2H_2) and acetonitrile (CH_3CN) at 700 °C over a 10% Fe-Co supported on calcium carbonate ($CaCO_3$) catalyst.

7.2 Experimental

7.2.1 Materials

C_2H_2 (Afrox), CH_3CN (Aldrich), N_2 (Afrox), HNO_3 (Aldrich), benzyl alcohol, hydrogen peroxide (H_2O_2) (50% mass concentration in water), $RuCl_3.xH_2O$ (Aldrich) were used as purchased. All other chemicals and reagents used were of analytical grade and purchased from Sigma Aldrich and used without any further purification.

7.2.2 N-CNTs* synthesis

N-CNTs* were synthesized using a procedure similar to that reported by Tetana et al [1]. The synthesis of N-CNTs* was carried out in a tubular quartz reactor (51 cm × 1.9 cm internal .diameter.) placed in a horizontal furnace under nitrogen (N_2) carrier gas. C_2H_2 and CH_3CN were used as carbon and carbon/nitrogen sources, respectively. For each synthesis, 1 g of the catalyst was uniformly spread onto a quartz boat (120 mm × 15 mm) which was then placed in the centre of quartz tube. The furnace was then ramped to 700 °C at 10 °C min^{-1} under flowing N_2 gas (40 mL min^{-1}). Once the desired temperature was reached, the N_2 (240 mL min^{-1}) and C_2H_2 (100 mL min^{-1}) were simultaneously bubbled through CH_3CN for 1 h. After this, the bubbling of the gases through CH_3CN was stopped and the system was left to cool down to room temperature under N_2 (40 mL min^{-1}). The quartz boat was then removed from the reactor and the black soot was then collected. The resulting nitrogen-containing materials were purified using 55 % HNO_3 under reflux in an oil bath held at 110 °C for 4 h to remove the CaO, residual Fe-Co particles and introduce oxygen surface groups. The acid-treated carbon materials were then filtered and washed several times with distilled water (to remove the residual HNO_3). The nitrogen-containing materials were dried at 120 °C for 12 hours.

7.2.3 Catalyst preparation

The catalyst was synthesised via a microwave irradiation procedure as described in [2]. Ru nanoparticles were deposited on N-CNTs* using the microwave assisted polyol method in a microwave teflon vessel. In the reaction 50 mg of N-CNTs* and $RuCl_3.xH_2O$ were mixed with 80 mL ethylene glycol and sonicated for 10 min to afford a homogenous suspension. Ru/N-MWCNT mixtures were chosen to give two different Ru loadings (3 and 5 wt. %.) The suspension was then placed in a microwave reactor (Anton-Paar Multiwave 3000) and heated to 200 °C and the reaction mixture was kept at this temperature for 5 min at 500 W. The

resulting clear suspension was filtered and the residue was washed with 20 mL acetone, then with 50 ml deionised water and dried at 110 °C overnight. The material was then calcined at 400 °C. The samples were named according to the wt. % of Ru expected *viz* 3Ru/N-CNTs* and 5Ru/N-CNTs*. The ICP analysis confirmed the amount of ruthenium to be 3.26 and 5 23 for 3Ru/N-CNTs* and 5Ru/N-CNTs* respectively.

7.2.4   Characterisation

The samples were characterised by XRD patterns collected in air at room temperature on a X'Pert Pro PANalytical X-ray diffractometer using Cu Kα radiation and the size of Ru particles was determined on carbon using a JEOL 2100 TEM. The morphology of the N-CNTs* was evaluated using a LEO 1525 FE-SEM. The SEM was equipped with an energy dispersive spectroscopy (EDS) facility, which was used for elemental analysis of the MWCNTs. Raman spectra were collected before and after synthesis using a Horiba Jobin Yvon T64000 Raman spectrometer. The spectra were recorded from 150 - 3000 cm^{-1} with a 514.5 nm excitation with energy setting 1.2 mW from a Coherent Innova model 308 Ar-ion laser in measured backscattering geometry with a cooled charge-coupled device array detector. Thermal analyses were performed by simultaneous thermogravimetric-differential procedures using a TA Q500 thermal instrument. The amount of Ru supported on the N-CNTs* was quantified using inductively coupling plasma (ICP) spectroscopy (Spectro-Acros).

7.2.5   Catalytic activity

The styrene oxidation reaction was carried out in a 50 mL two–neck round bottomed flask equipped with a magnetic stirrer and a reflux condenser under continuous stirring (1400 rpm), and was heated in an oil bath. The reaction was carried out at different temperatures (60 - 100 ºC), different times (2 - 18 h) and using various solvents (DMF, 1,4-dioxane, toluene and acetonitrile) (Table 7.3). After reaction, the catalysts were washed

with 20 mL acetone and recovered. The composition of the oxidation products was analysed using a Varian 3700 gas chromatograph equipped with a DBI capillary column (30 m x 0.32 mm x 0.53 µm) and a flame ionisation detector (FID). The injector and the column temperature were kept at 220 °C and 148 °C respectively. The column temperature was programmed to ramp at 10 °C/min. The identification of products was carried out by comparison of their retention time with known standards.

7.3   Results and discussion

7.3.1   Characterisation

Nitrogen doped CNTs were synthesised according to the procedure outlined in the experimental **section 7.2.2**. All the samples were washed with acid (HNO_3) prior to characterisation. The advantage of using HNO_3 rather than HCl is that, HNO_3 leads to surface functionalisation, specifically at high temperatures. Further, the use of HCl is not desirable when the CNTs are to be used in catalysis applications.

7.3.1.1 TEM analysis of N-CNT*

The SEM image in Figure 7.1a shows the N-CNT* material contains no impurities. The morphology and structure of the as-grown N-CNTs* are clearly visible in the TEM image (Figure 7.1b) with internal diameters ranging from 10 - 19 nm, and outer diameters ranging from 20-70 nm. The TEM images clearly show that the N-CNTs* are bamboo-shaped. XPS analysis confirmed the presence of 2.23 at.% nitrogen in the N-CNTs* [1].
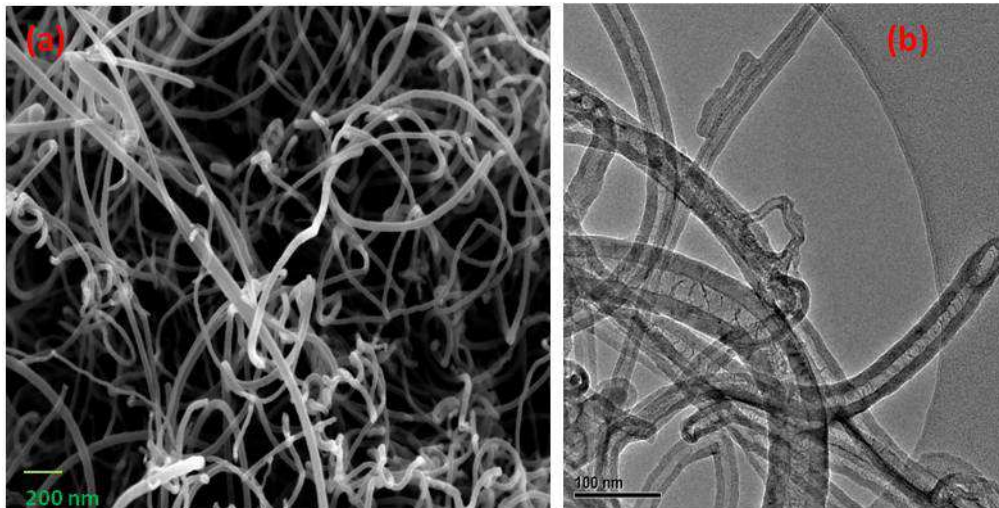
Figure 7.1. SEM and TEM images of N-CNTs*

7.3.1.2 TGA analysis

Thermogravimetric analysis (TGA) of nanotubes under air is a technique used to study the thermal stability and the purity of the as-prepared and the purified N-CNTs* samples. In this study the TGA data of the N-CNTs* is shown in Figure 7.2. The shape of the TGA gives information about the presence of carbon by-products, such as amorphous carbon [3,4]. The TGA curves of the as-prepared N-CNTs* (i.e unpurified) show that there was no mass loss below 400 °C, which confirms that there is no amorphous carbon in the N-CNTs*. The weight gain at 433 - 454 °C, is due to the formation of metal oxide from incompletely oxidized residual Fe catalysts. Furthermore the derivative curve shows there is a two-step weight loss during the heating processes In the first step around 560 °C as shown in the derivate (Figure 7.3), the weight loss correspond to the decomposition of carbon nanotubes. The second step, at around 600 °C, is ascribed to crystalline carbon materials or undoped MWCNTs [1].
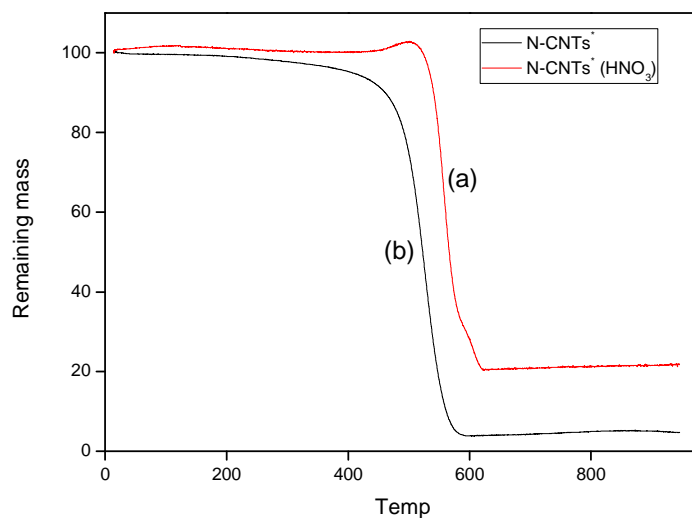
Figure 7.2. TGA of the (a) N-CNTs* and (b) N-CNTs* purified with HNO_3
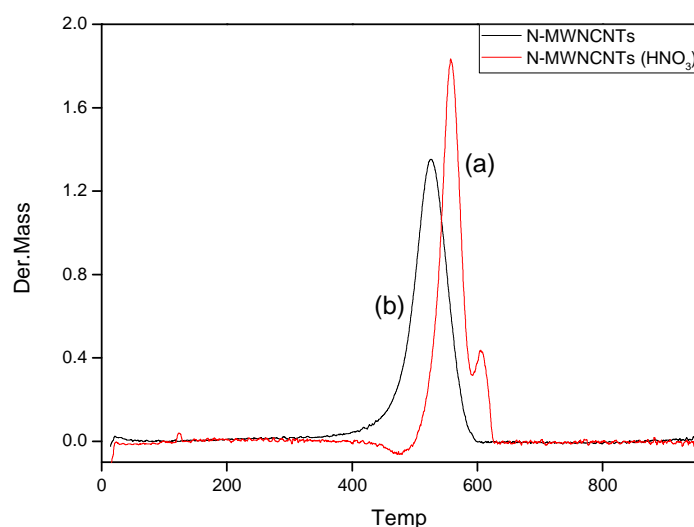
Figure 7.3. Derivative of the (a) N-CNTs* and (b) N-CNTs* purified with HNO_3

TGA curves of the acid purified N-CNTs* (Figure 7.2a) show a. small weight loss occurred below 400 °C. This is credited to the presence of acid groups and defects introduced during purification. There is an increase in thermal stability of the purified N-CNTs* from 526 to 558 °C. This improvement is attributed to the removal of fe catalyst which is known to

aid the oxidation of carbon. After purification about 20 % residual weight due to the metal oxides from the catalysts, was reduced to 1 % in purified N-CNTs*.

7.3.1.3 Raman spectroscopy analysis

To further investigate the graphitic nature as well as the disorder of the N-CNTs*, the as-prepared N-CNTs* were studied by Raman spectroscopy (Figure 7.4). the spectra showed peaks very similar to those reported in the literature for carbon fibers, with a characteristic strong, relatively narrow band around 1598 cm^{-1}, corresponding to graphitic species (G-band) and a band at 1341 cm^{-1}, corresponding to sp^3 carbon species (D-band) [5]. The bands at 1598 cm^{-1} and 1352 cm^{-1} may be ascribed to the graphite-like and disordered structure of carbons, respectively [6]. The ratio of the D-band to the G-band (I_D/I_G) was used to compare N-CNTs* before and after purification. The slightly higher I_D/I_G ratio (1.45) of purified N-MWNCNTs in comparison to I_D/I_G ratio (1.42) of the as-prepared N-CNTs* is due to the defects introduced during purification with the acid. These results are in agreement with the TGA results.
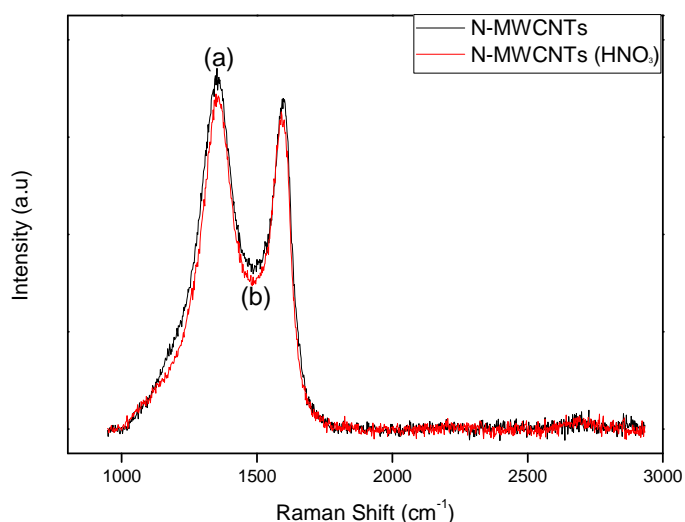
Figure 7.4. Raman spectra of (a) N-CNTS* and (b) purified N-CNTs*

7.3.1.4 XRD analysis

The formation of the metal nanoparticles on N-CNTs* was confirmed by XRD studies. The XRD peaks of the N-CNTs* and 5Ru/N-CNTs* are displayed in Figure 7.5. The peaks at 26° and the broad peak around 43° is due to carbon associated with the CNTs, these correspond to (002), (004) planes present in all three XRD patterns [7]. Figure 7.5a shows the XRD pattern of the pristine N-CNTs* while Figure 7.5b shows the pattern of 5Ru/N-CNTs*. The pattern did not change from the pristine N-CNTs* pattern even though the presence of Ru was detected by EDS (Figure 7.6).

The inability to detect Ru by XRD relates to the small size of Ru particles. As a result, the average crystallite size for Ru on the Ru/N-CNT catalyst could not be measured using XRD. Figure 7.5c shows the XRD pattern pattern of the Ru/N-CNTs* after heat treatment in air at 400 °C. now the Ru can be detected; peaks at 28°, 35° and 54° correspond to (110), (101) and (211) planes of RuO_2 with a tetragonal rutile-type structure. This agreed well with the RuO_2 data listed in ICDD powder diffraction pattern (00-040-1290) list.

The average metal particle of for the RuO_2 as calculated from the Scherrer formular;

$$D = \frac{0.89 \; \lambda}{\beta \, \text{Cos} \; \theta}$$

where D is the average crystallite size, λ is the wavelength (0.154 nm), β is the full width at half maximum, and θ is the Bragg diffraction angle. RuO_2 crystallites were found to be 9.2, 9.1, 8.5 using peaks at 28°, 35° and 54° respectively with average size = 9.0 nm [8].
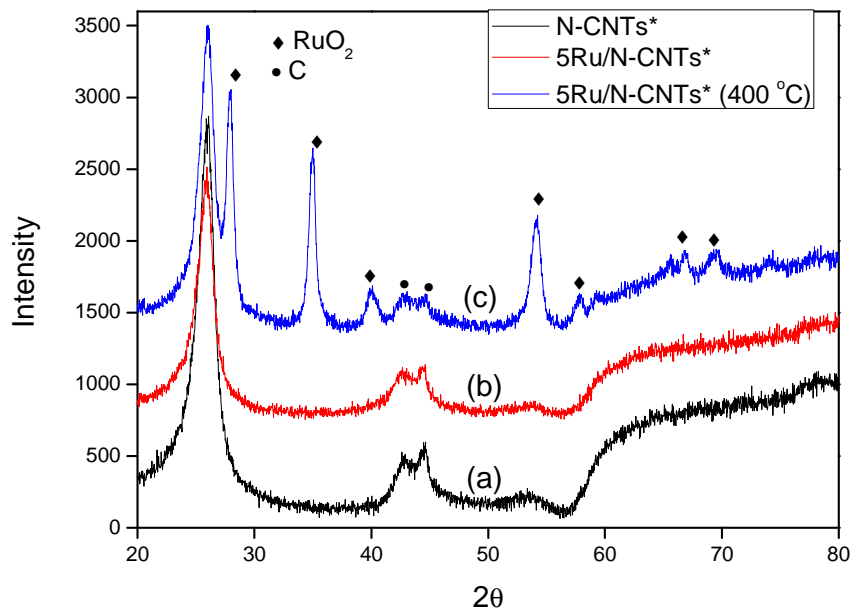
Figure 7.5. XRD pattern of (a) N-CNTs* (b) uncalcined 5Ru/N-CNTs* and (c) 400 °C calcined 5Ru/N-CNTs*
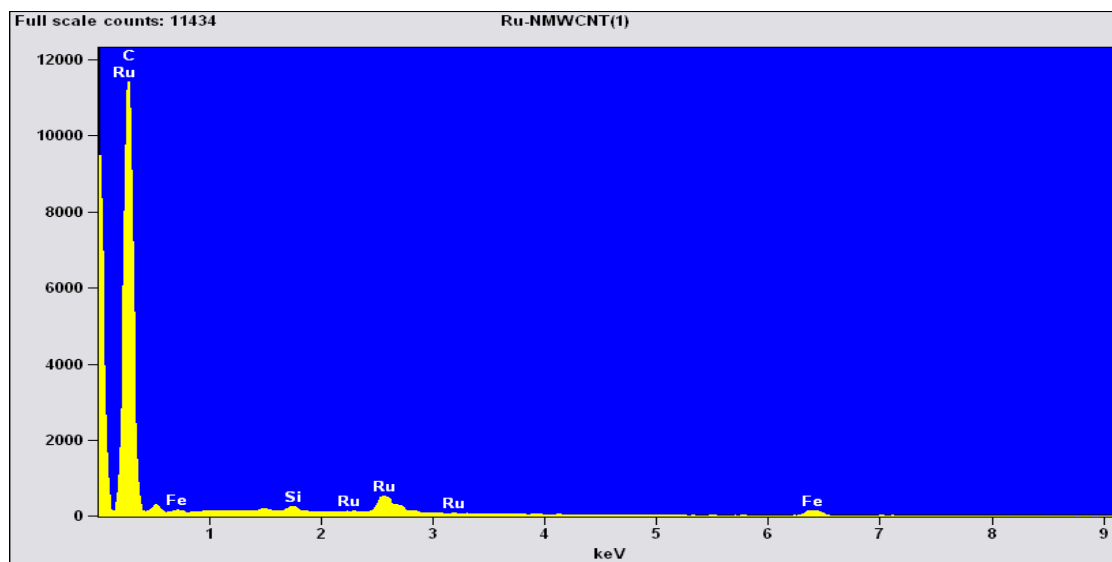
Figure 7.6. EDS of the 5Ru/N-CNTs*

7.3.1.5 TEM analysis of 5Ru/N-CNTs*

The particle size distribution and the position of the ruthenium particles on the N-CNTs* were studied using TEM. Figure 7.8a show a representative TEM image of Ru particles supported on the N-CNTs*. The material is characterised by a narrow uniform Ru nanoparticle, with a particle size distribution of 2 - 3.9 nm (Figure 7.7).
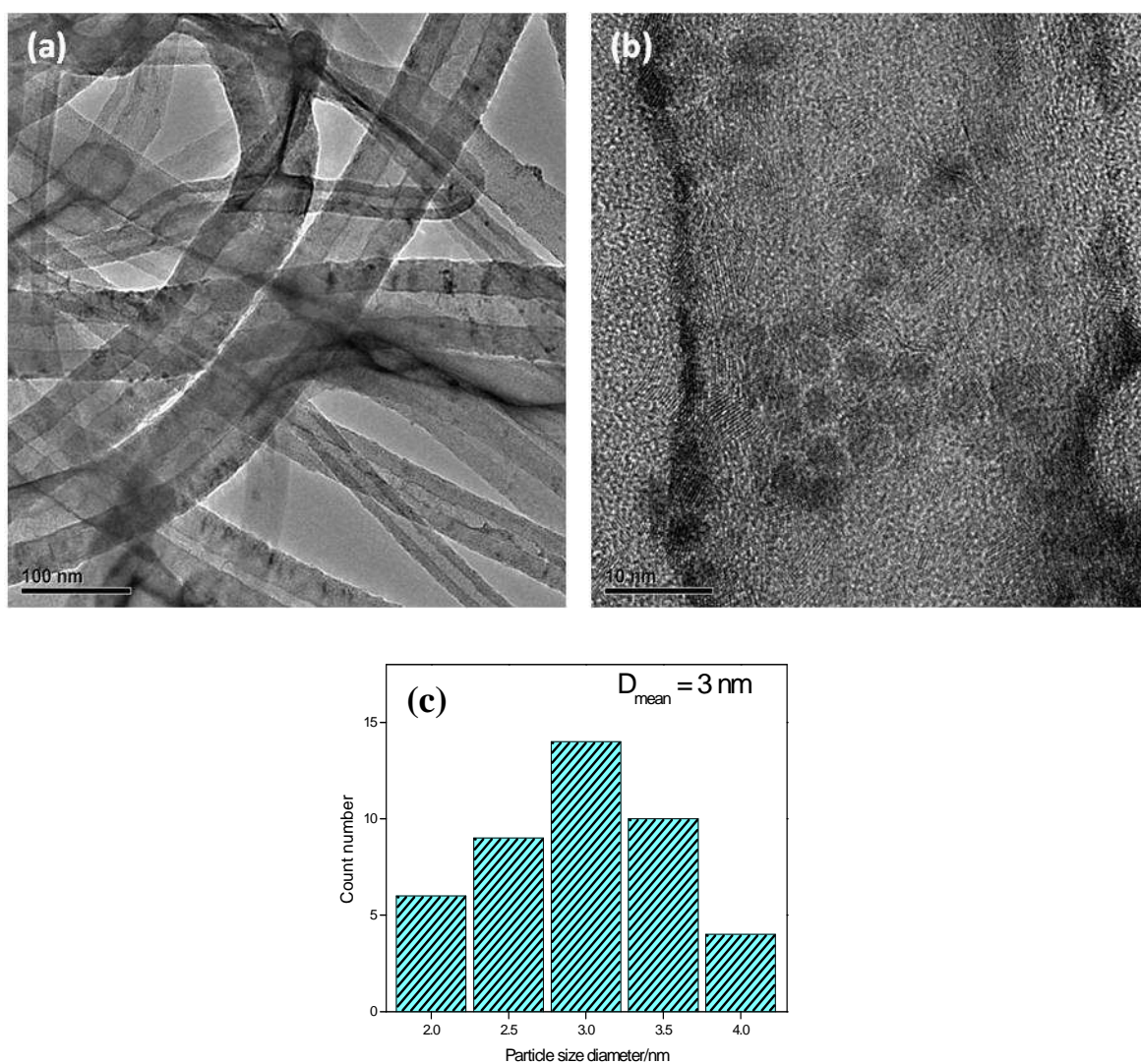
Figure 7.7. The TEM images low resolution (a) Ru/N-CNTs*, (b) high resolution Ru/N-CNTs and (c) histogram of the Ru/N-CNTs*
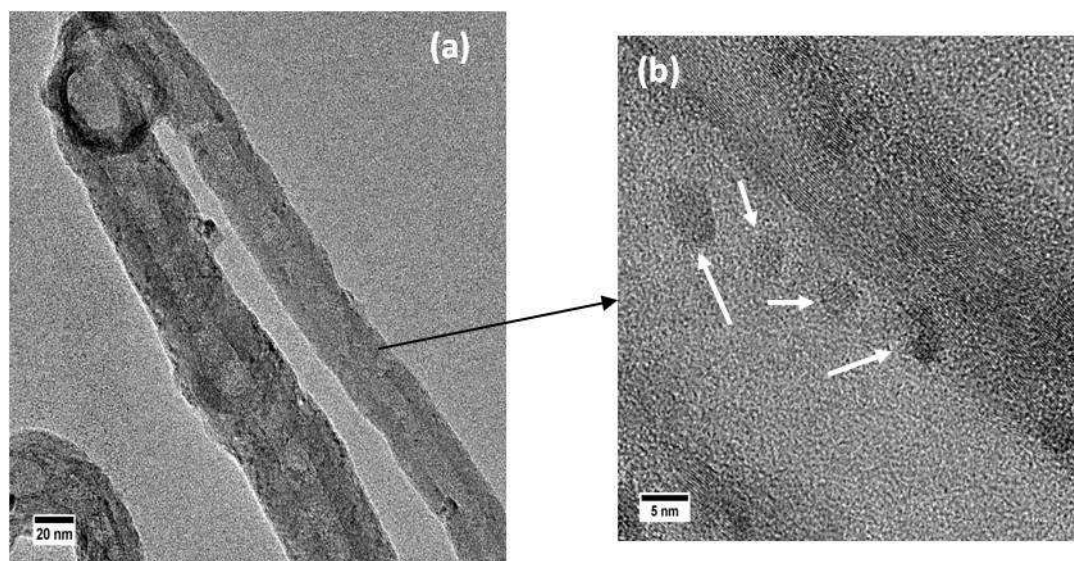
Figure 7.8. The TEM images (a) Ru/N-CNTs* calcined at 400 °C and (b) high resolution of calcined Ru/N-CNTs*.

Figure 7.8 shows the TEM images after the calcination of 5Ru/N-CNTs*, The RuO_2 metal particles appear as light spots embedded in the matrix of the N-CNTs* as shown by white arrows in Figure 7.8d. It was not easy to calculate the size of the RuO_2 nanoparticle from the TEM Image because the contrast between the support and metal nanoparticle was not clear. The oxide formation contributes to the particles to be less dense. Therefore the average 9 nm particle size obtained from the XRD analysis was applied. These data confirm that after calcination the size of the particles increased.

7.3.2   Reaction Analysis

The catalytic activity of the Ru/N-CNTs*, was evaluated by studying the oxidation of styrene with H_2O_2 as primary oxidant. In the investigation, suitable reaction conditions in terms of the styrene conversion and the product selectivity, the effect of temperature, oxidant concentration, catalyst amount, and the nature of the solvent were examined.

7.3.2.1 Effect of calcination temperature

The reaction activity of 5Ru/N-CNTs* catalysts in the oxidation of styrene was found to be affected by the catalyst calcination. The calcination of 5Ru/N-CNTs* at 400 ºC resulted in the decrease catalyst activity from 40 to 28 % but the selectivity to benzaldehyde increased from 75 to 92 %. The decrease of the activity after calcination might be due to the increase in the size of the metal particles. Similar results were observed for the study reported in Chapter 6 where the bigger particles of RuO_2 showed better selectivity. At the equi-conversion of styrene oxidation (28 %) the selectivity towards styrene oxide is also higher which shows the epoxidation route (route 2) is also favoured. As the calcined catalyst was found to be more selective further discussion were based on the calcined catalyst (RuO_2/N-CNTs*).

Table 7.1 Effect of calcination temperature

	Styrene Conversion (%)	Selectivity (%)			
		BZA	SO	BAc	PhAAc
5RuO$_2$/N-CNTs*	28	92	8	0	0
5Ru/N-CNTs*	40	75	6	6	11
[a]5Ru/N-CNTs*	28	62	38	0	0

[a] The styrene conversion at 3h. Reaction conditions: catalyst 0.04 g, styrene:H_2O_2 = 1:6 1,4-dioxane = 10 ml, T= 90 ºC and t = 5 h. Error bar = +/- .1.

7.3.2.2 Effect of temperature

The effect of the reaction temperature on the catalytic performance of the 5RuO$_2$/N-CNTs* is shown in Figure 7.9. As expected by increasing temperature from 60 to 100 ºC, styrene conversion increased from 3 to 43 mol % (5 h). The behaviour is due to the competitive thermal decomposition of H_2O_2 to water and oxygen at higher temperatures [9]. The reaction gave a higher selectivity to benzaldehyde at all temperatures. The selectivity to benzaldehyde decreased with an increase in

temperature, due to over oxidation to benzoic acid. The results shows that the cleavage of C=C bond (Route 1, Scheme 8.1) is high at low temperature which leads to the formation of benzaldehyde. On the other hand at higher temperature of 90 - 100 ºC the epoxidation (Route 2, Scheme 8.1) starts to compete against C=C bond cleavage which helps to form styrene oxide.

Figure 7.9. Effect of reaction temperature on the oxidation of styrene.   .
Reaction conditions: catalyst 0.04 g, styrene:H_2O_2 = 1:6   1,4-dioxane = 10 mL and t = 5 h

7.3.2.3 Effect of Time

The change of styrene oxidation was monitored and plotted with respect to the time as shown in Figure 7.10. The conversion of styrene increased with time and was completely converted after 18 h with 60 % benzaldehyde selectivity. By-products, such as benzoic acid were found to be formed when the reaction was allowed to run for a long time. After 6 h, the selectivity to benzaldehyde decreases and formation of by-products increased. This suggests over-oxidation of benzaldehyde with prolonged

152

time [10]. After 6 h of reaction over the catalyst, there is a decline in benzaldehyde selectivity due to the enhanced formation of side-products. The results indicate that benzaldehyde is a primary, product whereas, styrene oxide, benzoic acid, and phenyl acetic acids are secondary products.
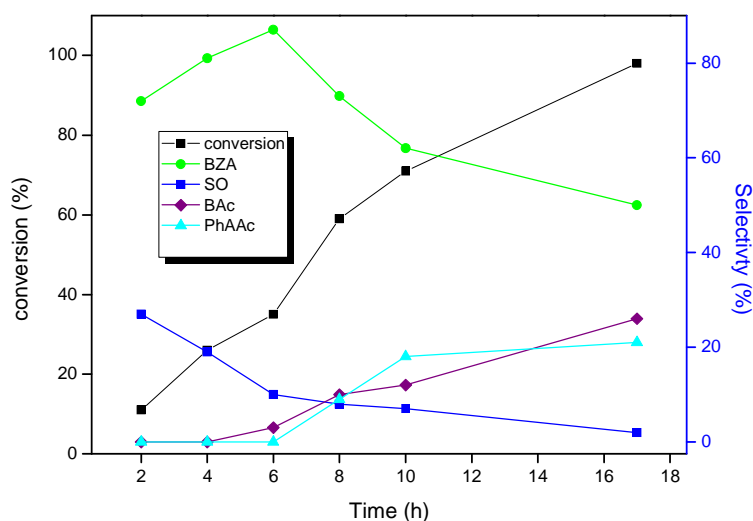
Figure 7.10. Effect of reaction time on the oxidation of styrene. Reaction conditions: catalyst 0.04 g, styrene:H_2O_2 = 1:6 1,4-dioxane = 10 ml, and T= 90 ºC

7.3.2.4 Effect of catalyst amount and loading

Three different amounts of catalyst (0.02, 0.04 and 0.06 g), were evaluated to study the effect of catalyst amount on the styrene oxidation reaction. When 0.02 g of 5RuO$_2$/N-CNTs* catalyst was used the styrene oxidation formed only benzaldehyde. The reaction was carried out for 5 h and the products were analyzed (Figure 7.11). With an increase in catalyst amount from 0.02 to 0.04 g, the conversion of styrene also increased from 14.0 mol % to 32 mol %, but the selectivity of benzaldehyde decreased from 100 to 85 mol % along with the formation of styrene oxide (15 mol %). The conversion increased with an increase in the amount of

catalyst because of an increase in catalytic active sites [11]. Once more, the increase in active site increases the competition of nucleophillic attack on styrene; leading to formation of styrene oxide.
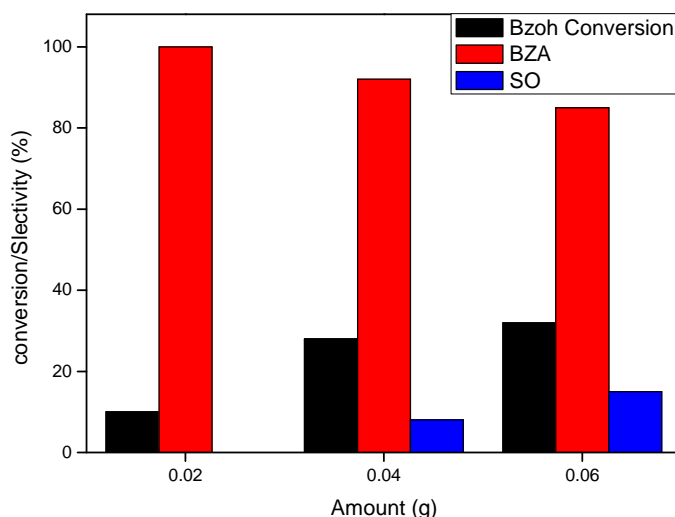
Figure 7.11. Effect of amount of catalyst on the oxidation of styrene. Reaction conditions: styrene:H_2O_2 = 1:6 1,4-dioxane = 10 ml, T= 90 ºC and t = 5 h

Table 7.2. Effect of loading

	Styrene Conversion (%)	Selectivity (%)			
		BZA	SO	BAc	PhAAc
5RuO$_2$/N-CNTs*	28	92	8	0	0
3RuO$_2$/N-CNTs*	20	96	4	0	0

Reaction conditions: catalyst 0.04 g, styrene:H_2O_2 = 1:6 1,4-dioxane = 10 ml, T= 90 ºC and t = 5 h. Error bar = +/- 1.

The amount of active sites available plays a major role in the reaction. The decrease in loading from 5 - 3 wt.% gave a decrease in the conversion of the styrene conversion (28 - 20 %) with an increase in selectivity to benzaldehyde. The selectivity to benzaldehyde was 92 and 96 %, for

5RuO$_2$/N-CNTs* and 3RuO$_2$/N-CNTs* respectively Similar conduct was experienced above with the amount of catalyst used.

7.3.2.5 Effect of oxidant

The influence of styrene to H$_2$O$_2$ molar ratio on the conversion and selectivity was studied and the results are shown in Figure 7.12. Different styrene/H$_2$O$_2$ molar ratios (1:2, 1:6, 1:8, and 1:10) were assessed. It is found that when the styrene to H$_2$O$_2$ molar ratio is increased from 1:2 to 1:8 styrene conversion increases from 13 % to 60 mol %. While the selectivity to benzaldehyde decreased from 100 to 85 mol %.
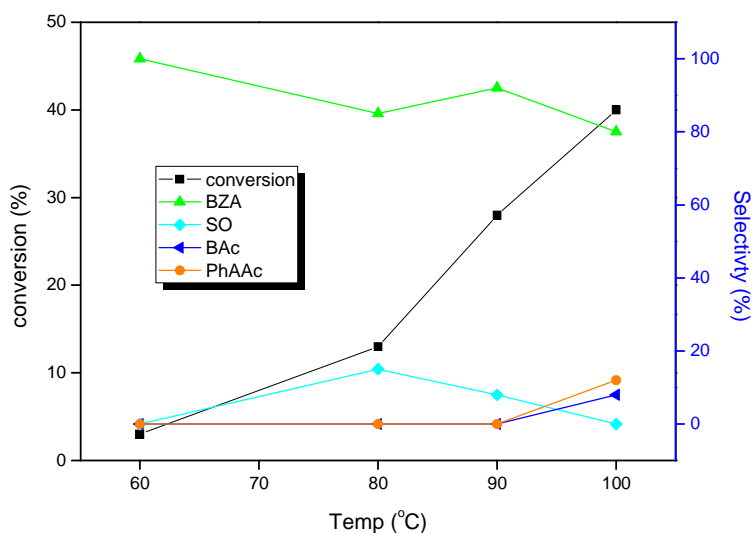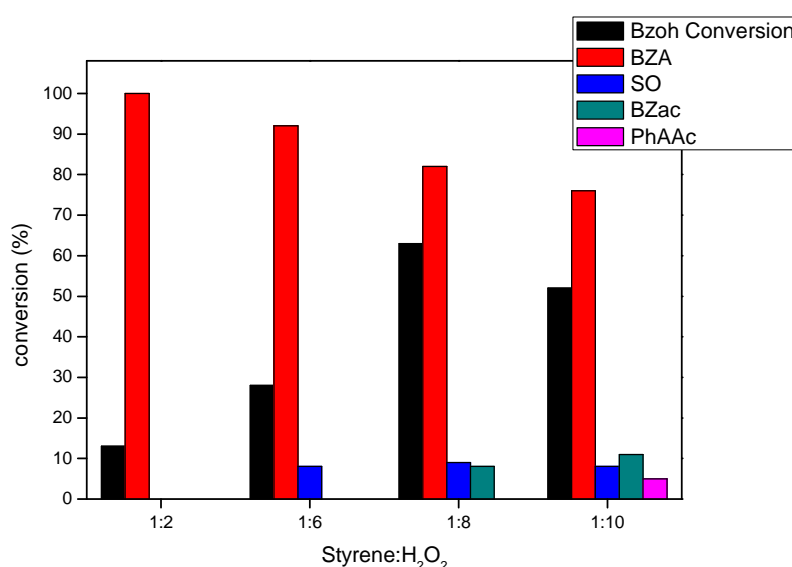

Figure 7.12. Effect of oxidant concentration the oxidation of styrene. Reaction conditions: catalyst 0.04 g, styrene:H$_2$O$_2$ = 1:6 1,4-dioxane = 10 ml, T= 90 ⁰C and t = 5 h.

When small amounts of H$_2$O$_2$ were used, H$_2$O$_2$ may compete with excess styrene for coordination sites, and hence formation of OH radicals might be significantly reduced. Thus, the conversion is reduced. With an increase in molar ratio, H$_2$O$_2$ coordinates to the metal and decomposes to form OH radicals. Hence, higher styrene conversions are noted [12]. A Further increase to a 1:10 ratio indicates a slight decrease in the styrene

conversion. Therefore, 1:6 molar ratio of styrene to H_2O_2 was found to be optimum in terms of conversion for this study.

7.3.2.6 Effect of solvent

To investigate the solvent effect on the styrene oxidation reaction, solvents such as: 1,4 dioxane, acetonitrile, DMF and toluene were used. The effect of different solvents on styrene conversion and product selectivity, at 90 ºC, over RuO_2/N-CNTs* catalysts, are summarized in Table 7.3

When DMF is used as a solvent no styrene oxidation occurred. Also, when the acetonitrile and toluene were used as solvents for the oxidation reaction, the catalytic activity of the catalyst was reduced to 5 and 3 % respectively; this is probably due to the adsorption of these solvents on the active species at the surface of catalyst [13].

When toluene was used as solvent, route 2 (Scheme1) dominated and led to the formation of styrene oxide. Acetonitrile resulted in route 1 being. favoured and hence the formation of benzaldehyde.

Table 7.3. Effect of solvent on styrene oxidation[a]

Temp (°C)	Styrene Conversion (%)	Selectivity (%)			
		BZA	SO	BAc	PhAAc
1,4-dioxane	28	92	8	0	0
Acetonitrile	5	100	0	0	0
Toluene	3	0	100	0	0
DMF	0	0	0	0	0

[a]The conversion of Styrene at 5 h. Reaction conditions: catalyst = 0.04 g, styrene:H_2O_2 = 1:6 1,4-dioxane = 10 ml and T= 90 ºC. Error bar = +/- 1.

7.3.2.7 Effect of recycling

After the completion of the catalytic reaction, the supernatant was decanted and the catalyst was washed several times with acetone. It was then dried at 150 for 3 h and used three more times following the same process conditions (Figure 7.13). It was observed that the recycled catalyst retained +/- 90 % of the initial conversion of the catalyst. There was an increase in the selectivity of the by-products specifically the acids after recycling. The ICP analysis of the reaction filtrate showed no detectable Ru in solution after the styrene oxidation reaction.
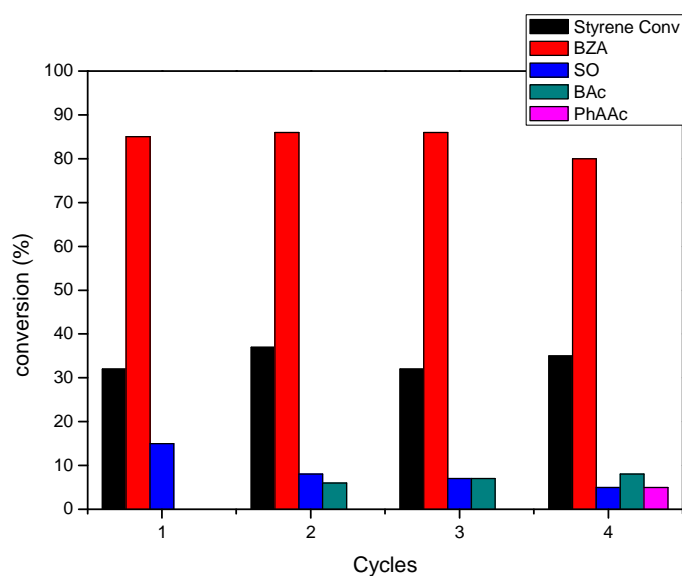

Figure 7.13. Effect of recycling on the oxidation of styrene. Reaction conditions: styrene:H_2O_2 = 1:6 1,4-dioxane = 10 ml, T= 80 ºC and t = 5 h.

7.3.2.8 The role of catalyst and oxidant

The role of the catalyst and oxidizing agent was determined. The conversion of styrene was to 2 % in the presence of RuO_2/N-CNTs* catalyst without using oxidant H_2O_2. Similarly, in the absence of

RuO$_2$/N-CNTs* catalyst but using H$_2$O$_2$ under similar reaction condition (1,4 dioxane, 90 °C, 5 h), no styrene conversion was noted. It suggests that no reaction takes place in the absence of catalyst. This observation ruled out the possibility of reaction taking place due to the thermal decomposition of hydrogen peroxide.

7.4   Activity comparison

Table 7.4. Comparison of the activity of the 5Ru/N-CNTs and 5Ru/N-CNTs*

	h	Styrene Conv (%)	Selectivity (%)			
			BZA	SO	BAc	PhAAc
5RuO$_2$/N-CNTs	4	34	87	3	3	6
5RuO$_2$/N-CNTs*	4	24	82	18	0	0
5RuO$_2$/N-CNTs	8	70	61	7	14	18
5RuO$_2$/N-CNTs*	8	60	75	8	8	9

In this section the activity of nitrogen doped carbon nanotubes used for styrene oxidation were compared. The N-CNTs and N-CNTs* contain 0.8 and 2.2 at. % nitrogen content respectively. It was realized that the nitrogen present in the support plays a major role. With the increase in the nitrogen content in the CNTs the conversion of styrene decreased but with an increase in selectivity.

7.5   Conclusion

RuO$_2$/N-CNTs* catalysts are active in catalysing the oxidation of styrene; the main product was benzaldehyde. This resulted from the nucleophilic attack of H$_2$O$_2$ on styrene oxide, followed by cleavage of the intermediate hydroxy–hydroperoxystyrene, and also from a cleavage of the C=C bond. The catalyst has shown to be highly selective as compared to the previous supported catalysts used for styrene oxidation; CNTs and N-CNTs.

Comparing the support it was deduced that the nitrogen present in the support plays a major role. With the increase in the nitrogen content in the CNTs the conversion of styrene decreased but with an increase in selectivity. The selectivity towards benzaldehyde was 92 mol % after 4 h when N-CNTs* was used as support for the styrene oxidation reaction. The conversion for CNTs and N-CNTs as support for Ru in the styrene conversion was 85 and 87 % respectively. N-CNTs* as support also slowed down the formation of by-products. The catalyst was also shown to be recyclable without a substantial loss of its catalytic activity, at least in three cycles.

In conclusion Ru particle size plays a role in catalytic reaction as does the amount of nitrogen present in the CNT support.

References

1   Z. N. Tetana, S. D. Mhlanga, G. Bepete, N. J. Coville, R. W. M. Krause, S. Afr. J. Chem. South African Journal of Chemistry 65 (2012) 39-49.

2.   L. F. Mabena, S. S. Ray, N. J. Coville, Ceramic Engineering and Science Proceedings 32 (2011) 33-42.

3.   A.M.F. Lima, A.W. Musumeci, H.-W. Liu, E.R. Waclawik, G.G. Silva, J. Therm. Anal. Calorim. 97 (2009) 257.

4.   D. Bom, R. Andrews, D. Jacques, J. Anthony, B. Chen, M.S. Meier, J.P. Selegue, Nano Lett. 2 (2002) 615.

5   S. Shang, X. Yang, X.-m. Tao, Polymer 50 (2009) 2815-2818

6   T. Kyotani, N. Sonobe, A. Tomita, Nature 331 (1988) 331-333

7   R. I. Zhao, Y. Ma, J. Zhang, F. Li, W. Liu, Q. Cui, Materials Science-Poland 28 (2010) 189-198.

8.   S. Qiu, S. J. Kalita, Materials Science and Engineering: A (2006) 327-332.

9.   C. Saux, L. B. Pierella, Applied Catalysis A: General 400 (2010) 117-121

10.   V. R. Choudhary, R. Jha, N. K. Chaudhari, P. Jana, Catalysis Communications 8 (2007) 1556-1560.

11   V. K. Bansal, P. P. Thankachan, and R. Prasad, Applied Catalysis A: General 381 (2010) 8.

12   S. K. Pardeshi, R. Y. Pawar, Materials Research Bulletin 45 (2010) 609-615.

13   C. Xiong, Q. Chen, W. Lu, H. Gao, W. Lu, and Z. Gao, Catalysis Letters 69 (2000) 231.

CHAPTER 8

SELECTIVE OXIDATION OF BENZYL ALCOHOL TO BENZALDEHYDE OVER CARBON NANOTUBE SUPPORTED RUTHENIUM

8.1   Introduction

Currently more than 20 % of industrial organic chemicals are produced by catalytic reactions [1]. One example is the development of novel and effective catalysts for the selective oxidation of alkenes/olefins to aldehydes and ketones. This is important in the chemical industry and the reaction is currently of considerable interest [2,3,4,5]. The liquid-phase oxidation of benzyl alcohol into the corresponding carbonyl compound, benzaldehyde, is an important reaction in organic synthesis. Oxidation of benzyl alcohol to benzaldehyde, is important as it provides chlorine-free benzaldehyde [6]. Generally oxidation of benzyl alcohol provides benzaldehyde and benzoic acid but other by-products such as benzyl benzoate, toluene and benzene can form depending on the reaction conditions and metal catalyst employed. These by-products are likely to be the outcome of side reactions as shown in scheme 8.1: (A) decarbonylation (benzene), (B) hydrogenolysis (toluene), (D) overoxidation (benzoic acid) and (E) esterification (benzyl benzoate) reaction pathways [7,8]. The main product benzaldehyde is a non-enolizable aldehyde. Formation of this aldehyde reduces the number of possible by-products that can form and allows an easier understanding of the reaction mechanism [9,10].
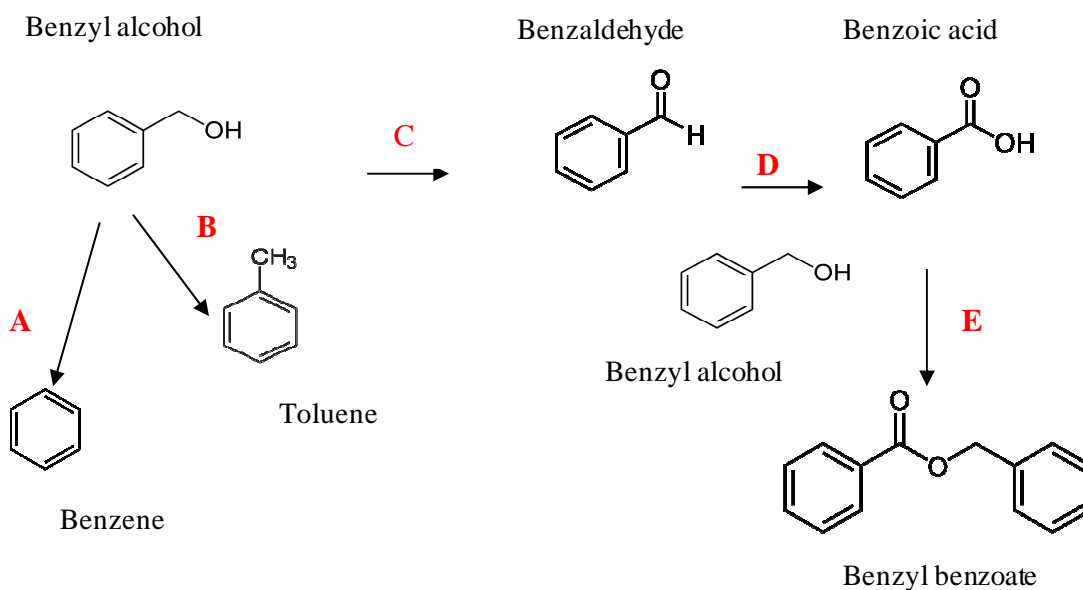
Scheme 8.1. Possible reaction pathways for benzyl alcohol oxidation

Benzaldehyde is a valuable chemical which has widespread applications as an intermediate for the production of perfumes, dyes stuffs and agro chemicals [11,12,13,14,15,16]. Alcohols are traditionally oxidised by non-catalytic methods with stoichiometric oxidants such as dichromate or permanganate [7,17,18]. The oxidation process is complex and it can be difficult to control. Hence, improvements to the reaction by the use of new catalytic materials can lead to the reduction in by-product formation [1,19,20].

An important consideration in developing a new catalyst system relates to finding appropriate support materials. Hence, the catalytic performance can be improved by the use of appropriate supports that controls dispersion of both metal particle and the metal-support interaction [21].

Supported heterogeneous catalysts have been studied for the selective oxidation of organic compounds such as alcohols [22,23]. The catalytic role of the supported metals for selective oxidation of benzyl alcohol has

been extensively studied and the most promising heterogeneous catalysts are currently based on the platinum group metals. Gold and palladium have also attracted significant attention due to their superior catalytic performance [8,10,24]. Supports used include zeolites silica, titania, and alumina [25]. Although these supports can be separated from the product at the end of the reaction by centrifugation or extraction it is often difficult to use these processes in industry.

Carbon materials are currently attractive as supports because they can be easily separated from reactants and products [26]. Carbon nanotubes (CNTs) have many advantages when used as support since metal particles are expected to be readily exposed to reactants on the non porous exterior of the CNT and as a result generate an effective catalyst. Metal deposition commonly requires use of an activated CNT surface [27] and this means that the inert surface of pristine CNTs must be chemically modified. For instance, by doping CNTs with heteroatoms such as nitrogen, a practical path to tailor both the physical and chemical properties of the CNTs, by modifying the CNT electronic structure, can be achieved [28,29]. Nitrogen atoms entering the graphene sheets as a substituent for carbon could also modify the adsorption strength of the nanotube towards foreign atoms/molecules quite significantly. This will in turn, greatly modify the overall catalytic activity as well as the selectivity of a catalyst [30].

Table 8.1 lists some of the reactions that have been reported in the literature on the benzyl alcohol reaction using supported heterogeneous catalysts.

Table 8.1. Studies of the oxidation of benzyl alcohol to carbonyl compounds

Metal	Support	Oxidant	Ref
Ag	Hexagonal mesoporous silicas	O_2	[31]
Au	Hexagonal mesoporous silicas	O_2	[32]
Ru	Al_2O_3	O_2	[18]
Ru	CNT	O_2	[3]
Pd	CNT/AC	O_2	[8]
Au–Pd	N-CNs/AC	O_2	[27]
Au	C/TiO_2	O_2	[7]
Au-Pd	TiO_2	O_2	[13]
Fe	FeAPO-5	H_2O_2	[33
Au/Au-Pd	SBA-15	O_2/air	[2]
Pd/Au-Pd	SBA-16	O_2	[10]
Ag	Ni-Fiber	O_2	[15]
Au-Cu	SiO_2	O_2	[34]
Pd	$MnCeO_x$	O_2	[9]

Most reported studies on the oxidation of benzyl alcohol to carbonyl compounds have used oxygen as an oxidant. This is an environmentally friendly oxidant and it provides a green route to product formation when compared to stoichiometric oxidations using a metal or a metal containing inorganic oxidant such as dichromate or permanganate. However, the presence of oxygen may result in overoxidation and explosions, or the flammability of the organic solvent or alcohol reactants [35]. These issues make safety a problem in a large scale production process. To overcome this issue hydrogen peroxide can be used as an oxidant and in this study peroxide will be used as an oxidant. Yu et al, [3] reported the use of a 9.3 wt. % Ru supported on CNT catalyst for the aerobic oxidation of benzyl alcohol. Air was used as the oxidant at ambient pressure.

Yamaguchi et. al., [36] achieved a 99 % yield of benzaldehyde by using molecular oxygen and Ru/Al$_2$O$_3$ catalyst. In this chapter, the influence of a Ru supported catalyst for the oxidation of benzyl alcohol is reported. The Ru was supported on CNTs and on nitrogen doped carbon nanotubes (N-CNTs) and the liquid phase oxidation of benzyl alcohol was studied.

8.2 Experimental

8.2.1 Materials

CNTs with inner diameters of 5-10 nm and outer diameters of 40-80 nm were obtained from Sigma Aldrich. The N-CNTs used, with inner diameters of 5 - 10 nm and outer diameters of 35 - 100 nm, with nitrogen content of 0.8 at.%. were synthesised in-house (Chapter 3). Benzyl alcohol, hydrogen peroxide (H$_2$O$_2$) (50% mass concentration in water), RuCl$_3$.xH$_2$O (Aldrich) were used as purchased. All other chemicals and reagents used were of analytical grade and purchased from Sigma Aldrich and used without any further purification.

8.2.2 Catalyst preparation

The catalyst was synthesised via a microwave irradiation procedure as described in [37]. Ru nanoparticles were deposited on N-CNTs using the microwave assisted polyol method in a microwave teflon vessel. In the reaction 50 mg of CNTs or (N-CNTs) and RuCl$_3$.xH$_2$O were mixed with 80 mL ethylene glycol (EG) and sonicated for 10 min to afford a homogenous suspension. Ru/CNT and Ru/N-CNT mixtures were chosen to give four different Ru loadings (2, 3 4 and 5 wt. %.). The suspension was then placed in a microwave reactor (Anton-Paar Multiwave 3000) and heated to 200 °C and the reaction mixture was kept at this temperature for 5 min at 500 W. The resulting clear suspension was filtered and the residue was washed with 20 mL acetone, then with 50 mL deionised water and dried at 110 °C overnight. The material was then calcined at 350 °C.

The samples were named according to the wt. % of Ru expected *viz* 2Ru/CNTs, 2Ru/N-CNTs, 3Ru/CNTs 4Ru/CNTs and 5Ru/CNTs.

8.2.3   Characterisation

The samples were characterised as described in chapter 6. The Ru loadings were determined by the inductively coupled plasma (ICP) (Spectro-Acros) technique, XRD patterns were collected in air at room temperature on a X'Pert Pro PANalytical X-ray diffractometer using Cu Kα radiation and the size of Ru particles was determined on carbon using a JEOL 2100 TEM.

8.2.4   Catalytic activity

Benzyl alcohol, the Ru/CNT catalyst and the 1,4-dioxane solvent in the required ratio were added to a 50 mL two–neck round bottomed flask. The flask was equipped with a magnetic stirrer and a water circulated condenser under continuous stirring of 1400 rpm, while heated in the oil bath. The progress of the reaction was determined by analysing the reaction mixture using an Agilent 7890A gas chromatograph system fitted with a SPB 50 fused silica capillary column (30 m x 0.25 mm x 0.25 µm) and a FID detector. Small aliquots (1 mL) of the reaction mxture were withdrawn after specific time intervals. The injector and the column temperature were set at 220 ºC and 148 ºC respectively. The conversion of benzyl alcohol and the selectivity to benzaldehyde were calculated by the peak area normalization method. After the reaction the catalyst was collected and then washed with 20 mL acetone and heated at 110 °C prior to reuse.

8.3   Results and discussion

8.3.1   Benzyl alcohol oxidation

The Ru/CNT catalytic oxidation of benzyl alcohol to benzaldehyde was monitored by GC. A typical GC spectrum showing the benzyl alcohol oxidation product is shown in Figure 8.1. The peak area corresponding to each molecule detected was taken to correspond to the number of moles of that molecule passing through the detector. The conversion and selectivity data were calculated as follows:

$$\text{Conversion/\%} = \frac{\text{moles of reactant converted}}{\text{moles of reactant in feed}} \times 100\%$$

$$\text{Selectivity /\%} = \frac{\text{moles of product formed}}{\text{moles of all products}} \times 100\%$$
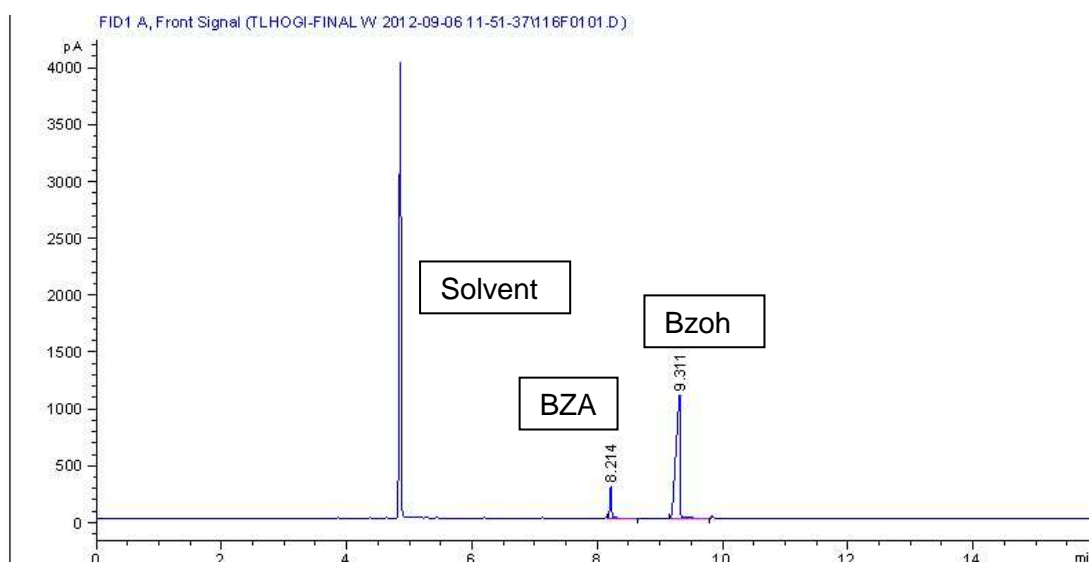
Figure 8.1. A typical benzyl alcohol oxidation spectrum for products obtained from an FID GC

167

The synthetic method gave Ru particles that were, highly dispersed, small and homogenous (chapter 4). Ru nanoparticles were produced on both CNTs and N-CNTs. Four different Ru loadings (2, 3, 4 and 5 wt. % Ru) were deposited on the CNTs. The ICP analysis showed that the Ru loading ratio was 1.87, 2.93, 3.80 and 4.81 % for 2Ru/CNTs, 3Ru/CNTs, 4Ru/CNTs and 5Ru/CNTs materials respectively (Table 7.2). The particle sizes were observed to increase with the increase in loading of Ru, with sizes of 5.2, 5.2, 5.6 and 6.2 nm for the 2Ru/CNT, 3Ru/CNT, 4Ru/CNT and 5Ru/CNT materials respectively. The loading of the Ru on N-CNTs was found to be 3.12 wt. % with a nanoparticle size average diameter of 2.90 nm. The particle size of RuO_2 supported on both CNTs and N-CNTs increased after calcination at 350 °C.

Table 8.2 The loading, particle size of Ru/RuO_2 on CNTs and N-CNTs before and after calcination

Support	Ru loading (wt. %)	Particle size (nm)	
		Before calcination (Ru)	After calcination (RuO_2)
2Ru/CNTs	1.87	5.2	7.3
3Ru/CNTs	2.93	5.2	7.2
4Ru/CNTs	3.80	5.6	8.4
5Ru/CNTs	4.81	6.2	9.8
3Ru/N-CNTs	3.12	2.9	5.1

8.3.1.1 Effect of temperature

It had been reported that reaction temperature has a strong influence on the process of benzyl alcohol oxidation [12]. The results of benzyl alcohol oxidation over the $3RuO_2$/CNT catalyst in 1,4-dioxane solvent for 5 h in the temperature range of 80 - 110 °C are given in Table 8.3. As expected, the conversion of benzyl alcohol increased with an increase in reaction

temperature. This might be due to the competitive thermal decomposition of H_2O_2 to H_2O and O_2 with increase in temperature and/or to an increase in the rate of the benzyl alcohol to benzaldehyde reaction [26,38]. The conversion increased from 4 - 11 % but the selectivity of benzaldehyde decreased with an increase in temperature (Table 6.7).

Table 8.3 Effect of temperature on benzyl alcohol oxidation[a]

Temperature (°C)	Conversion (%)	Selectivity (%)	
		BZA	BAc
80	4	100	0
100	6	88	12
110	10	85	15

[a]Reaction Conditions: Bzoh:H_2O_2 =1:6, catalyst = 40 mg, T = 5 h.
BZA - Benzaldehyde
BAc - Benzoic acid
Error bar = +/- 1.

8.3.1.2 Effect of reaction time

The oxidation of benzyl alcohol was monitored with respect to time. The results are shown in Figure 8.2 The conversion of benzyl alcohol increased slowly and continuously when the reaction time was increased. It was seen that 10 % conversion was observed after 5 h; when the reaction was allowed to continue for 18 h, 21% conversion was observed. The benzyl alcohol conversion and selectivity to benzoic acid increased whereas the selectivity to benzaldehyde decreased with increasing reaction time. The decrease in the selectivity to benzaldehyde and the increase in the selectivity to benzoic acid with increasing reaction time indicates an over oxidation process (Scheme 8.2).

Scheme 8.2. Benzyl alcohol reaction pathway to benzoic acid
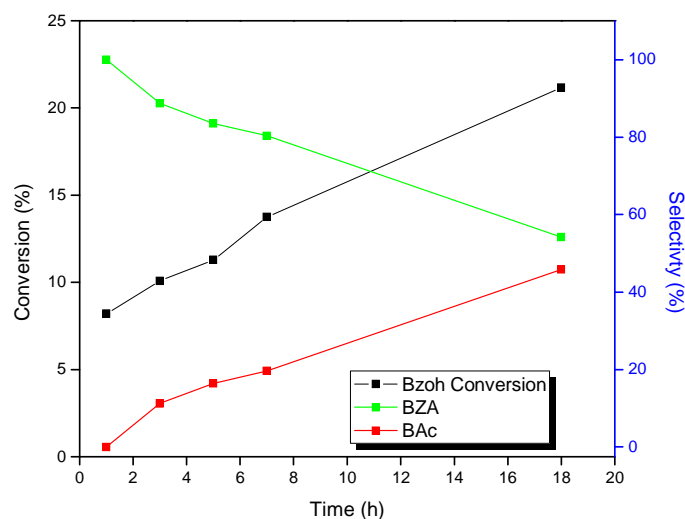
Figure 8.2. Effect of reaction time on the oxidation of benzyl alcohol. Reaction Conditions: catalyst = 0.04 gBzoh:H_2O_2 =1:6 and T =110 ºC

8.3.1.3 Effect of loading

The influence of the RuO_2 loading on the RuO_2/CNT catalyst performance in the benzyl alcohol oxidation is shown in Figure 8.3. The supported RuO_2/CNT catalysts were found to be active and selective for the oxidation of the benzyl alcohol at all ruthenium loadings. The conversion of benzyl alcohol increased from 4 to 25 % on increasing the Ru loading from 2 to 5 wt. %. However, on increasing the Ru loading the selectivity to benzaldehyde decreased to 74 % along with an increase in formation of benzoic acid. At higher loadings there are more active sites and hence a greater chance of both benzyl alcohol and benzaldehyde being simultaneously adsorbed on the RuO_2 [39].

Figure 8.3. Effect of Ru metal loading on the oxidation of benzyl alcohol. Reaction Conditions: catalyst = 0.04 g, Bzoh:H_2O_2 = 1:6, T = 110 °C and t = 5 h.

8.3.1.4 Effect of H_2O_2 concentration

The amount of oxidant used in the system is an important factor that influences the oxidation of alcohols. The effect of H_2O_2 concentration on the oxidation of benzyl alcohol was investigated by varying the molar ratio of substrate to H_2O_2 (1:4, 1:6, 1:8, 1:10 and 1:12) and the results are shown in Figure 8.4. An increase of oxidant concentration ratio from 1:4 to 1:10 enhanced the rate of the benzyl alcohol oxidation with conversion increasing from 8 to 23 %. Benzaldehyde selectivity increased up to a 1:6 ratio only (70 to 85 %) then decreased while benzoic acid formation increased. When the benzyl alcohol to H_2O_2 molar ratio was increased to 1:12, both the catalytic activity and the benzaldehyde selectivity decreased.
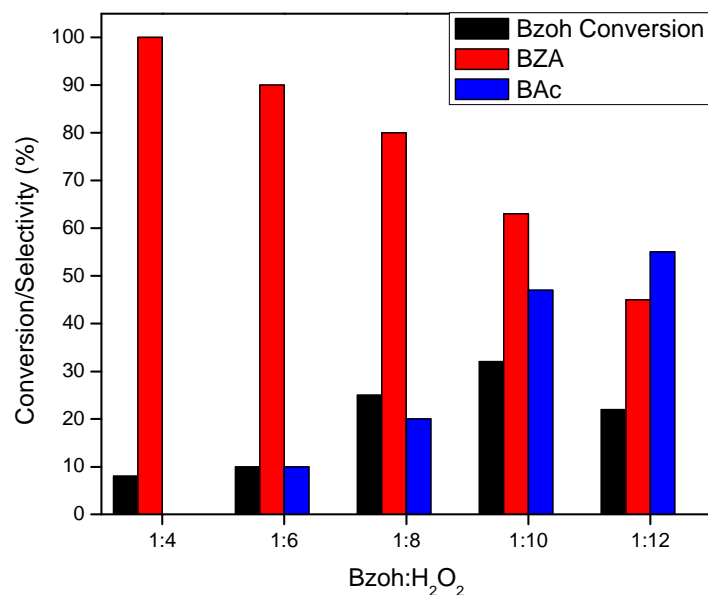
Figure 8.4. Effect of oxidant concentration the oxidation of benzyl alcohol. Reaction Conditions: catalyst = 0.04 g, T = 110 ºC and t = 5 h.

The amount of benzoic acid increased at the expense of benzaldehyde due to over-oxidation. The reason for the decreasing % conversion of benzyl alcohol at higher H_2O_2 concentration and temperature is due to self-decomposition of oxidant. Further, dilution of the reaction mixture takes place, since H_2O_2 contains a considerable amount of water (50 %) [3,8].

8.3.1.5 Effect of the amount of catalyst

The amount of catalyst has a significant effect on the oxidation of benzyl alcohol. Four different amounts of catalysts viz., 20, 40, 60 and 80 mg were used, while keeping all other reaction parameters constant (reaction temperature, benzyl alcohol to peroxide ratio and reaction time). The results are shown in Figure 8.5. Benzyl alcohol conversions of 6, 10, 22 and 20 % corresponding to the 20, 40, 60 and 80 mg catalysts used were measured.
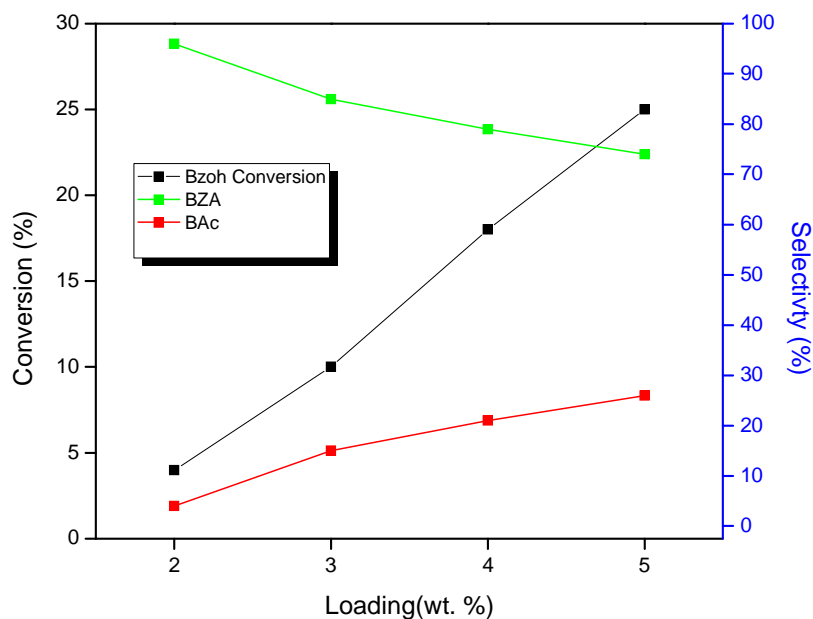
Figure 8.5. Effect of amount of catalyst on the oxidation of benzyl alcohol. Reaction Conditions: catalyst = 0.04 g, Bzoh:H_2O_2 =1:6, T =110 °C, and t = 5 h.

The results indicated that the benzyl alcohol conversion increased with increasing catalyst amount, which is due to the increase in the number of RuO_2 active sites available for reaction [12,40]. With an increase in the amount of catalyst from 20 to 80 mg the selectivity to benzaldehyde also decreased from 100 to 71 %. The increase in the amount of catalyst aids the decomposition of more hydrogen peroxide to oxygen and water leading to a lower conversion [41].

8.3.1.6 Effect of recycling

The recyclability of a used catalyst $3RuO_2$/CNT was tested in the benzyl alcohol oxidation reaction. The reaction mixture was filtered after a contact time of 5 h. (110 °C). The catalyst was then re-used after washing with acetone and after drying in an oven at 120 °C for 2 h.
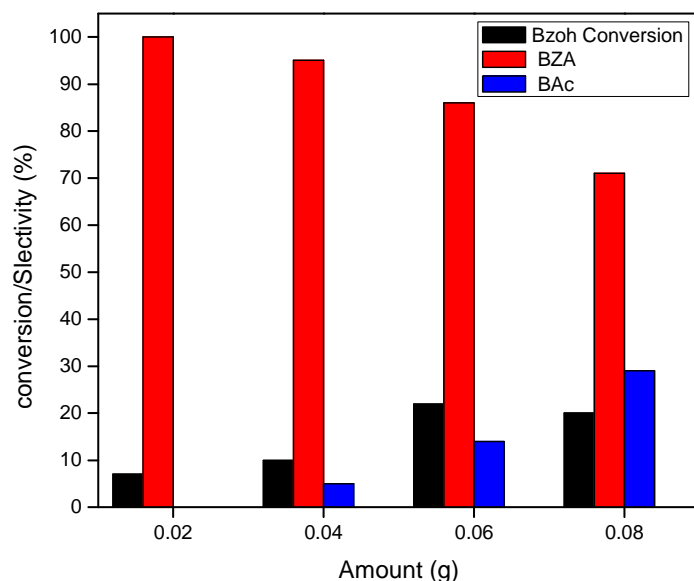
Figure 8.6. Effect of recycling on the oxidation of benzyl alcohol. Reaction Conditions: catalyst = 0.06 g, Bzoh:H_2O_2 = 1:4, T = 110 °C and t = 5 h.

Figure 8.6 shows that the re-use resulted in a decrease in the selectivity of benzaldehyde with an increase in selectivity to benzoic acid formation. Recycling for a second time continued this trend (selectivity 37 %). The conversion of benzyl alcohol remained almost unchanged after another re-use (21 %) from an initial conversion of 23 %. The conversion is not affected but the selectivity to benzaldehyde decreased as a function of re-use. This suggests a change in the surface of the Ru and oxygen atoms. The catalytic particles could rearrange in the presence of H_2O_2 and this could lead to the changed selectivity. It is possible that sintering also occurred. The ICP-OES analysis of the reaction for the reaction mixture was performed and no Ru metal was detected in the filtrate after reaction. These rules out a homogenous oxidation reaction involving Ru salts.

8.3.1.7 Effect of N-CNTs

Figure 8.7 demonstrates the results of the benzyl alcohol reaction over RuO_2 supported on the N-CNTs and on the CNTs. The RuO_2 supported on

the N-CNTs shows better activity and benzaldehyde selectivity than the RuO$_2$ on the CNTs. The conversion of 3RuO$_2$/N-CNTs after 5 h was 18 % with 80 % selectivity to benzaldehyde. After 18 h the conversion of alcohol using the N-CNT support increased to 41 % even though the selectivity to benzaldehyde decreased significantly to 25 %. For 3RuO$_2$/CNTs the conversion was only 10 % after 5 h with 70 % selectivity to benzaldehyde. The conversion increased to 16 % after 18 h but with a benzaldehyde selectivity of 32 %. At equi-conversion (8 % conversion), RuO$_2$/N-CNTs showed 95 % selectivity to benzaldehyde. This reveals that the catalytic activity of supported Ru nanocatalysts can be attributed not only to Ru nanoparticles but also to the interaction of the Ru particles with the support; the latter plays an important role in controlling the catalytic activity of the supported Ru nanoparticles.
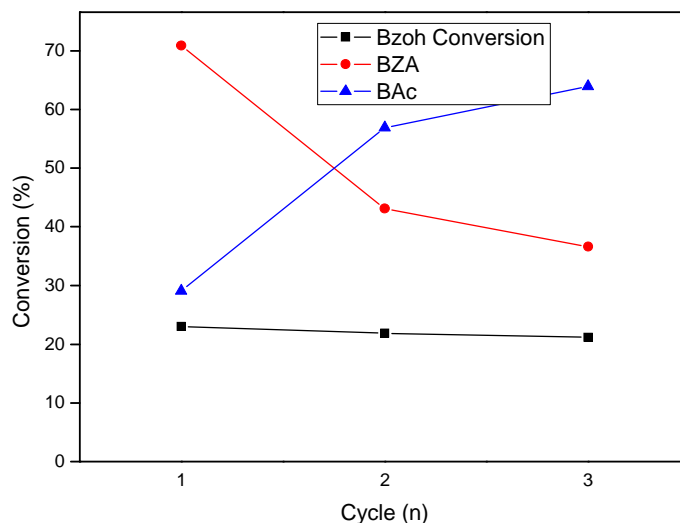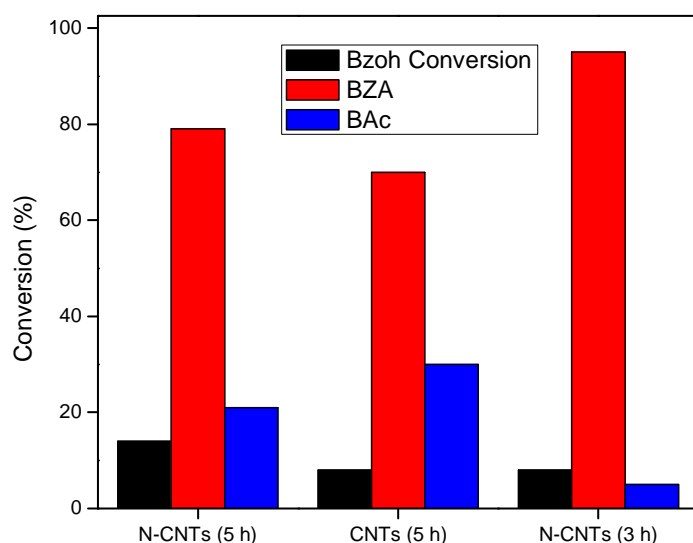

Figure 8.7. Effect of N-CNTs on the oxidation of benzyl alcohol. Reaction Conditions: catalyst = 0.04 g, Bzoh:H$_2$O$_2$ = 1:6, T = 110 ºC, and t = 5h.

The increase in the activity of RuO$_2$/N-CNTs can be related to the higher dispersion of the Ru and a good interaction between the support and the Ru particles associated with the introduction of the N-functionalities.

[27,42] Nitrogen introduced chemically active sites that are required for anchoring of the nanoparticles [43]. In addition, nitrogen is able to generate defects on carbon, which increases the edge plane exposure and as a result enhances the catalytic activity [44].

8.4   Conclusion

The synthetic method gave Ru particles that were, highly dispersed, small and homogenous. RuO_2 nanoparticles were produced on both CNTs and N-CNTs by calcination. The catalysts were tested for benzyl alcohol oxidation to benzaldehyde. The structural features of a Ru catalyst, as well as the reaction conditions strongly affect the behaviour of the benzyl alcohol oxidation reaction with hydrogen peroxide. The main product of the benzyl alcohol oxidation reaction is benzaldehyde with benzoic acid as by-product. The product ratio depends on the nature of the catalyst. The functionalised RuO_2/N-CNT based catalyst was also tested for the selective oxidation of benzyl alcohol and compared to the RuO_2/CNT based catalysts. After 5 h at 110 ºC benzyl alcohol conversion was 10 and 14 % for $3RuO_2$/CNTs and $3RuO_2$/N-CNT catalyst respectively and benzaldehyde selectivity of 70 and 85 % respectively. The nitrogen functionalities incorporated in the network structure of CNTs led to an improvement of the catalytic performance and the selectivity towards benzaldehyde. The activity improvement for $3RuO_2$/N-CNT was due to a better dispersion and smaller particle size (5.1 nm) of the metal nanoparticles on the surface but also due to the interaction of the Ru particles with the support. The Ru particles-support interaction plays an important role in determining the catalyst performance in the process of benzyl alcohol oxidation.

In conclusion, the results for supported Ru catalyst for different reactions show that the catalytic properties of catalyst depend on the support, Ru loading, and also on the reaction catalysed by the catalyst.

References

1.   S. Mandal, A. SinhaMahapatra, B. Rakesh, R. Kumar, A. Panda, B. Chowdhury, Catalysis Communications 12 (2011) 734-738.

2.   C. Y. Ma, B. J. Dou, J. J. Li, J. Cheng, Q. Hu, Z. P. Hao, S. Z. Qiao, Applied Catalysis B: Environmental 92 (2009) 202-208.

3.   H. Yu, Y. Zhang, X. Fu, F. Peng, H. Wang, J. Yang, Catalysis Communications 10 (2009) 1752-1756.

4.   L. Nie, K. K. Xin, W. S. Li, X. P. Zhou, Catalysis Communications 8 (2007) 488-492.

5.   L. Xinrong, X. Jinyu, L. Huizhang, Y. Bin, J. Songlin, X. Gaoyang, Journal of Molecular Catalysis A: Chemical 161 (2000) 163-169.

6.   V. Choudhary, D. Dumbre, Topics in Catalysis 52 (2009) 1677-1687.

7.   N. Dimitratos, J. A. Lopez-Sanchez, D. Morgan, A. Carley, L. Prati, G. J. Hutchings, Catalysis Today 122 (2007) 317-324.

8.   A. Villa, D. Wang, N. Dimitratos, D. Su, V. Trevisan, L. Prati, Catalysis Today 150 (2010) 8-15.

9.   Y. Chen, H. Zheng, Z. Guo, C. Zhou, C. Wang, A. Borgna, Y. Yang, Journal of Catalysis 283 (2011) 34-44.

10.   Y. Chen, H. Lim, Q. Tang, Y. Gao, T. Sun, Q. Yan, Y. Yang, Applied Catalysis A: General 380 (2010) 55-65.

11.   G. Wu, X. Wang, J. Li, N. Zhao, W. Wei, Y. Sun, Catalysis Today 131 (2008) 402-407.

12.   Y. Yu, B. Lu, X. Wang, J. Zhao, X. Wang, Q. Cai, Chemical Engineering Journal 162 (2010) 738-742.

13.   P. Miedziak, M. Sankar, N. Dimitratos, J. A. Lopez-Sanchez, A. F. Carley, D. W. Knight, S. H. Taylor, C. J. Kiely, G. J. Hutchings, Catalysis Today 164 (2011) 315-319.

14.   N. Jamwal, R. K. Sodhi, P. Gupta, S. Paul, International Journal of Biological Macromolecules 49 (2011) 930-935.

15.   M. Deng, G. Zhao, Q. Xue, L. Chen, Y. Lu, Applied Catalysis B: Environmental 99 (2010) 222-228.

16.   T. Harada, S. Ikeda, F. Hashimoto, T. Sakata, K. Ikeue, T. Torimoto, M. Matsumura, Langmuir 26 (2010) 17720-17725.

17.   L. Qi, X. Qi, J. Wang, L. Zheng, Catalysis Communications 16 225-228.

18.   K. Yamaguchi, N. Mizuno, Angewandte Chemie International Edition 41 (2002) 4538-4542.

19.   J. Liu, F. Wang, Z. Gu, X. Xu, Catalysis Communications 10 (2009) 868-871.

20.   V. Hulea, E. Dumitriu, Applied Catalysis A: General 277 (2004) 99-106.

21.   M. Oubenali, G. Vanucci, B. Machado, M. Kacimi, M. Ziyad, J. Faria, A. Raspolli-Galetti, P. Serp, ChemSusChem 4 (2011) 950-956.

22.   D. Gao, Q. Gao, Catalysis Communications 8 (2007) 681-685.

23.   C. Chiappe, A. Sanzone, P. J. Dyson, Green Chemistry 13 (2011) 1437-1441.

24.   P. J. Miedziak, Q. He, J. K. Edwards, S. H. Taylor, D. W. Knight, B. Tarbit, C. J. Kiely, G. J. Hutchings, Catalysis Today 163 (2011) 47-54.

25.   D. K. Chakrabarty, Adsorption and Catalysis by Solids, Wiley Eastern Limited, 1990.

26.   H. Zhang, Y. Liu, X. Zhang, Chinese Journal of Catalysis 32 (2011) 1693-1701.

27.   A. Villa, D. Wang, P. Spontoni, R. Arrigo, D. Su, L. Prati, Catalysis Today 157 (2010) 89-93.

28.   M. Silva, C. Freire, B. de Castro, J. L. Figueiredo, Journal of Molecular Catalysis A: Chemical 258 (2006) 327-333.

29.   M. S. Saha, R. Li, X. Sun, S. Ye, Electrochemistry Communications 11 (2009) 438-441.

30.   J. Amadou, K. Chizari, M. Houllé, I. Janowska, O. Ersen, D. Bégin, C. Pham-Huu, Catalysis Today 138 (2008) 62-68.

31. L. Jia, S. Zhang, F. Gu, Y. Ping, X. Guo, Z. Zhong, F. Su, Microporous and Mesoporous Materials 149 (2012) 158-165.

32. C. Y. Ma, J. Cheng, H. L. Wang, Q. Hu, H. Tian, C. He, Z. P. Hao, Catalysis Today 158 (2010) 246-251.

33. L. Qi, X. Qi, J. Wang, L. Zheng, Catalysis Communications 16 (2011) 225-228.

34. C. Della Pina, E. Falletta, M. Rossi, Journal of Catalysis 260 (2008) 384-386.

35. W. Fang, J. Chen, Q. Zhang, W. Deng, Y. Wang, Chemistry – A European Journal 17 (2011) 1247-1256

36 K. Yamaguchi and N. Mizuno, Angewandte Chemie International Edition 41 (2002) 4538

37. L. F. Mabena, S. S. Ray, N. J. Coville, Ceramic Engineering and Science Proceedings 32 (2011) 33-42.

38. C. Saux, L. B. Pierella, Applied Catalysis A: General 400 (2010) 117-121.

39. S. K. Pardeshi, R. Y. Pawar, Materials Research Bulletin 45 (2010) 609-615.

40. V. K. Bansal, P. P. Thankachan, R. Prasad, Applied Catalysis A: General 381 (2010) 8-17.

41. X. Gao, J. Xu, Applied Clay Science 33 (2006) 1-6.

42. K. Chizari, I. Janowska, M. Houllé, I. Florea, O. Ersen, T. Romero, P. Bernhardt, M. J. Ledoux, C. Pham-Huu, Applied Catalysis A: General 380 (2010) 72-80.

43. R. I. Jafri, N. Rajalakshmi, S. Ramaprabhu, Journal of Power Sources 195 (2010) 8080-8083.

44. T. C. Nagaiah, S. Kundu, M. Bron, M. Muhler, W. Schuhmann, Electrochemistry Communications 12 (2009) 338-341.

CHAPTER 9

GENERAL CONCLUSION

The objective of the study was to synthesise and characterise ruthenium supported on N-doped carbon nanotubes (N-CNTs). The Ru catalysts prepared were used in different applications; the oxygen reduction reaction (ORR) for fuel cells application and in liquid phase oxidation reactions.

The initial chapters introduced the evolution of catalysis until the current era of nanotechnology. A comprehensive literature review of nitrogen doped carbon nanotubes as a catalyst support and their applications were outlined. The review showed that currently most applications related to the use of N-CNTs as a catalyst support are fuel cell applications. N-CNTs are still in their early stages of development but they have been show to be exceptional nanomaterials due to their chemical and physical properties.

SECTION A

In **chapter 3,** N-CNTs were synthesised using a thermal-CVD method in a two stage horizontal split-tube furnace. Cyclohexanol was used as carbon source, aniline as a nitrogen source and ferrocene as catalyst. Since alcohols have been found to produce cleaner CNTs which contain less amorphous carbon and impurities, an alcohol was used as the source of carbon. The choice of cyclohexanol was suggested as it contains a benzene structure and it has a boiling point which is similar to that of aniline. Additionally, it is a good solvent for the ferrocene and this allows the generation of a homogeneous solution. It was shown that the yield, and purity of the CNTs produced were influenced by the

cyclohehexanol/aniline/ferrocene ratios, temperature and flow rate. Under optimum conditions (reaction temperature: 900 °C, nitrogen flow rate: 100 mL/min, ferrocene:aniline:cyclohehexanol ratios of 1:5:34), high quality nitrogen doped CNTs were obtained The obtained as-prepared N-CNTs were refluxed in 30 % nitric acid for 4 h in order to remove the residual growth reagents. The N-CNTs were fully characterised using a range of instrumental techniques such as transmission electron microscopy (TEM), scanning electron microscopy (SEM), thermogravimetric analysis (TGA), Raman spectroscopy and X-ray photoelectron spectroscopy (XPS).

The N-CNTs that formed had a fairly crystalline structure, constituted by a periodical bamboo like structure with tube diameters of 35 - 100 nm and a nitrogen content of up to 1.3 at %.

Even though clean N-CNTs were obtained the issue with the synthesis approach is the different vapour pressures of the cyclohehexanol, aniline and ferrocene mixture which makes it difficult to maintain a constant reactant ratio with time. The recommendation is to use a one furnace system and using a syringe injection system in order to have a constant reactant ratio.

Chapter 4 describes the synthesis and characterisation of Ru nanoparticles that are formed on the N-CNTs using a microwave irradiation technique. For the optimum conditions, commercial CNTs were used to support the Ru while varying the microwave heating power between 350 and 1000 W; 500 W was determined to be the optimum power to use.

TEM images of the ruthenium catalysts supported on N-CNTs, and CNTs revealed that the catalyst particles were homogenously dispersed on the surface. The Ru particles had a narrow size distribution and small particle size with an average Ru diameter of 2.5 and 6.2 nm for the N-CNTs, and

for the pristine CNTs respectively. The nitrogen containing carbon nanotubes are preferred to the CNTs as support for Ru as it generates a catalyst with a better homogenously and narrow Ru dispersion than the CNTs. The N-CNTs support also generates a catalyst with smaller Ru particles than those formed on the CNT as support. The catalyst support played an important role in controlling the Ru deposition and Ru particle size through a strong Ru particle-support surface interaction presumably at the defects sites. This dispersion controls the catalytic activity of the supported nano-Ru catalysts.

ICP analysis of the Ru supported on carbon materials revealed that the metal ratios obtained were very close to those predicted from the catalyst preparation.

SECTION B

Part A

The electrocatalytic activity of Ru supported catalysts on the ORR activity was investigated and presented in **Chapter 5**. The activity of the prepared N-CNTs towards the reduction of oxygen in alkaline electrolyte was compared to that of commercial CNTs without N using the onset potential at 1500 rpm. The onset potential of commercial CNTs was more negative at -0.184 V while that of N-CNTs was more positive at -0.144 V thus indicating improved ORR kinetics on N-CNTs than on the commercial CNTs. For this reason the study focused on the activity of a range of Ru/N-CNT materials. The Ru nanoparticles of mean diameter of 2.9 nm were uniformly distributed on the N-CNT surface. The 4 electron reaction of ORR was found to be more favourable on 2Ru/N-CNTs and 5Ru/N-CNTs. 2Ru/N-CNTs i.e. a 2 % Ru loaded sample and the (5 % Ru) 5Ru/N-CNTs nanocatalysts showed the oxygen within the solution diffused to the surface of the electrode and reacted to form hydroxyl ion through a four-electron reaction. With the increase of the loadings from 2 - 5 to 10 wt. % the n value in the equation decreased to 3.7 and 3.2,

respectively. This was due to the formation of the isolated metallic Ru particles, since isolated 3d transition metals tend to produce H_2O_2, thereby causing a low n value. The lower loading of Ru metal nanoparticles on the 2Ru/N-CNT catalyst proved to give a better catalyst, which makes it a potential material for the ORR catalysis in fuel cells in alkaline media.

Part B

Ru/N-CNTs and Ru/CNT catalysts were calcined to form RuO_2/N-CNT and RuO_2/CNT respectively, and the catalytic activity and product selectivity of RuO_2/N-CNT and RuO_2/CNT catalyst for the liquid phase oxidation of styrene and benzyl alcohol was investigated. Reaction variables such as catalyst amount, catalyst loading, solvent, temperature and substrate oxidant ratio were explored. Possible reaction pathways were proposed for the reactions. Both styrene and benzyl alcohol oxidation reaction gave benzaldehyde as the major product.

In **Chapter 6** $5RuO_2$/CNT catalysts were found to be active in catalysing the oxidation of styrene with relatively high benzaldehyde selectivity (85 %) using hydrogen peroxide as oxidant. Other products such as benzoic acid, phenyl acetic acid and traces of styrene oxide were obtained with very low selectivity. The $5RuO_2$/N-CNT catalyst showed a better selectivity to benzaldehyde (88 %) but at lower conversion (34 %) as compared to $5RuO_2$/CNTs after 4 h reaction.

In the previous chapter the Ru/N-CNTs were shown to exhibit some activity. To further explore this issue Ru was deposited on nitrogen doped CNTs prepared differently from those in chapter 6. In **Chapter 7** further investigations on the activity of the new nitrogen doped carbon nanotubes (N-CNTs*) was investigated for styrene oxidation. In this case, the nitrogen doped carbon nanotubes (N-CNTs*) with 2.2 at.% nitrogen content were synthesized by the catalytic decomposition of acetylene (C_2H_2) and acetonitrile (CH_3CN) at 700 °C over a 10 % Fe-Co supported on calcium carbonate ($CaCO_3$) catalyst. Optimisation of this synthesis process was

done by other co-workers in our group. N-CNTs* were prepared, characterised and tested for styrene oxidation. The bamboo structured material with a diameter range of 30 – 90 nm was made. The Ru was supported on the N-CNTs* using the same conditions as the one used for supporting Ru on N-CNTs using a microwave method. The Ru particle size obtained was narrower with the average particle size of 3 nm. After calcination the size of the particle increased to 9 nm average particle size. RuO_2/N-CNTs* catalysts were active in catalysing the oxidation of styrene; the main product was benzaldehyde. This resulted from the nucleophilic attack of H_2O_2 on styrene oxide, followed by cleavage of the intermediate hydroxy–hydroperoxystyrene, and also from a cleavage of the C=C bond. The catalyst has shown to be highly selective as compared to the previous supported catalysts used for styrene oxidation in this study. Comparing the support it was deduced that the nitrogen present in the support plays a major role. With the increase in the nitrogen content in the CNTs the conversion of styrene decreased but with an increase in selectivity

3 % Ru loaded on N-CNTs (3RuO_2/N-CNT) based catalyst was also tested for the selective oxidation of benzyl alcohol and compared to the 3RuO_2/CNT based catalysts in **Chapter 8**. After 5 h at 110 ºC benzyl alcohol conversion was 10 and 14 % for 3RuO_2/CNTs and 3RuO_2/N-CNT catalyst respectively with benzaldehyde selectivity of 70 and 85 % respectively. The catalyst was shown to have a lower activity for benzyl alcohol oxidation than styrene oxidation.

In general the results reveal that the nitrogen functionalities incorporated in the network structure of carbon nanotubes led to an improvement of the selectivity towards benzaldehyde in the styrene oxidation reaction. Furthermore, the catalytic activity of the supported Ru catalyst depends on the support, Ru loading and Ru particle size but also on the reaction catalyzed by the catalyst.

The results indicate a strong influence of the support used for the supported Ru catalyst for the styrene conversion and benzaldehyde selectivity. Further detailed studies are necessary for understanding the influence of nitrogen on the support for improving the catalyst performance.

The thesis was successful in achieving the research objectives proposed of synthesising ruthenium catalysts that are active in different catalysis application.

Future studies may entail:

- Use of a one furnace system for the synthesis of N-CNTs to maintain constant reactant ratios as it is difficult to control the ratios because of different vapour pressures of the reactants.

- Investigate different oxidants for the benzyl alcohol oxidation reaction using Ru/N-CNT and Ru/N-CNTs* as catalysts.

- Determining the maximum nitrogen content in the nitrogen doped carbon nanotubes that can give maximum selectivity towards benzaldehyde in the styrene oxidation reaction.